5-2015

Biomechanical Characterization and Modeling of Human TMJ Disc

Gregory Wright
Clemson University, mrgregjwright@gmail.com

BIOMECHANICAL CHARACTERIZATION AND MODELING OF THE HUMAN TMJ DISC

A Dissertation
Presented to
the Graduate School of
Clemson University

In Partial Fulfillment
of the Requirements for the Degree
Doctor of Philosophy
Bioengineering

---

by
Gregory John Wright
May 2015

Accepted by:
Hai Yao, PhD, Committee Chair
Zhi Gao, PhD
Michael Kern, PhD
Martine LaBerge, PhD

ABSTRACT

Temporomandibular joint (TMJ) disorder affects over 10 million people in the US each year. The signs and symptoms of temporomandibular joint disorders (TMDs) include limited mouth opening, clicking and locking of the jaw, and significant pain in the craniofacial region. A majority of these cases involve the pathology of the TMJ disc, a large fibrocartilage responsible for joint function. Treatments aimed at restoring joint function, such as corticosteroid injections and joint replacements, have been met with limited success due to the gap in understanding about the complex biomechanical function of the TMJ disc and the events that lead to pathology of the disc. As a result, significant advances in research are essential to understand the pathophysiology of joint degeneration for early diagnosis and management. It is generally believed that pathological mechanical loadings, e.g. sustained jaw clenching or malocclusion, trigger a cascade of molecular events leading to TMJ disc degeneration. A deeper understanding of the biomechanics, i.e. mechanical environment and effect on the nutrient environment, could lead to developments in TMJ disorder diagnosis and management. Therefore, the objective of this research study is to determine the mechanical and transport properties of the human TMJ disc and begin to simulate joint biomechanics using patient specific finite element models. Our **central hypothesis** is that sustained mechanical loading can alter solute transport and nutrient levels in the TMJ disc as well as mechanical function

resulting in disc derangement and degeneration. **Aim 1: Determine mechanical properties of human TMJ discs and correlate the mechanical properties to the tissue composition and structure. Aim 2: Determine strain-dependent transport properties of human TMJ discs.** The outcome of this study will yield a model of the human mechanical environment of the TMJ disc that will build a pathway between biomechanics and pathobiology.

ACKNOWLEDGMENTS

My sincerest thank you goes out to all those that stood with me during this work. I could not have completed this work without the support and encouragement from many people. In addition, I would like to extend special appreciation to several individuals.

I would like to thank my advisor, Dr. Hai Yao, for his patience, guidance and commitment to my training and success, and for the amount of time he dedicated to my development.

I would like to thank my committee members Dr. Martine LaBerge, Dr. Bruce Gao, and Dr. Michael Kern for their wisdom and support through my study.

I would like to additionally thank Dr. Richard Swaja and Dr. Ed Krug for timely advice during my study, and a special thank you to Maria Torres and LuAnne Harley.

I want to thank my friends and lab partners, Dr. Yongren Wu, Dr. Wenjun He, Dr. Andy Shi, Sarah Cisweski and David Butts for your consistent support and help in moments that made this work possible.

I would like to thank my brother Rob Wright and my family for all their love and encouragement. I would also like to thank Mike and Lynn Varn, and John A. Zeigler for their tremendous support.

And finally I would like to give the deepest thank you to my love and my all Meredith Varn, who believed in me and the work. Thank you for showing me the moments along the way. This work is dedicated to you.

Funding for this research was provided by the National Institutes of Health for T32 DE017551 and F31 DE023486.

TABLE OF CONTENTS

Page

Table of Contents (Continued) Page

LIST OF TABLES

Table Page

LIST OF FIGURES

Figure Page

List of Figures (Continued)

Figure Page

List of Figures (Continued)

Figure

Page

1 GENERAL INTRODUCTION

The temporomandibular joint (TMJ) is a joint unlike any other in the body. The articular tissues of the joint along with the TMJ disc are derived from neural crest cells which give the tissues a unique cell type and matrix compared to articular cartilage of the knee and the intervertebral disc in the spine [1]. These tissues give rise to the unique diarthroidial function and translation of the jaw [2-6]. But these tissues may also be responsible for the unique onset of TMJ disorder (TMD) which involves a much younger population 25-45 than many other cartilage disorders and could contribute to a significant gender disparity, with women being affected 2-3 times more than men [7, 8].

In 2005 the NIDCR (National Institutes of Dental and Craniofacial Research) launched the OPPERA (Orofacial Pain Prospective Evaluation and Risk Assessment) program. The program was a prospective evaluation to determine which risk factors were at play in developing temporomandibular joint disorders (TMDs) [9-13]. Although it confirmed the gender disparity but challenged population age, the study found that a complex range of risk factors, including gender, genetic, and psychological factors, were likely correlated, unlike many other cartilage disorders that feature injury or age related causes. In 2012, the NIDCR director declared TMDs a top priority, establishing research on TMDs a major research initiative of the NIDCR. This was an effort to bring TMJ research up to speed with current advancements in biomedical research as few treatments have advanced in TMJ disorder while dramatic progress has provided much more success in other joints. One of the key areas of research focuses on the large articular TMJ disc, a

cartilage tissue responsible for a significant portion of biomechanical function of the joint. Most researchers agree that a large majority of late stage progression of TMDs involves the loss of the biomechanical function of the TMJ disc [5, 14-16]. In the early 1990's, researchers began to characterize the cell type and extracellular matrix (ECM) composition of the TMJ disc in an effort to begin to understand the cellular and matrix environment that may contribute to the molecular events leading to degradation [17-22]. During that time and increasingly in the early 2000's, a significant number of biomechanics studies began to correlate matrix composition with mechanical strength of the TMJ disc in an effort to begin to understand the disc's biomechanical capacity for joint loading and ECM mechanisms for load dissipation [23-34].

In the past two decades, these animal models were used to test TMJ disc tissue [14, 35]. These models have provided a significant understanding in the field of TMJ disc biomechanics. However, due presumably to the scarcity of human tissue, human studies were relatively few compared with animal studies. Therefore, the work of this dissertation seeks to provide a better understanding of the human biomechanical environment by determining the human transport and biomechanical properties using human cadaveric tissue. Currently large animal models such as porcine and bovine models are used to conduct biomechanics studies, such as tissue biomechanical characterization and tissue engineering implantation. Results from human characterization will allow researchers working with these large animal models to better compare the results to the human mechanical environment. In addition, this dissertation will determine the biomechanical properties of the disc with new electrokinetic

methodologies which can determine the solid, fluid and charged matrix effects on the TMJ disc and measure the diffusion of ions within the disc under strain. This new understanding could provide valuable insight into the complex biomechanical function of the TMJ disc. Data from these studies will be used to begin to model the *in vivo* mechanical environment of the disc.

This research study will use human tissue properties to develop a model of the TMJ disc based on the solid matrix, interstitial fluid and charged ion phases of the disc in reaction to mechanical load. The timeliness of this project comes with the wide variety of large animal models such as pig and bovine models being used to make biomechanical assumptions about the behavior of human TMJ disc. Current finite element models use porcine tissue modulus and diffusivity values to construct human models from MRI and patient anatomy. A comprehensive characterization of human tissues will better equip scientists to judge the *in vivo* multiphasic environment of the disc as well as enhance our understanding of previous and future animal studies due to the comparison with a human baseline. As an outcome, the combined stress, strain, electrical conductivity and fixed charge density of the disc will be modeled to investigate the *in vivo* physiochemical environment of the disc. Future animal studies may then reference this study as a basis for the biomechanical behavior of the disc compared to the human.

The purpose of this study is to experimentally determine the diffusivity, fixed charge density, and viscoelastic, tensile material properties of the disc so that we can better understand the TMJ disc biomechanical function. As a result, we may be able to identify key biomechanical factors that significantly alter the disc's homeostasis, such as

condyle translation against weak collagen fiber alignment within the disc or prolonged clenching (bruxism) effects on nutrient transport across the disc. **Our overall long term goal** is to understand the TMJ disc's biomechanical function from a macroscopic to microscopic scale, which includes understanding TMJ disc biomechanical function and the influence of mechanical loading on cell metabolism and matrix production. Finally, if we can set a baseline for human biomechanical function we may be able to model more accurately the events that lead to TMJ pathology. This understanding would allow us to develop better prevention strategies and treatments in the future.

Anatomy, Composition, and Structure of the TMJ disc

The TMJ disc is a dense, avascular fibrocartilage (19 mm x 14 mm) interposed between the condyle of the mandible and the glenoid fossa of the temporal bone [2, 25]. The disc articulates with the condyle during function, acting to lubricate the joint and shield articular surfaces from large contact stresses [36, 37]. Finite element models have determined the TM joint to be a load bearing joint, while additional studies have indicated the TMJ disc is central to joint function [38-44]. Many TMJ disc disorders involve mechanical dysfunction of the disc [45-48]. Therefore, understanding the precise mechanical function of the disc is central to understanding dysfunction [3, 49-51]. It was through failed implants and massive FDA recalls along with biomechanical studies that we learned the disc is a load bearing cartilage structure that performs a complex biomechanical role in jaw movement and mastication [52]. A disruption in this complex biomechanical function initiates damage in the ECM architecture and corresponds to changes in cell synthesis and maintenance of the surrounding ECM [4, 49, 53-56].

The TMJ disc has a very unique cell type, given the designation fibrochondrocyes since they maintain multiple cell type characteristics [1, 17, 26, 35]. The TMJ disc is mainly composed of an abundant amount of water ~70-85% and type I collagen (75~90% dry weight) with small amounts of proteoglycan containing fixed charges (~3-10% dry weight) [14, 25, 27, 57]. SEM studies have found type I collagen aligned in the anterior-posterior direction within central regions of the disc [24, 58]. By comparison, the outer bands of the disc assume a random, circumferential orientation of type I collagen alignment [24, 58]. The combination of different collagen fiber alignment is likely responsible for the disc's complex biomechanical function requiring anisotropic mechanical properties between regions of the disc.

Solute Diffusion and Nutrition: A Potential for a Large Nutrient Concentration Gradient

Transport of solutes and fluids is a large directive for bioengineers specifically in the field of cartilage tissue engineering [3, 49-51]. In avascular cartilage, passive diffusion is responsible for nutrient transport across tissues [53, 59, 60]. In humans, nutrients are required to diffuse over long distances due to the size of the tissues. Interestingly, these distances are much smaller in small animal models such as the mouse and rabbit models. The smaller differences could offer one possible explanation as to why tissue engineering implants and growth factor delivery therapies have been successful in small animals but not in humans. This gives greater emphasis for the need to develop a human model of nutrient transport properties. We do not currently have a constitutive relation for the tissue to predict solute diffusion accurately in the presence of

mechanical loading accounting for additional factors such as the charge density of the tissue, typical in many cartilage types.

Nutrients required by disc cells for maintaining disc health are supplied by synovial fluid at the margins of the disc as well as nearby blood vessels [61]. The transport of small nutrients (i.e., oxygen and glucose) within the TMJ disc depends primarily on diffusion. The balance between the rate of nutrient diffusion through the matrix and the rate of consumption by disc cells establishes a concentration gradient inside the disc [61-63]. Our studies have shown that solute diffusivities in the TMJ disc are only ~50% of the values in IVD tissues of the spine [58, 61, 62]. Furthermore, our cell metabolic studies have shown that the oxygen and glucose consumption rates of TMJ disc cells are at least 5 times and 2 times higher respectively, than cells from articular cartilage and IVD [64]. These results suggest that a steep nutrient concentration gradient likely exists in the TMJ disc and that this nutrient environment is uniquely vulnerable to pathological mechanical loadings (e.g. clenching/bruxism and trauma). Therefore, a central aim of this research is to determine the transport properties of the human TMJ disc and to understand the influence of mechanical loading upon these properties.

Mechanical Function of the TMJ Disc: Importance of Strain Dependent Properties

Modeling the physical signals within biologic tissue allows researchers to simulate the physicochemical environment surrounding cells in response to joint loads. Rather than focus on tissue composition and static mechanical behavior, the focus of this dissertation is on the dynamic biomechanical environment of the TMJ disc. The TMJ disc's unique ECM environment requires the characterization of the viscoelastic strain-

stress relationship. Experiments were conducted at the tissue level to determine the material properties using appropriate biphasic (solid, fluid) and triphasic (solid, fluid, and charged ion phase) model assumptions. These material property values were used to construct a computer generated finite element model of the tissue based on patient anatomy from reconstructed MRI/CT scans.

TMJ disc degeneration is likely multifactorial in origin, however, pathological loading such as sustained clenching (bruxism) and injury could trigger a cascade of molecular events which could lead to disease in certain individuals [65]. Sustained mechanical loading has been shown to affect tissue response to load, such as the loss of fluid pressurization from fluid exudation. In addition, increased loading can cause increased friction through loss of lubrication leading to excessive tissue deformation and wear. Under normal physiologic conditions, mechanical loading at the tissue level effects physicochemical signals at the cellular level initiating cell responses to generate ECM capable of withstanding the loading environment. In the case of disc degeneration, changes in tissue morphology and biochemistry occur in which the tissue can no longer support the loading environment resulting in further damage to the tissue. The molecular cascade of events is still poorly understood, but a significant research objective is to understand the primary mechanical environment supported by the tissue and the corresponding ECM structure. Once this biomechanical characterization of the tissue is elucidated, we can begin to understand the central role pathological mechanical loading plays in disc degeneration.

1.1 Specific Aims

The ***goal of this research study*** is to characterize the mechanical properties and transport properties of human TMJ disc tissues to develop a finite element model of the TMJ disc to understand the nutrient environment under mechanical strain. *Our central hypothesis is that sustained mechanical loading can alter solute transport and nutrient levels in the TMJ disc as well as mechanical function resulting in disc derangement and degeneration.*

Aim 1: Determine mechanical properties of human and porcine TMJ discs and correlate the mechanical properties to the tissue composition. Knowledge of mechanical properties of the TMJ disc and its relationship with tissue composition is crucial for elucidating the mechanical function of the TMJ disc and studying the effect of mechanical strain on fluid and nutrient transport. Therefore, we will: 1a) obtain the tensile instantaneous and relaxed moduli using stress relaxation tensile test.

Aim 2: Determine strain-dependent transport properties of human and porcine TMJ discs. The rates of fluid and solute transport in tissue are mainly governed by transport properties, i.e., hydraulic permeability and solute diffusivity, respectively. The TMJ disc is a charged, hydrated soft tissue. Due to the mechano-electrical coupling effect, the measured transport properties depend on the fixed charge density of the ECM. Therefore, we will: 2a) simultaneously determine hydraulic permeability, fixed charge density, and electrical conductivity of TMJ disc under various mechanical strains using our novel methods; 2b) obtain ion diffusivities from electrical conductivity data and develop new constitutive relationships between transport properties (hydraulic

permeability and solute diffusivity) and tissue hydration to establish strain-dependent transport properties.

Framework and Content: A Dissertation Based on a Combined Experimental and Theoretical Approach

This dissertation addresses the relatively scarce amount of human mechanical properties available on the TMJ disc. The lack of human properties is likely the result of the availability of human tissues. It is the unique research environment of a Bioengineering Program located on the same campus as a Dental School that gives access to these human tissues. The central focus of this research is the mechanical function of the human TMJ disc. Is it similar to the IVD and knee cartilage in terms not only of material strength but how the cartilage dissipates loading? This analysis is also correlated with the biochemical make-up of these specimens. In addition to mechanical function, this dissertation addresses another main concern for TMJ research, to understand the transport properties of the TMJ disc whereby the avascular tissue is supplied with nutrients. This problem is central to understanding disease mechanisms in the onset of mechanical loading and is also fundamental to tissue engineering.

In **Chapter 2**, the background and significance for this research study was presented. The section defined the TMJ disc's unique cellular, anatomical, and biochemical composition as it relates to the disc's biomechanical function. After the disc's composition was established, TMJ disorders and their risk factors were presented along with current treatments. The limited success of current treatments combined with the

limited clinical tools that track the progression of TMJ disorder emphasized the need to define the TMJ disc's biomechanical function so that healthy function can be understood. A detailed review of past biomechanical studies was described, including tensile, shear, and compression studies of the TMJ disc. These biomechanical tests were described by methodology and species. Finally, finite element models of the disc were presented based on assumptions about TMJ disc material properties and mechanical function with and without TMJ disc displacement.

In **Chapter 3**, a study was conducted to determine the electrical conductivity of human TMJ discs. The electrical conductivity was determined based on 0%, 10% and 20% mechanical strains for five disc regions (anterior, lateral, intermediate, medial and posterior). These results were compared for male and female tissues, along with porcine tissue results, which indicated that mechanical strain significantly affected conductivity/diffusivity of the TMJ disc. This supports our overall hypothesis that mechanical strain could play a significant role in impeding nutrient transport across the tissue.

In **Chapter 4**, cartilage storage solutions were investigated using the electrical conductivity method. The ECM permeability of articular cartilage samples in different solutions were evaluated for permeability using conductivity methods similar to Chapter 3. In clinical use, donor osteochondral tissue grafts are stored up to 42 days before

transplantation. In this study, a 30 day storage period was used to evaluate storage solution effects on cell viability and matrix permeability. Ideally, the optimum storage solution preserves both the cell viability and the matrix. This study evaluated two intracellular-type preservation solutions compared with two extracellular-type storage solutions. This study found that extracellular isotonic culture medium (DMEM 10% FBS) preserved cell viability and matrix permeability better than other storage solutions. The results for conductivity were similar to previous studies of articular cartilage. Techniques discovered in this study were applied to the TMJ disc. First, the conductivity method was improved to investigate slight changes in matrix permeability by using a hypotonic bathing solution. This reduced the osmotic pressure surrounding the tissue and exaggerated permeability changes caused by the depletion of glycosaminoglycans (GAGs) which enhanced the sensitivity of the conductivity method. Further, we measured not only the change in matrix permeability of the cartilage but also changes in the charge density of the matrix (fixed charge density) by using the conductivity measurements in different ionic salt concentrations. The technique derived in this study was used on the TMJ disc and presented in Chapter 5.

In **Chapter 5**, the fixed charge density (FCD) of the human TMJ disc was determined using a two point electrical conductivity method. The FCD values were determined for male and female TMJ discs. The fixed charge density is a material property of cartilage. The FCD is determined by the amount of proteoglycan with sulfated GAG chains carrying fixed negative charges. This property plays a significant mechanical role in

articular cartilage as described by the triphasic theory and measured by Maroudas et al. and Mow et al [66-69]. Fixed negative charges in cartilage play a significant role in load support by resisting interstitial fluid exudation upon mechanical compression and by steric interference when GAG chains are compressed closer to one another with like charges repelling. The fixed charge density also affects the diffusivity of the tissue, which previously we have considered negligible. The GAG content was also measured in these tissues and correlated with FCD content. This study brings the TMJ research community in biomechanics to the level of current studies of articular cartilage and IVD studies aimed at advanced triphasic modeling of the solid, fluid and charged solid matrix components of the TMJ disc.

In **Chapter 6**, the tensile mechanical strength of human TMJ discs was determined by incremental tensile stress-relaxation methods. To our knowledge, the tensile properties of human TMJ disc tissue have only been compared in few studies before (i.e. one study used two discs from a discectomy removing degenerated tissue) [70, 71]. This study used 24 discs from 12 cadavers. The samples in this study were loaded at a uniform load rate. The tensile moduli, expressed as instantaneous and relaxed modulus, were compared to previous studies using porcine tissues. The sample's stress response to increments of constant strain was also analyzed through YC Fung's quasilinear viscoelastic theory which accounts for nonlinear behavior in viscoelastic response [56]. The theory has been used to analyze tendon and other articular cartilaginous tissues.

In **Chapter 7**, current progress was presented on the formulation of a finite element (FE) model based on experimentally measured biomechanical properties of the TMJ disc. A 2D axial symmetric FE model was first described followed by a 3D FE model of the human TMJ disc. The 3D FE model was explored through its creation of the solid model of patient anatomy using Mimics software and MRI/CT scans. Finally, a dynamic model was constructed using rigid body jaw tracking data collected from patients. Future simulations were discussed such as modeling the stress field translation of the condyle acting on the disc which could be used for diagnosing pathologies based on patient specific joint function.

In **Appendix 1**, a spine biomechanics study was presented. The translational study was completed with the MUSC Orthopaedic Surgery Department. The study investigated two methods of surgical instrumentation in upper thoracic fixation used to treat pediatric patients (8-12 years old) with severe early onset scoliosis (COBB angle > 45) in the presence of severe kyphosis (>45 degrees or hyperkyphosis). The control method was a commonly used method whereby pedicle screws were used in upper thoracic fixation but experience pullout failure in the presence of kyphosis. The test method developed by the pediatric spine surgeon, used lamina hooks for fixation on the ribs to prevent pullout failure. The implants were applied to an immature porcine model (n=6 for each group) with the full spine intact, so a pure bending load could be applied to the spine to mimic kyphosis. The study found the rib construct to be superior in maintaining a larger angle

of deflection and carried a similar load without failure, whereas the pedicle screw fixation experienced dramatic pullout failure in all six samples.

2 A REVIEW OF TMJ DISC BIOMECHANICS

TMDs are a major musculoskeletal disorder. In the US, over 10 million people are affected with signs and symptoms of the disorder (NIDCR 2010). Of those that seek treatment, over 70% suffer from disc derangement believed to be a consequence of TMJ disc degeneration [16, 65].

Currently there is a gap in understanding of how mechanical injury can bring about molecular processes that lead to disc degeneration. Our hypothesis is that sustained mechanical loading can alter solute transport and nutrient levels in the TMJ disc, thereby altering the cellular metabolism, tissue composition, and mechanical function leading to degeneration**.** The rationale for this literature review comes on the basis of our findings in the lab and the absence of knowledge dealing with the combined effect of mechanical strains damaging the nutrient environment within the human TMJ disc.

Current methods aimed at understanding the mechanical function of the TMJ disc can only investigate *in vitro* tissue mechanical properties along with the nutrient transport properties based on animal models. With all tests results combined, however, the level of knowledge is still not enough to gain an accurate portrait of the tissue under physiologic mechanical loads *in vivo*. In order to simulate the TMJ disc *in vivo*, finite element (FE) methods must use tissue properties along with the patient's specific anatomy and mechanics to gain a better understanding of mechanical effects that could lead to degeneration.

First, before proposing an experimental plan, a thorough examination of the literature must provide a firm foundation of discovery and room for advancement. The

literature review provides a perspective from previous mechanical and transport studies, as well as developments in finite element models and motion tracking tools used to study the TMJ disc.

2.1 Anatomy and Biomechanical Function

Similar to other joints in vertebrates, the temporomandibular joint (TMJ) consists of bone to bone interfaces with cartilage protecting bone surfaces from impact and friction build-up. Cartilage in the joint provides a unique load dissipating environment that allows the joint to function through the life of the patient. In the closed jaw position or central occlusal position, the strongly convex mandible condyle of the mandible bone rests within the concave surface of the glenoid fossa of the squamous portion of the temporal bone. A thin layer articular cartilage lines both the mandible condyle and glenoid fossa; and unique to the joint is the articular disc or TMJ disc that is positioned between the two boney surfaces and divides the joint into an upper and lower joint compartment (Figure 1).

Figure 1 Cross-sectional view of temporomandibular joint and overhead view of TMJ disc outlining specific regions. [1]

The articular disc is ovid shaped in dorsal view and biconcaved shaped in the parasagital section [35]. Both inferior and superior joint compartments are filled with synovial fluid that aid in lubrication of the condyle and disc and supply surrounding avascular cartilage and TMJ disc with nutrients [2, 35].

During initial jaw motion, the mandible condyle first rotates in central occlusal position within the inferior joint compartment [2]. As the mandible elevates, the temporalis, masseter, and medial pterygoid muscles contract. The mandible condyle further translates out of the resting glenoid fossa concavity and down the posterior slope of the fossa eminence. The ability of the joint to rotate (diarthroid joint) and translate (ginglyo joint) gives rise to the classification of *ginglymoarthroidal* joint [2]. The TMJ disc translates with the condyle through lateral and medial pole attachments through robust insertion of capsular ligaments. The posterior attachment to the TMJ disc is through a massive pad of fibrous retrodiscal tissue with inner clusters of adipose cells [35]. The posterior band of the TMJ disc is attached to the surrounding ligaments through large, thick fibrous tissues with interspersed adipose cell, with insertion into the condyle and temporal bone [35]. The posterior attachment is believed to assist the disc's recovery in retrusion back to central intercuspal positon [35, 72]. The disc has anterior attachment to the lateral pterygoid muscle and anterior to the condyle. As the mandible closes or depresses, the masseter and inferior lateral pterygoid muscles act, as the disc is positioned back to central intercuspal position [2].

Thin layers of articular cartilage protect the mandible condyle (0.2-0.5 mm) and fossa along with eminence (0.1-0.3 mm) [2, 28]. The articular disc on the other hand is

much thicker (2-4 mm) along the posterior and anterior zones and (1-2 mm) along the intermediate zones. It is believed that the disc supplies the majority of joint load dissipation, lubrication and protection of articular surfaces. The disc is believed to act to fill joint areas of low areas of contact, in order to reduce high contact stresses and distribute them through the disc.

Another key aspect of the TMJ anatomy and function is the unique loading environment to the joint. The joint is said to operate as a 1) a rotating hinge joint with 2) secondary gliding motion [2]. However, the joint motion must be further examined. For example, the joint has two condylar poles with muscle attachments. As the joint functions, muscles contract and release bilaterally. This caused protrusive and retrusive movement, opening and closing with translation and rotation within the joint. However, during mastication the mandible also undergoes lateral shifts and orbital motions, which create grinding motion and rotation of the condyles about multiple axes. Therefore, the joint not only rotates and translates, but when analyzing both condylar poles, the joint is allowed complex six degrees of freedom (6 DOF) about its condylar axis [6, 37, 73, 74]. Finite element studies have determined the TM joint is a load bearing joint [37]. This gives rise to a very unique mechanical function in the TMJ disc. The disc is highly anisotropic functioning under tensile, compressive, shear, as well as frictional and traction forces often during the same masticatory stroke.

2.2 TMJ Disc Cell Characterization and Extracellular Matrix Composition

Fibroblasts

In porcine TMJ disc, fibroblasts were found to comprise 70% of the cell population. In the anterior posterior axis, the anterior and posterior regions of the disc had higher fibroblast content than the intermediate portion of the disc, 3.5% and 6.3% greater respectively. The overall cell density from histology was 681±197 cells/mm^2. Fibroblasts appeared to exhibit uniform ultrastructural characteristics between regions of the disc. The ultrastructural characteristics included a large nuclei, minimally visible rough endoplasmic reticulum and even less visible smooth endoplasmic reticulum. Golgi apparatus and mitochondria were rarely observed. Similarly, ribosomes were observed in scarce amounts; however few fibroblasts had an abundant amount of ribosomes.

Fibroblasts were also found in greater amounts along the periphery of the disc, specifically at the anterior and posterior attachment sights [19, 75]. Fibroblasts appeared to align with surrounding collagen fibrils.

Chondrocytes, Chondrocyte-like cells, and Fibrochondrocytes

Chondrocytes are generally identified in articular cartilage and the nucleus pulposis of IVD. During embryonic development, chondrocytes provide major functional growth of the skeleton through endrochondral ossification mainly due to the remarkable ECM synthesizing ability of chondrocytes. The flexibility of cartilage as opposed to mineralized bone also helps in the development. As the growth tapers and the skeleton becomes mature, chondrocytes are mainly found in cartilage at the end of long bones,

IVD, and nasal septum for the purpose of distributing mechanical loads, providing flexibility, and protecting boney surfaces [76].

Chondrocytes in the TMJ disc were distinct from other designated chondrocyte-like cells found in the disc. Chondrocytes exhibited well-organized rough and smooth endoplasmic reticulum, Golgi apparatus and many ribosomes. While the chondrocytes exhibited a well-defined electron-lucent zone or pericellular matrix, the pericellular capsule was not found [26].

Chondrocyte-like cells on the other hand were found to have very few organelles with a lack of pseudopodia and pericellular matrix, including a small amount of rough endoplasmic reticulum and lesser amounts of smooth endoplasmic reticulum [26]. Few cells had identifiable Golgi apparatus. However, the chondrocyte-like cells did have an abundant amount of mitochondria and large nucleus, with moderate amounts of ribosomes [1, 26, 77-79]. Chondrocyte-like cells were found in abundant concentrations in the center of the TMJ disc which corresponds well to the greater amounts of chondroitin sulfate and higher compressive modulus found for this region [32, 80]. Berkovitz et al described the human TMJ disc as a dense fibrous connective tissue with chondrocyte-like cells scattered sparsely. Overall, the ratio of fibroblast to chondrocyte-like cells was 2.35 to 1 [26].

Often cells of the TMJ disc are referred to as fibrochondrocytes since these cells lack a pericellular matrix but still retain chondrocyte markers [49]. Overall, the cells within the disc appear to exhibit more fibroblast like characteristics resembling synovial fibroblasts due to proteinase and proteinase inhibitors [81]. Among the cell types in the

TMJ disc, fibroblasts, chondrocytes and fibrochondrocytes have been shown to express different markers based on normal and pathologic discs.

Collagen

Collagens are considered a main structural protein of connective tissue. In humans, collagens account for one third of the total proteins, being the most prevalent protein in the ECM. Collagen is known for its triple helix formation of three parallel, staggered polypeptide chains. The triple helixes interweave to form fibrils; fibrils align and bind together to become microfibrils in fibrillar collagens. Of the types of collagen, the first five are fibrillary and the most common is type I collagen , which makes up 90% of the collagen found the body and can be found in dermis, bone, tendon and ligaments [56].

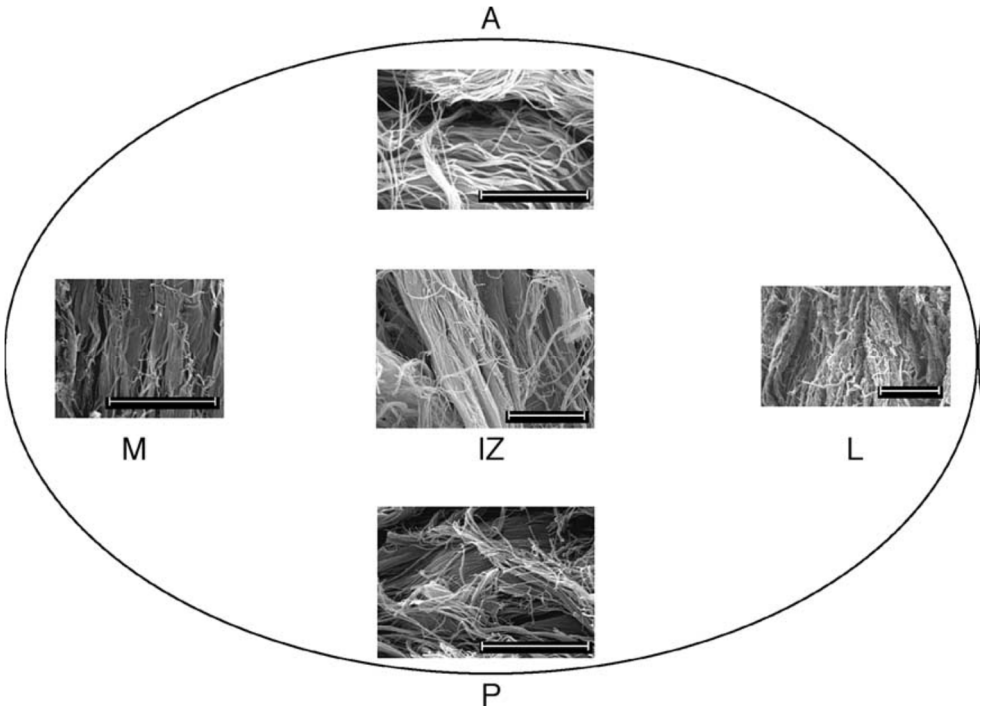

Figure 2 SEM image from porcine TMJ disc
SEM image shows the collagen fiber type I alignment. The fibers appear to run anterior-posterior along the intermediate zone and run circumferentially along the perimeter.[82]

The TMJ disc is primarily composed of type I collagen, whereas hyaline cartilage and the nucleus pulposus of the intervertebral disc is composed mainly of type II collagen [17, 19, 75, 83]. For primate TMJ discs, only minute amounts of collagen type II was detected in areas near chondrocyte-like cells and also along the periphery of the disc [75]. The largest concentration of collagen II was found in the intermediate region suggesting a higher concentration of chondrocytes in the region where researchers believe the disc may undergo a greater amount of compressive loading in this region [27]. See Table 1 below for species comparison [3].

Type I collagen is aligned in a ring like fashion around the perimeter of the disc and runs anterior-posterior along the intermediate region of the disc (see Figure 2 above). Biomechanical studies have correlated anisotropy in tensile strength to collagen alignment. Collagen accounts for 80-95% of the TMJ disc dry weight and up to 50% of the volume by wet weight [84-87]. Average collagen fiber diameter has been reported as ~18 μm ± 9 μm [27]. Collagen fibers have been observed to have a wavy and crimped pattern across the entire thickness of the disc [23, 88-90].

Table 1 Regional collagen content of various animal models.

Authors	*Ref. no.*	*Location*	*Content (mg/g)*	*Species*	*Dry/wet weight*	
Gage *et al.* (1995)	70	Posterior band	334 ± 6	Human	Wet	I
		Anterior band	342 ± 10	(diseased)		
		Anterior attachment	365 ± 18			
		Medial attachment	372 ± 18			
		Lateral attachment	360 ± 17			
		Posterior attachment	368 ± 21			
Berkovitz and Robertshaw (1993)	80	Periphery (anterior)	52.3 ± 6.7% (v/v)	Rabbit	Dry	I
		Center	58.0 ± 6.6% (v/v)			
Gage *et al.* (1990)	64	Posterior attachment	377 ± 21	Human	Wet	I
		Lateral attachment	372 ± 18			
		Disc	304 ± 5			
Nakano and Scott (1989)	59	Disc	830	Bovine	Dry	I

Elastin

Elastins are highly elastic proteins found in connective tissues, with as much as 50-70% by dry weight found in arterial tissue of canines. Elastin is believed to provide recovery after deformation, as well as provide load support after ~50% deformation in some tissues. The TMJ disc has been found to deform up to 35%, so elastin in the TMJ disc may provide recovery after small deformations instead of significant amounts of

loading. Elastin content in TMJ disc has been reported to be very low by dry weight, in bovine TMJ disc 3-7% [91, 92]. Although elastin has been found to be cross-linked with collagen in the TMJ disc, due to the scarce amount it is unlikely that elastin contributes to the mechanical loading of the tissue [25, 75, 89]. Additionally, the presence of elastin has varied between regions of the disc and between inferior and superior surfaces [22, 92].

GAG/Proteoglycans

Proteoglycans (PGs) are synthesized by almost all types of mammalian cells. PGs have been found within cells, on the cell surface, and in the ECM. PGs contribute to material properties in tissues as well as carry out roles in cell adhesion and cell signaling [93].

There are a wide variety of PGs defined by their construction of polysaccharide units. PGs are composed of a core protein covalently connected to linear polymers of disaccharides, known as glycosominoglycans (GAG). PGs can have one GAG chain as present in decorin or as many as a hundred in aggrecan. PGs are named according to the type of GAG chains, such as chondroitin sulfate, dermatan sulfate, keratin sulfate, and heparan sulfate [93].

It is common in tissues for PGs to form large aggregates where PGs are connected to hyaluronan (HA) through non-covalent interaction with LINK protein. Additionally, these large PG aggregates are contained within a collagen matrix. The interconnectedness between the ECM components, like the hyaluronan interaction with large PG aggregates, give tissues unique biomechanical properties especially in cartilage

which has a very high concentration of PGs. Often, PGs have GAG chains which contain a high concentration of negative charges due to sulfated end groups [93].

The negative charges on the GAG chains give cartilage very unique material properties. First, the negative charges make PGs extremely hydrophilic which cause the tissue to resist the fluid exudation from the tissues. The PGs are trapped by a network of collagen and the small pore spaces created by this network combined with the incompressibility of water allow cartilage to resist instantaneous compressive forces due the fluid pressurization [69]. A diagram of PGs inside a collagen network is shown in Figure 3 below. Secondly, collagen retains highly negatively charged GAGs creating a high osmotic swelling pressure responsible for up to 50% of cartilage's compressive modulus [69]. Finally, the fixed charge density is also responsible for electrokinetic effects such as streaming potential, as a pressure gradient is applied to the charged tissue an electric potential develops. These electro-kinetic phenomenon can have significant influence on cartilage behavior from the diffusion of nutrients within the tissue to cell signaling based on physicochemical signals at the cellular level [94-101].

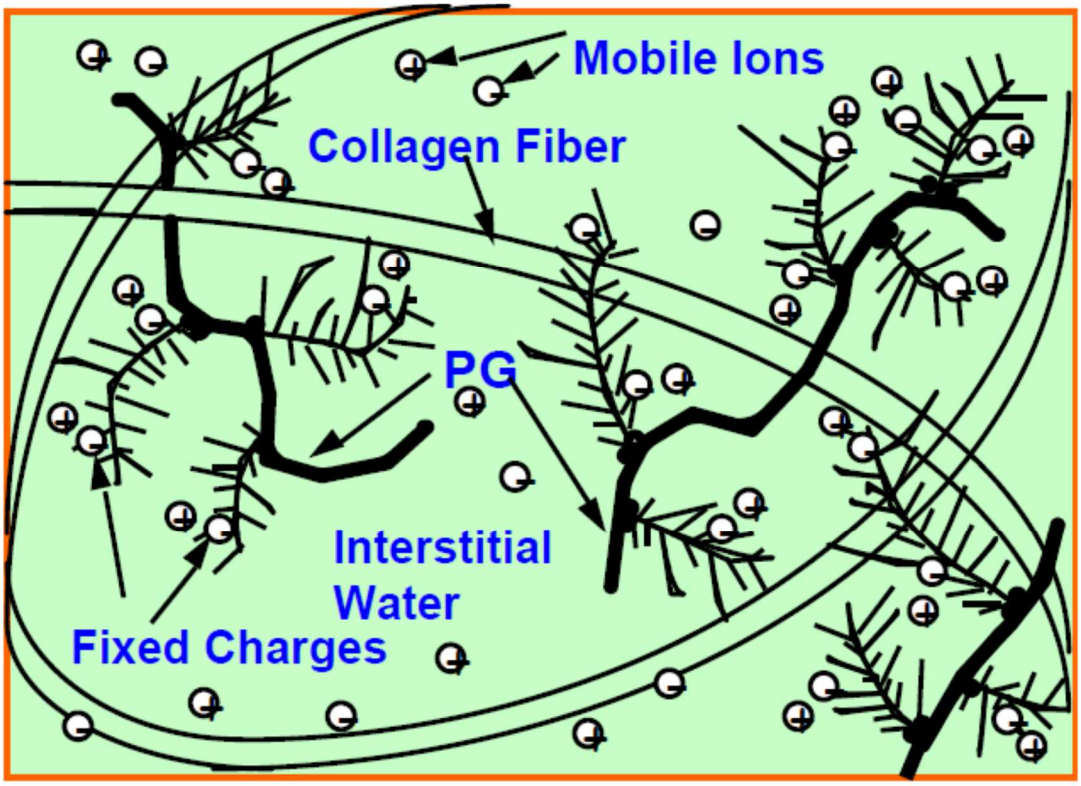

Figure 3 A diagram of proteoglycans with fixed negative charges inside a collagen network [69].

In porcine TMJ discs, GAGs have been found to comprise 5.3±1.2% of the total dry weight and only 1.5±0.3% of the wet weight [27]. In many other studies, the typical average GAG content was at, or below, 5% [27, 57, 75, 102, 103]. In our own human study using TMJ discs in compression, GAG content was ~3.2% by dry weight.

The primary GAG in the porcine TMJ disc was chondroitin sulfate which represented 74% of the GAG content in the disc, followed by dermatan sulfate, keratan sulfate and hyaluronic acid [27]. Other studies have found chondroitin sulfate and dermatan sulfate amounts between 75-93% [27, 80, 102, 103]. These research studies have found the GAG content in the TMJ disc to be much lower than reports of GAG

content in hyaline cartilage [3]. The low GAG content in the TMJ disc may indicate the disc plays a much less significant role in compressive loading and may have a distinct mechanical role from other types of cartilages that rely on a high PG content and high fixed charge density [49, 57, 104]. Kalpakci et al. has conducted a GAG, collagen type I and DNA for cell count comparison between species shown in Figure 4.

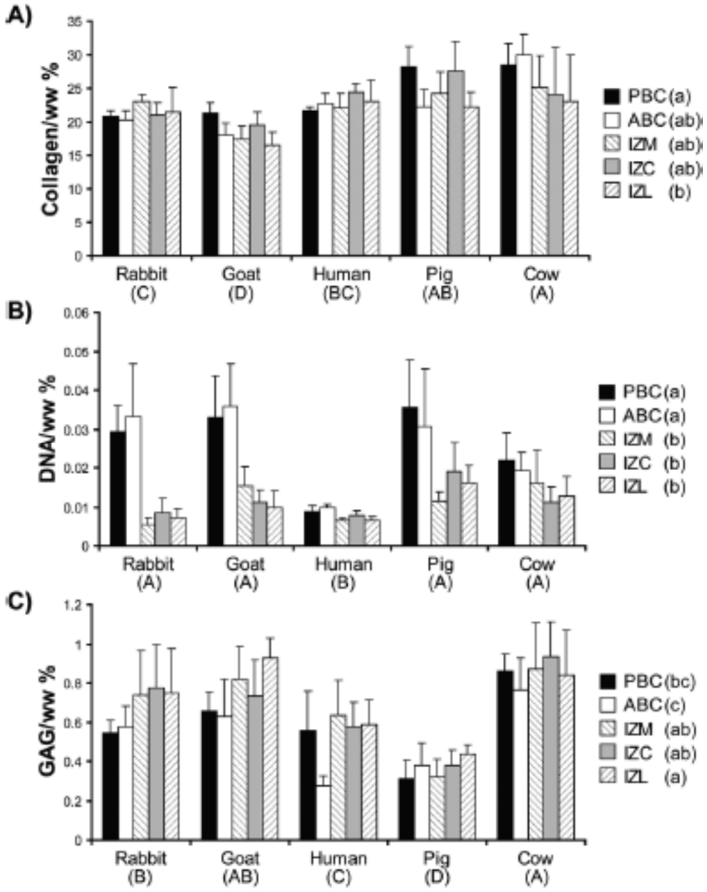

Figure 4 Biochemistry comparison of the TMJ disc between species
A comparison of biochemistry from different species by Kalpakci et al. Collagen compared is type I. Regional comparison within species noted by: PBC-Posterior Region, ABC-Anterior Region, IZM- Medial Region, IZC-Intermediated Region, and IZL-Lateral Region [141].

Water content

Water content is the major component in cartilage as well as the TMJ disc. Water content is also considered a significant mechanical component of cartilaginous tissues, affecting the diffusivity of the tissue and the compressive strength as water exudes from the tissue. Water content has also been used as a marker for tissue degeneration as proteoglycans and collagens are cleaved during enzymatic degradation resulting in loss of matrix retention and tissue swelling [69, 80].

The average water content found in human TMJ discs from our studies were between 76-80% involving subjects with an average age of 78 years [62]. In previous studies using porcine tissues, the water content value was somewhat lower around 71±2%. This could be due to the water content increasing with age. Regional differences were found in the porcine study; however, they were not found in our human studies [27].

2.3 Temporomandibular Joint Disorder

Temporomandibular Joint Disorders is a broad term used to describe a group of over 20 pathological conditions and collectively represents the most common type of chronic orofacial pain. Symptoms include orofacial pain, muscle pain in the head and neck, periauricular pain, clicking and locking of the jaw with limited jaw opening [2]. In the US population, five percent of adults were reported to suffer from TMD like pain, with 6% women and 3% men. In 2011, the NIDCR released the results of the first ever prospective study, Orofacial Pain: Prospective Evaluation and Risk Assessment

(OPPERA), which began in 2005 and sought to elucidate the associations and risks for progression of TMD [9-13].

Risk Factors and OPPERA Study

The OPPERA study found that psychosocial factors lead to an increased risk in developing TMDs, such as higher levels of psychological distress, and greater levels of perceived stress and catastrophizing, along with somatic awareness and greater levels of preexisting pain sensitivity [9, 10]. Pain amplification was the most significant indicator for increased risk of development and progression of chronic TMD pain [11]. Pain amplification refers to changes in the peripheral and central nervous system which cause increased perception and response to nociceptive stimuli. The response could be generated by genetic predisposition or it can be developed as a neurological response to biological processes or environmental stimuli. In the most conclusive finding in the prospective study, patients with a preexisting chronic pain condition, for example fibromyalgia and low back pain, were most likely to develop chronic TMD pain [9]. The study further reported that there were clear indications that genetics did play a role in the development of TMDs as several genes were identified as potential markers of risk for TMD [13]. Of the population sampled, the gender disparity confirmed previous levels as women to men ratio was 3:1; however, socioeconomic status was not a significant factor in the development of TMD. Race was indicated as a factor with Caucasians having an increased odds ratio for development as compared to African Americans. Finally, age did have an effect on the increased risk of development. The sampled age group was

from 18-44 years of age, with an increased risk of development highest amongst the 36-44 age group [12].

Gender Differences

TMJ disorders are primarily found in female patients between the ages of 20 and 40 years of age [8, 105]. This discrepancy in treatment by gender is believed to be attributed to hormonal differences because these symptoms primarily appear during childbearing ages in females. While the mechanistic role of hormones remains to be elucidated, many studies have indicated that estrogen and progesterone could act on the nervous system to enhance nociceptive processing. In one rat study, estrogen appears to increase the number of localized nociceptors and also enhance signaling of those receptors in parts of the hippocampus [106].

Studies have been conducted to determine effects of hormones on connective tissues such as cartilage [7, 105]. These hormones have been found to have a significant effect on differentiation and metabolism. In a study on female rats, collagen was produced at significantly lower levels than male controls but when the females were ovariectomized the differences were removed [107]. This may indicate significant differences in biochemical composition and thus affect biomechanical properties providing the rationale to investigate both male and female tissue in our biomechanical studies.

In our electrical conductivity study on male and female TMJ discs, we found differences in conductivity and porosity between male and female tissues and these differences were magnified by mechanical loading [62]. At the present time, the exact

pathways and specific receptors responsible for the gender paradox are unknown. However, studies have demonstrated clinically and experimentally that gender differences exist, indicating the need for further research to examine fundamental differences in tissue composition and structure along with comparing male and female tissue response to hormones such as 17β estradiol [51].

Mechanical Dysfunction

Studies have indicated that changing biomechanical stresses can cause TMJ disc tissue to quickly adapt to maintain efficiency of the joint. Studies have shown that the TMJ disc requires normal physiological loading to maintain tissue growth and function, while excessive hydrostatic stresses result in enzymatic degradation of ECM and apoptosis [108]. These stresses damage cartilage tissue resulting in the production and accumulation of free radicals [21, 109, 110]. Free radicals are produced by degenerative cell responses that reduce oxygen in situ resulting in reactive oxygen species. Reactive oxidative species such as superoxide, hydrogen peroxide and hydroyl radicals can result in ECM and cell damage [21, 109, 111]. The appearance of free radicals has been observed during normal masticatory function as well as during abnormal movements such as clenching [21]. An example of free radical damage to the TMJ synovial joint cavity is illustrated by increased articular pressure as a result of inflammation which induces localized hypoxia. Hypoxic conditions arise due to the upset of balance of pressure between synovial capsule chamber and the capillary perfusion pressure [54]. Temporary hypoxia leads to the free radical production. The reduction environment cleaves hyaluronan chains in hyaluronic acid leading to the degradation of synovial fluid

[54, 112]. The fluid becomes ineffective, increasing joint friction and in-turn causing accelerated joint degradation.

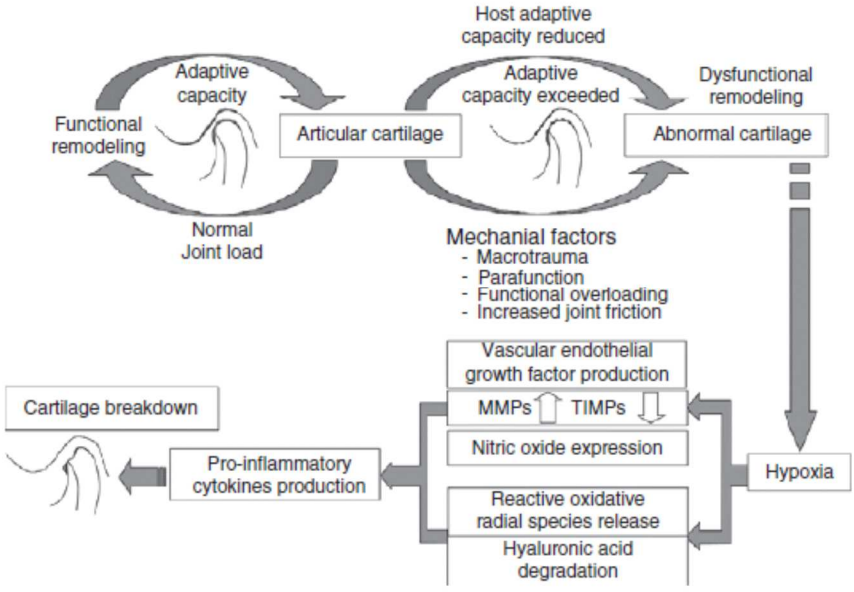

Figure 5 Possible effects of mechanical dysfunction in the TMJ disc
Abnormal mechanical loading leading to TM Joint dysfunction and tissue degradation [112].

These factors are usually concomitant with increasing joint load. Inflammation occurs as a response to the localized hypoxia and reduction to available nutrients. The result of inflammation causes the release of pro-inflammatory cytokines upregulating MMP9, specifically interleukins (IL- 1, 3, 6, 8, 12, and 17), along with tumor necrosis factor-α (TNF-α) [112].

Another possible cause of TMD is the loss of physiological nutrition transport within the disc. The living cells of the TMJ disc require nutrients to maintain growth and development and waste products must be removed to keep the environment from becoming toxic. Since the TMJ disc is avascular, solutes must be transported passively

via diffusion to all of the cells. Studies have shown that sustained loading decreases the rate of diffusion and transport properties of the cartilage significantly, thus decreasing the nutrient levels deep within the tissue. Increasing joint load causes decreased diffusivity of oxygen and glucose into the joint, leading to a further degenerative state. The local pH can also significantly drop as lactic acid builds up and the cells begin to die at low nutrient levels (i.e. oxygen and glucose) within 24 hours [113].

Changes in the tissue as a result of inflammation or response to mechanical dysfunction over time can result in degeneration of the disc. With degeneration, the mechanical properties of the tissue are affected altering the physiological function of the TMJ disc. The TMJ disc becomes displaced and no longer travels in smooth congruent motion protecting the condyle and fossa [37]. As disc displacement or disc derangement worsens, the disc can limit the jaw's range of motion and in some cases block the jaw from opening or closing (known as derangement without reduction) [48]. Disc displacement and derangement are common events for patients who seek treatment for TMDs [15].

Disc Displacement and Other Derangement

In patients who seek treatment for TMDs, disc displacement is present in nearly 70% of cases [5]. This emphasizes the importance of the TMJ disc's biomechanical role in TMDs. The disc exhibits a highly biconcave shape in humans and appears to exhibit some anisotropy based on regions within the tissue. The TMJ disc translates with the condyle during function because it is supported by an anterior attachment to the lateral pterygoid and anterior insertion into the condyle and a posterior attachment to the

retrodiscal tissue [114]. During opening and closing of the jaw the disc translates anteriorly with the condyle [2]. The translation requires the disc to support tension as it is stretched anteriorly and posteriorly over the condyle during motion. Alterations in normal TMJ disc translation can cause pathological loadings resulting in damage to the disc and surrounding boney surfaces. One of the first symptoms of disc displacement is clicking and popping in the joint when the mouth is opened and closed. This is caused by the disc being displaced anteriorly or posteriorly until the discal attachments force the disc back into normal position over the condyle. The joint is said to be *reduced* or restored to normal position, clinically know as disc displacement *with reduction*. If the disc is displaced anteriorly or posteriorly and prevents the joint from opening or closing without moving into normal position, the symptom is disc displacement *without reduction* [48]. Disc displacement has been found to create high stress distributions and increase friction between articular surfaces resulting in osteoarthritis in patients with internal disc derangement [29, 42, 43, 115].

TMDs are generally classified by stages of TMJ disc displacement and derangement. In early stage TMDs, the TMJ disc appears healthy but mild displacement is present indicated by possible clicking. In the intermediate stage, pain is more prevalent and the disc begins to show signs of deformation through MRI/x-rays. This can lead to progressive development of joint locking and hardening of disc tissue. In late intermediate stage progression, more pain is present accompanied by severe joint dysfunction, including locking and morphologic changes in bone structure and

surrounding tissues. In late stage progression, severe pathology of TMJ disc tissues and surrounding bone along with severe loss of joint function is present [45, 46].

Treatments

Current practice uses medications in 90% of TMD related disorders. Commonly used agents are corticosteroids, muscle relaxants, antioxidants, opiates and anti-inflammatory drugs. The effectiveness of the prescribed medications has come under considerable debate due to their ability to treat the symptoms and not the underlying mechanism of pathophysiology [116]. In the meantime, even though considerable progress has been made toward discoveries on the molecular mechanism of TMJ disorder, decisive treatments and delivery methods have been extremely complex in dealing with the individual patient. One of the main reasons for lack of empirical evidence in support of drugs is the lack of randomized clinical studies [116].

The majority of TMD patients can be successfully treated by non-surgical therapies and surgical interventions may be required for only a small portion of the TMD population. Some of the ways that patients can personally alleviate pain and keep symptoms from worsening are performing jaw exercises, avoiding extreme or rapid movements, applying hot and cold compresses to the region, and eating soft foods [2]. Patients may also be given splint devices to fit over the teeth to prevent the effects of clenching and grinding. Grinding of the teeth or bruxism is believed to cause TMD through tooth erosion, muscular strain, and inflammation of the tissue within the joint space [36]. Splints are therefore prescribed in the hopes of controlling the consequences of bruxism and slowing the onset of TMDs [117, 118].

Surgical repair covers a range of invasive from arthrocentesis and arthroscopy, to finally total joint replacement, arthroplasty, if minimally invasive treatments fail. Arthrocentesis has become a very popular choice among surgical interventions due to the minimal invasiveness of the procedure, time of operation of one hour, and its cost effectiveness.

Arthrocentesis

Arthrocentesis is prescribed for acute TMJ disorder, including internal derangement, OA, chronic closed lock and open lock, synovitis, rheumatoid arthritis and adhesions [119]. Arthrocentesis is an office outpatient procedure taking less than 1 hour with treatment and recovery (the procedure is performed with intra-venous deep sedation). Two 18 gauge needles are atraumatically inserted in the superior joint space and the space is insufflated and irrigated with 150-300cc of lactated ringer's solution, washing out inflammatory mediators and relieving pain. An inlet and outlet is required for this process to irrigate the joint space removing boney/cellular particles causing inflammation and inflammatory mediators. The mandible is manipulated to ensure return of maximum opening. A steroid (Dexamethasone 6mg) and local anesthetic (Marcaine .5% with epinephrine 1:200,0001cc) are administered by flushing through the inflow/outflow needle ports. Finally, a sodium hyaluronate is applied through injection which replaces synovial fluid that was previously washed from the joint. The sodium hyaluronate aids in the lubrication of the joint and also reduces inflammation and pain [119-121].

Nitzan et al. first documented treatment of TMJ dysfunction using arthrocentesis in 1991 [119]. Since then numerous clinical treatments have been carried out. Treatment success has been evaluated by visual analog scale (VAS) pain scales and a comparison of jaw mobility after surgery measured by maximal interincisal opening (MIO) [121]. Arthrocentisis have been shown to improve immediate symptoms of TMDs such as pain relief, however the long-term effects are debatable. This is often a reoccurring follow-up procedure, with temporary relief of pain which seems to restore joint function but could be causing damage to the TMJ tissues further since the symptoms are masked but the underlying causes are still present.

Arthroscopy

During arthroscopy, a small incision (6.35 mm) is made anterior to the ear and an athroscope is inserted into the superior joint space. The arthroscope allows the oral surgeon to inspect the tissue, remove damaged tissue, and realign the disc and condyle if necessary. The arthroscope is connected to a video screen. The surgeon can then examine the joint, remove pathologic tissue, or position the disc back normal position through the use of anchors (see Mitek anchor in the next section). [36]. Afterwards, the disc is lavaged with saline and treated with drugs described above in the same way as athrocentesis.

With arthroscopy, a larger incision is required for the scope, disc inspection, and attachment. Athrocentesis requires less than 1 hour in the operating room, while arthroscopy can take longer given the procedures of inspecting the superior joint compartment. Success of the procedure is highly dependent on the concise placement of

the lavage needles and how well the inflammatory mediators can be removed in the process [119].

Success rates for arthroscopy have been reported between 79%-91% compared to success rates for arthrocentisis of 75%-91.8% [121]. A 6 to 30 month follow-up study of arthrocentisis with lavage indicated that only 1 out of the 46 patients did not report a significant improvement in pain, function, and maximum interincisal opening. While the results for the improvement of pain and jaw range of motion are generally accepted, questions on the sustainable restoration of TMJ tissue and sounding joint cavity tissue remain. The controversy lies in the follow-up after treatment. Over the long term, successful outcomes for pathologies such as disc degeneration are highly debatable and the question remains if the treatment simply relieves pain or if it accelerates disc degeneration.

Mitek Anchor

To help treat anterior disc displacement, common in TMDs, physicians implant a device called the Mitek mini anchor into the bone of the condyle [122, 123]. The device is a small titanium anchor with nitinol wings that expand when reaching medullary bone. Once the anchor is set in the condyle, the sutures insert into the posterior band to secure the disc. The Mitek anchor has been reported to have success rates of up to 90%. The anchor has shown favorable osseointegration and biocompativility through a 59 month follow-up. The Mitek anchor offers many advantages. It is applied minimally invasively through arthroscopy, it provides occlusal stability by anchoring the anterior portion of the

TMJ disc which is usually displaced, and it has been shown to reduce pain and improve joint function. [122, 124].

Joint Replacements

TMJ implants have had a history of recalls and complications due to the complex loading environment's effect on the implant. Evidence for recalls has come mainly from the immune reaction from wear debris. The investigation of biochemical, biomechanical, and degeneration studies were launched due in large part to the previous failure in TMJ implants.

The Christensen implant was in effect since the 1960's. The implant was comprised of a cobalt-chrome alloy for fossa and condyle head, with a molded polymethylmethylacrilate (PMMA) head on the alloy framework. For total TMJ joint replacement, the procedure creates metal wear debris. Patients developed metallosis, causing an increase in stress concentration at the fossa implant site, and resulted in hypersensitivity in the joint. In July 1993, the FDA halted use of implants made before the 1976 medical device law due to safety concerns and lack of supporting information demonstrating efficacy of those implants.

Techmedica developed a TMJ total joint prosthesis in 1989. A 5-year follow-up study was performed in 1993 at the request of the FDA. The study found a 90% success rate for occlusal and skeletal stability and an 89% reduction in pain. The product was re-admitted for approval in 1997. The fossa component of the device is made from pure titanium mesh with an articular surface of ultra-high-weight-polyethylene. The condyle component is made from medical grade titanium alloy with a head of cobalt-chromium

molybdenum alloy. Fit for the device is determined by CT imaging that generates a stereolithographic plastic model of the patient's jaw and condyle that is anatomically exact. Only four TMJ implants have been approved by the FDA since Dec. 30, 1998.

The Vitek Implant: A Need to Understand TMJ disc biomechanics.

The Vitek Proplast TMJ implant was recalled by the FDA in January 1991. A chemical engineer named Dr. Charles Homsy developed a soft Proplast material of silicon embedded in a wire mesh to reconstruct the glenoid fossa of the temporal bone. A Teflon disc, from DuPont, was reinforced with graphite and used between the condyle and fossa. The porous Proplast was believed to adhere to superior joint surfaces of the glenoid fossa combined with Teflon's ability to facilitate movement and withstand wear [125].

Vitek notified the FDA of plans to market the "interpositional implant" (IPA) in March 1983. Proplast had been used favorably to stabilize the femoral head and acetabulum in hip prosthesis. In turn Vitek sought 510 Premarket Notification citing substantial equivalence to existing silicon sheeting devices. To justify safety of the device, Vitek cited the "scarcity of probative scientific material" and cited Homsy's own research in related dental applications which were not related to the TMJ disc. When questioned about the Teflon fragmentation that had been discovered with hip implants, the team claimed the TM joint was "largely non-load bearing" [52, 125].

Oral surgeons began implanting the device in 1984. By 1986 a large patient group across North America was suffering. The surgical community was slow to report surgical failures and follow-up symptoms. Emphasis was placed on conservative

recovery of soft foods and the historical difficulty of recovery for this joint was cited. But during this time, a much deeper understanding of the problem emerged. MRI's showed inflammation of surrounding tissues and fragmentation of the implants. Emergency surgeries were conducted which found Giant cell reactions in response to wear particles. These were found throughout the joint and migrated to local lymph nodes [2, 52, 125].

In 1988, news of implant failure had reached the FDA. Vitek issued a voluntary safety alert under FDA guidance. In January of 1991, the FDA ordered a recall of all Vitek implants. During the recall the FDA issued a statement that failure of the prosthesis was mainly due to the lack of understanding TMJ disorders, specifically TMJ joint mechanics, and tissue function. It concluded that a prosthetic designed without clear understanding of the working joint would inevitably fail [52, 123, 125].

In total, over 26,000 implants were administered between 1984 and 1991, mostly in women. Often emergency surgeries were conducted to remove the implants to resolve immune response from implant fragmentation and wear debris. As many as six surgeries were required in some cases to rebuild the mandible and craniofacial tissues affected by Giant cell reactions, which resulted in chronic limited jaw opening. Patients reported loss of eyesight, itching and burning during chewing, tiredness and debilitating pain in the craniofacial region [52, 123, 125]. As a result of the delay between first reports of implant failure and FDA recall, new laws and regulations were enacted such as the Medical Device Reporting Regulations (1984) and Safe Medical Device Act (1990).

TMJ Disc Mechanical Properties

Mandibular Condyle Cartilage Mechanical Properties

The articular cartilage of the mandible condyle and glenoid fossa are primarily fibrocartilage with mainly type I collagen, unlike the articular cartilage of the knee which is hyaline cartilage and type II collagen. The fluid phase consists of water and dissolved electrolytes, which is over 80% of the tissue by volume. The intrinsic stiffness measured signified by the compressive modulus depends on Donnan swelling pressure generated by the fixed charged density (i.e. proteoglycan (PG) concentration) and the solid mesh. In hyaline cartilage the apparent stiffness is given as 30-50% by the Donnon swelling pressure [69].

To examine the mandibular condyle cartilage mechanical properties, a microindentation test was performed by Singh et al. 2009 [28]. The tests were completed under two conditions, an isotonic (0.15M PBS) condition that measured apparent compressive modulus (matrix solid and Donnan pressure) and intrinsic compressive modulus under hypertonic conditions (2.0M) that measured only the compressive modulus of the solid matrix. The mechanical response from the tissue in two different ionic concentrations was analyzed by curve fitting the load response. The two curves were used to determine the contribution of the solid phase versus the ion/fluid phase of the cartilage. The apparent aggregate, shear modulus and permeability were on average about 20% higher than the intrinsic mechanical properties. This indicates that although significant, the apparent mechanical properties are less dependent on the PG content than the solid matrix. In other joints, such as the knee joint with significant amounts of PG in

the hyaline cartilage, obtain as much as 30-50% of their mechanical compressive modulus from Donnan osmotic pressure resulting from PG content.

TMJ Disc Mechanical Properties

The TMJ disc experiences a complex range of forces under normal physiologic conditions such as mastication. These forces can be compression, tension and shear. Cells respond by producing matrix proteins and growth factors for the synthesis of collagen and aggrecan, along with maintaining cell phenotype and proliferation in response to mechanical loading. Intermittent mechanical loading within the physiologic range has been shown to maintain homeostasis of TMJ cartilage, while high sustained stress may introduce catabolic changes [37, 56, 69]. It is generally believed that a breakdown in this interrelated balance between mechanical loading and tissue homeostasis causes a cascade of biological signaling processes that could lead to degeneration of the disc [50].

The transfer of energy through a biologic material depends on the primary structure and function of the tissue [25, 37, 50]. In the case of the fibrocartilaginous TMJ disc, the collagen fibers primarily absorb tensile loads, such as stretching, while compressive loads are absorbed by fluid flow through the disc. The resistance of fluid flow increases significantly as the disc is compressed, since the porosity is significantly reduced under mechanical load. These properties are strain dependent. The physiological level of strain varies between tissues; some examples include skin at 40%, tendons at 2-5%, and around 4% for canine TMJ discs [56, 126].

Cartilaginous tissues are generally characterized as viscoelastic materials in which load response is dependent on load rate and load response changes with respect to time. The mechanical load response is usually highly related to fluid flow within the tissue, known as the viscous response. This is modeled as a dash pot in phenomenological models as the material supplies viscous stresses in response to loading. Also, collagen crimping and elastin levels give the tissue the elastic properties. Together the viscous and elastic response is highly rate dependent. Therefore, in order to compare tissue mechanical properties, the load rate and test protocol must be given consideration [69].

Mechanical tests on viscoelastic materials are rarely load-to-failure or dynamic load-to-failure tests, since maximum stress would be dictated by load rate. Instead, viscoelastic tests seek to characterize the material under different load rates or strain rates. These tests involve stress-relaxation, creep, or recovery experiments which provide information on the mechanical properties of load rate. Often a series of load rates are used or a series of increasing strains are used with a measured load response within the tissue. The load response characteristics are measured from the tissue and indicate how well the tissue absorbs stress and dissipates energy [37].

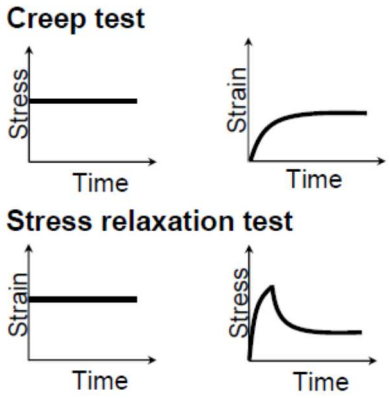

Figure 6 Example plots of creep test and stress relaxation test
In the creep test, stress is held constant while stain varies with respect to time, requiring displacement. While in the stress relaxation test, strain is held constant and the stress reaction is recorded with respect to time. The stress relaxation test was chosen in this dissertation to model the tensile properties of the human TMJ disc [22].

In a stress-relaxation test, the material is loaded by applying a set strain or set displacement which deforms the material invoking a stress response, see Figure 6 above. This stress response dissipates over time until a steady state level is achieved. The load response is measured over the time the material reaches steady state. The relaxation modulus is obtained by dividing the stress at steady state with the relaxation time. In a creep test, an instantaneous stress is applied to the material and kept constant while time-dependent strain levels are recorded. The response of the tissue is measured by strain, until the strain level becomes constant, reaching steady state. Finally, general recovery tests involve applying a load, then characterizing the response of the material after loading is removed. Numerous models for the behavior of TMJ discs have been proposed by assuming the material to be linearly elastic, but the time-dependent response

of cartilage suggests that more complicated constitutive models are required [53, 70, 127, 128].

Tensile

Since the tissue is a viscoelastic material, strain rate is highly correlated with stress response; therefore, the strain rate needs to match physiologic level simulated *in vivo*. In the case of the TMJ disc, finite element models have determined physiologic strain levels range from 0-30%, as most tissue tests use this as range for testing. This measures the energy absorptive capacity of the viscoelastic material which is more physiologically relevant, since the tissue operates underneath these conditions during everyday use.

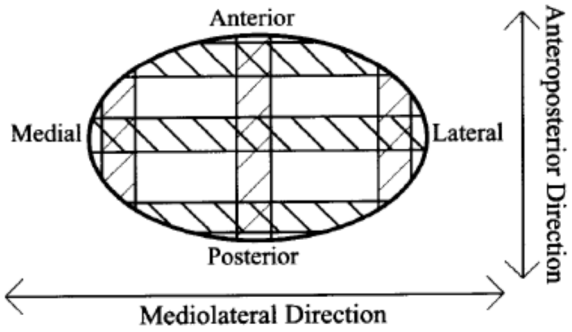

Figure 7 TMJ disc with anteroposterior and mediolateral sample orientations for tensile test
The TMJ disc is labeled with anteroposterior and mediolateral strips used for tensile tests. Note the diagram shows the orientation as an overlay, since in one TMJ disc samples can be extracted in *either* anteroposterior or mediolateral orientation [1].

During normal joint function, as the condyle translates anteriorly, the disc stretches anterior-posteriorly across the head of the condyle to protect articulating surfaces. Due to

the anisotropic range of forces the disc undergoes, the disc has adapted highly regional anisotropic material properties. As a result, the testing direction has a significant impact on tensile properties of the TMJ disc (see Figure 7 above for directional orientation). To illustrate, the porcine tensile modulus in the intermediate zone was found to be 37.4 MPa in the anteroposterior direction and 1.6 MPa in the mediolateral direction [129]. Further, in comparing the anterior, intermediate, and posterior zones, the canine central zone was found to have an ultimate tensile modulus of 14.7 MPa compared to the anterior (46.7 MPa) and posterior (69.7 MPa) zones [126]. The general overall trend is the anteriorposterior direction has a higher tensile modulus than the mediolateral direction. However, studies have produced results that vary greatly between species. This has been attributed to biologic variation as well as differences in models chosen to analyze material response. Many review papers have cited the need for consistent protocols to establish the mechanical properties of human TMJ disc tissue.

The anisotropic properties were gathered from creep and relaxation stress tests. A good example is supplied by Tanaka et al. 2002 using a creep test to evaluate the influence of creep duration on residual stress in bovine TMJ disc tissue in the mediolateral direction [130]. A 1.5 MPa stress was applied to the specimen for 20 minutes and the tissue response was measured for 20 minutes. The creep test showed a dramatic increase in stress within the first 5 seconds tapering to a constant stress at the 3 minute mark. A Burger's model was used to fit the stress relaxation curve. The model consisted of Maxwell model that accounted for residual strain after load removal and several Voight models to characterize creep features. The findings indicated that the disc

is able to absorb a significant amount of energy within the first 5 seconds of tensile loading, similar to that found in compression. This would indicate that the articular disc is responsible for absorbing joint forces and changing shape in-order to dissipate energy within the joint. Without this residual stress absorption, a stress concentration could occur to the surrounding surfaces of the mandible condyle and fossa of the temporal bone that would result in catabolic changes of injury.

M. Beek et al. 2001 analyzed human TMJ discs using dynamic indentation on the anterior, intermediate, and poster regions [32]. The study found the intermediate region to be 2 to 3 times stiffer, withstanding a significant amount more energy dissipation than the anterior and posterior regions. These findings may indicate the disc's ability to transfer stress from the stiffer intermediate region through hydrostatic pressure and into the anterior and posterior regions. In the process the disc can deform, increasing contact area that would decrease the stress concentration in the joint. The findings are in agreement with histological data that indicate a higher proteoglycan concentration along the intermediate region of the disc along with a greater collagen density found by Mills et. al 1994 [75]. The collagen alignment along the interior region in the anterior posterior direction would direct fluid flow to the peripheral anterior poster bands, which have a mediolateral alignment. In the process, proteoglycans would be trapped in the collage matrix further reducing fluid flow [37]. This accounts for high energy dissipation upon impact and the slow recovery after loading.

Compression

One of the original investigations into the viscoelastic properties of the TMJ disc was demonstrated on human TMJ discs under unconfined compression tests at two different load rates. The study concluded that the material did exhibit viscoelastic response under compression by finding two different compression moduli corresponding to two different load rates [131].

Additionally, several other studies assessed the regional dependency on compressive properties. Allen et al. investigated the five disc regions, as well as the superior and inferior surfaces of the disc using an unconfined compression incremental stress relaxation test [132]. The instantaneous modulus (500 kPa) was higher than the relaxed modulus (80 kPa) for combined samples, while regional differences in stiffness were found across the disc's surface regions. [132] The compressive moduli were significantly lower (100-1000 times) than the tensile moduli found in Detamore et al. 2003 porcine tensile study [24, 132]. The intermediate and medial regions of the disc had the highest relaxation modulus, while the anterior and posterior portion of the disc had the highest instantaneous modulus. Surface differences were only found in the relaxed modulus, where the inferior surface was more resistant to compressive forces than the superior surface [132]. Further studies also confirmed regional differences in compressive moduli [32, 133]

Along with finding regional variation of compressive moduli within the disc, studies have found a marked difference in compressive properties depending on how the compressive load was applied. This would indicate significant material reactions at work

and gives insight as to how the disc functions under physiologic loading. Increasing frequency of dynamic compressive load caused the disc to become stiffer [31, 134]. After preconditioning, repeatable stress strain curves were reached with clear hysteresis under low strains. This would indicate, under physiologic conditions, that hydrostatic pressure may be responsible for significant load dissipation within the joint, without significant dependency of the collagen network. Upon significant cyclic loading, the disc cannot keep the same levels of fluid pressurization and after several cycles at high strains, the relaxed compressive modulus was 1/2 to $1/7^{th}$ that of the original instantaneous modulus [134].

The general finding in regional differences was the central region possessed a greater dynamic compressive modulus and more rapidly dissipating energy than other regions. This trend has been correlated to motion studies and finite element models that predict that the central region, specifically the intermediate region experiences the greatest amount of compressive forces from the mandible condyle during normal joint movement [39, 104]. Biochemical analysis by region has confirmed the greatest levels of proteoglycans and few observed chondrocytes in the intermediate region. Finally, Willard et al. 2012 compared control regional samples to samples with GAG depleted through Chondroitinase ABS. The study found through unconfined compression stress relaxation tests that only the intermediate region had compressive moduli affected through the removal of GAGs. This would indicate not only a significant level of GAG present in the intermediate region but compressive moduli in the region dependent on

GAG to dissipate compressive forces. The particular mechanism of biphasic action is more similar to other types of cartilage such as hyaline in articular cartilage.

Shear

Shear forces in the TMJ disc are believed to be caused by incongruent articular surfaces acting on the disc during compressive loading. In addition, the disc is bioconcave with anisotropic material properties which could cause further non-uniform compressive loads across the disc, resulting in shear. Shear stresses are believed to cause mechanical injury such as fatigue and perforations along the disc [34, 135]. The shear modulus of the disc was found to be dependent on frequency and direction of the shear load [31]. Further studies revealed dynamic shear modulus increased with dynamic frequency which could indicate the shear properties of the disc are dependent on interstitial fluid flow (i.e. fluid exudation from the disc could increase shear stiffness).

The relationship of shear with compression in the disc is consistent with results found in bovine meniscus and articular cartilage [135, 136]. This correlation may be a result of fluid pressurization during compression that decreases the size of the pores in the ECM and decreases the permeability of fluid effectively stiffening the material to shear forces [137].

In studies in articular cartilage, shear stress has been found to cause mechanical injury such as fatigue with damage being irreparable [34, 136]. Injury to the disc as a result of shear stresses has been modeled extensively in finite element models of the TMJ disc [33, 38, 73, 74, 115, 138]. These models depend on accurate material properties from biomechanics studies.

Friction and Tractional Forces

The primary lubrication mechanism of the TMJ disc is a boundary layer lubricant, surface-active phospholipids secreted by synovites, fibrochondrocytes and osteoblasts [139]. The surface-active phospholipids bond to articular surfaces through hydrogen bonding on their polar end. The nonpolar moieties face opposite the articulating surface, being hydrophobic create a very low surface energy and much less conductive to surface friction. A lipid solvent applied to articulating surfaces was shown to increase friction 150%. Hyaluronic acid and lubricin are important lubricants also found in the synovial fluid of the inferior and superior joint capsules [139]. Another aspect of lubrication mechanism, particularly in the TMJ disc is the concept of weeping lubrication. A study by Nickel et al. showed a weeping lubrication mechanism was a significant method of joint lubrication, as the disc is compressed, interstitial water is compressed to the boundary of the disc surface for lubrication [140]. The study showed by measuring static friction on the surfaces of discs with a range of thicknesses that weeping lubrication had positive correlation of thickness to joint lubrication. The study also reported that impact loading due to trauma caused surface damage on fresh porcine discs that had a logarithmic effect on surface friction. The *in vivo* implications are that sustained clenching or bruxism may have a significant negative impact on the TMJ disc's ability to maintain lubrication. The results of the disc impact or trauma indicate that the level of impact may introduce surface damage to the disc surfaces that predispose the disc to degenerative changes similar to osteoarthiritis [140].

Large shear and compressive forces were observed in FEM in these regions which correlates well with the TMJ perforation findings in cadaverous tissues [33, 42, 141, 142]. Translational forces applied mediolaterally across the TMJ disc may be one cause of tissue failure because traction forces are applied at the surface where the disc is relatively weak [41]. Traction forces in the TMJ are composed of friction and plowing forces, which result from movement and fluid pressurization due to loading [143]. Studies have shown that plowing forces are approximately 10 times greater than frictional forces [144, 145].

Biomechanical property differences between species

The differences in mechanical properties between species have been noted abundantly within review papers that seek to establish baseline TMJ disc mechanical properties [25, 50, 71]. The rationale for establishing baseline material properties arises from the desire to set design criteria for tissue engineering replacements and reach a consensus on mechanical function.

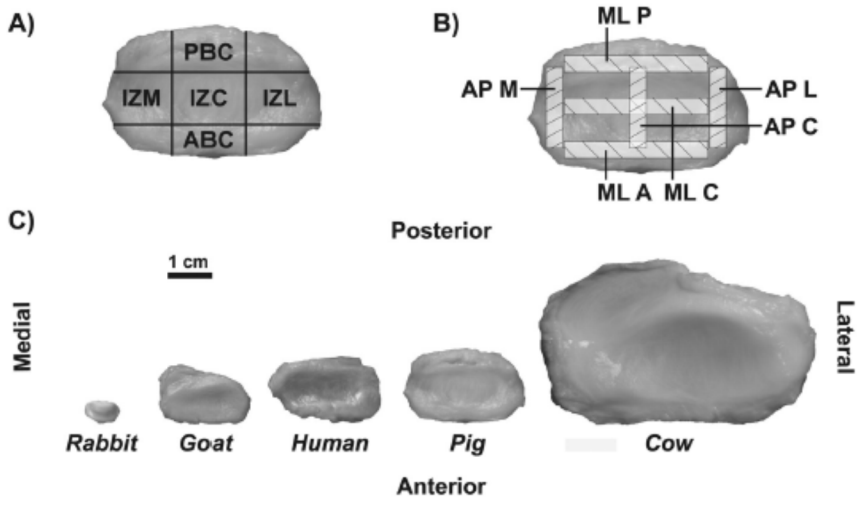

D)

	Rabbit	Goat	Human	Pig	Cow
Average Length M-L Direction (cm)	0.746 ± 0.0298 (D)	2.06 ± 0.121 (C)	2.36 ± 0.0609 (BC)	2.70 ± 0.236 (B)	4.46 ± 0.542 (A)
Average Length A-P Direction (cm)	0.387 ± 0.0264 (d)	0.952 ± 0.0476 (c)	1.40 ± 0.149 (b)	1.39 ± 0.129 (b)	2.35 ± 0.229 (a)

Figure 8 Morphological comparison between species
TMJ discs from different species. Notice the size and biconcavity similarities between the Human and Pig TMJ disc [71].

Establishing these properties has proven difficult due to differences between studies sample load rates, non-uniformity in sample preparation, different regional sampling, different testing protocols in different temperatures, the use of different ages in humans as well as variations in tissue quality. Figure 8 above shows an example of the differences in morphology of the TMJ disc between species. Though differences exist on the level of 10 to 100 fold, they do not entirely account for biological variations. The variation in species qualities have been justified by the structure meets function criterion, with herbivores (cows, goats, and rabbits) exhibiting highest compressive modulus across all disc regions. Animals tested exhibiting different food types, different masticatory patterns for the food quality, as well as the size and morphological development of the

animal. Therefore, each species resulting mechanical property has to be taken into consideration under the testing configuration that produced the results.

The overall elastic moduli for bovine samples were much lower than for human discs (25-65 MPa) which may be due to differences in chewing motion and diet [146]. In tensile tests, the overall strain rates varied from 6mm/min to 500 mm/min. The resulting variance between the porcine group central region had an anteriorposterior modulus of 18.5 MPa (6mm/min strain rate) versus 76.4 MPa (500 min/min). Between species the modulus varied between 14.3 MPa for porcine to 101 MPa for canine for anterioposter modulus, however strain rate varied between species tests. The mediolateral modulus was much lower than the anterioposterior orientation, when tested, regardless of species. In general, information on human TMJ disc was scarce. And in order to properly compare differences between species, such as the most commonly accepted equivalent animal model, the porcine to the human, the tests should be conducted under the same strain load rate, sample extraction, and test protocol.

The compressive properties of other animal models were found to be significantly higher than those of porcine samples. Unconfined compression tests on canine samples were found to have instantaneous modulus values of around 31 MPa while stress relaxation tests on bovine discs yielded an instantaneous modulus of ~15 MPa [128, 147]. Specific differences in protocols such as strain rate, frequency rate, and amplitude have all been found to have a significant impact on the compressive properties of TMJ disc tissue, but it is assumed that most of the variation is due to interspecies differences in disc composition [30, 132, 134, 148]. Regional and topographical variation during

compression has been observed for TMJ discs of several species. In tensile loading, variation between species and region is shown in Figure 9 below. The porcine sample had significantly lower moduli in the lateral region and large instantaneous modulus in the posterior region while these differences were not seen in the bovine model [132, 147, 148]. The general assumption is that the compressive properties vary between the mediolateral and anteroposterior directions, but the exact values and relationship are currently debated in the literature [49].

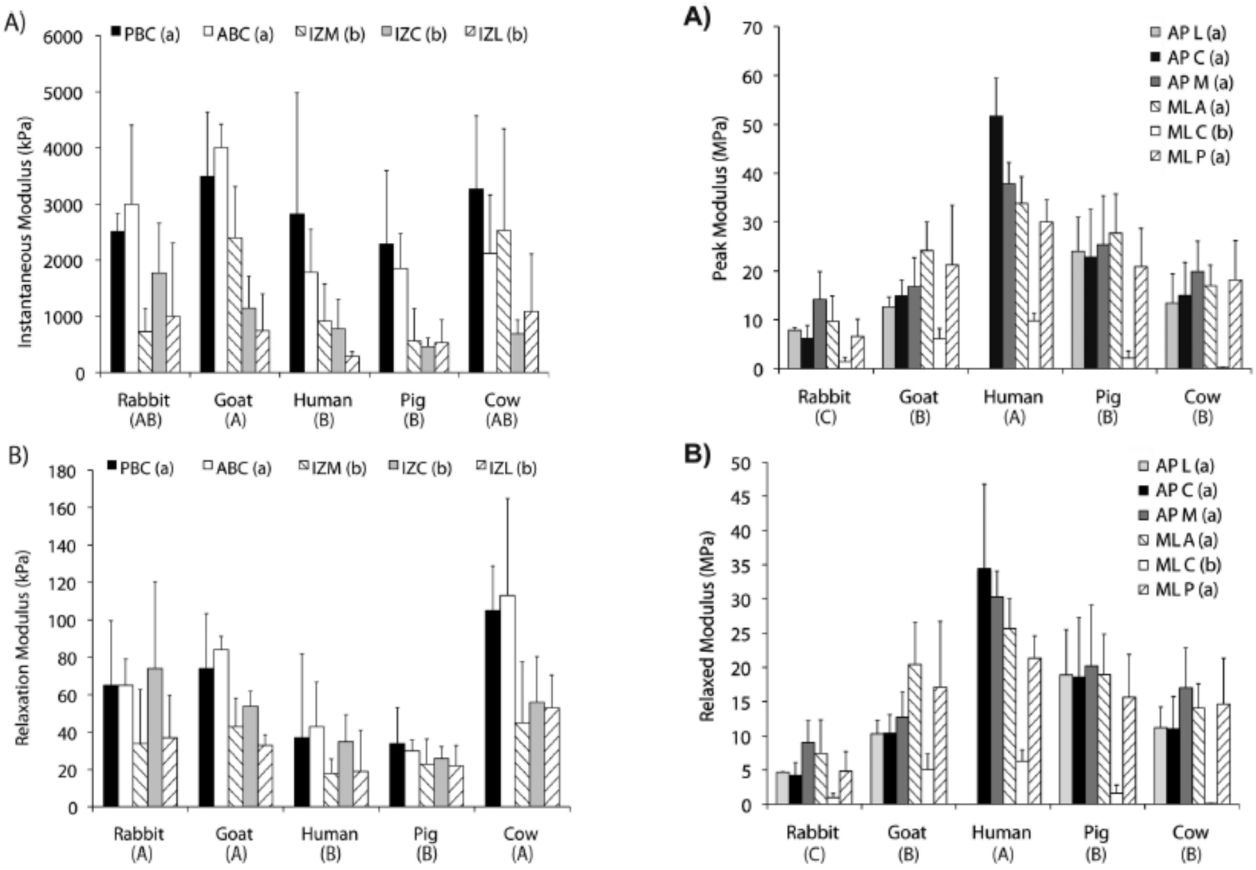

Figure 9 Comparison of the tensile modulus by species
The left figures A&B show a comparison of the tensile modulus by species by Kalapaki et al. The right figures A&B show a comparison of the compressive modulus by species at 20% strain. Regional moduli were

compared with PBC-Posterior Region, ABC-Anterior Region, IZM- Medial Region, IZC-Intermediated Region, and IZL-Lateral Region [141].

2.4 Transport Properties of the TMJ Disc

The nutrient transport in TMJ discs is believed to play a significant role in matrix remodeling. Currently studies from other cartilages must be relied upon like the intervertebral discs (IVD) to draw comparisons and analyze methods of diffusion studies due to the lack of TMJ disc transport properties. The TMJ disc and the IVD are similar in that both are large avascular tissues that require nutrient delivery through diffusion from the nutrient rich environment around the periphery of the tissue. The driving transport mechanism is the diffusive flux driven by high concentrations of nutrients around the periphery of the disc (synovial fluid) to areas of low nutrient concentration in the center of the avascular disc. As nutrients are being transported to the center of the disc, cells consume nutrients at a rate dependent on the concentration of the substrates and pH [149]. For solutes, such as oxygen which is consumed rapidly, a steep concentration gradient may occur that results in low concentrations at the center of the disc (less than 1%) [150, 151]. The concentration gradient can be described as a change in value of a quantity (nutrients/molecules) with a change over a distance. The concentration gradient depends on the diffusivity of the disc, a material property, as well as the consumption rate within the disc. Results from our lab have discovered a high nutrient gradient through the TMJ disc. Our transport study using the electrical conductivity method has found that the TMJ disc has very low diffusivity when compared to other cartilages such as hyaline and IVD [152]. Not only was the diffusivity

low, the material property was negatively affected by mechanical loading. With this understanding, there may exist a steep nutrient concentration gradient within the TMJ disc that is uniquely venerable to pathologic loading. Therefore the transport properties of the disc must be analyzed with the mechanical properties of the disc so that a clear understanding of the nutrient environment may be understood. Since direct measurements are not possible *in vivo*, only *in vit*ro measurements are collected and with the use of modeling techniques such as finite element models we are able to study the unique nutrient environment based on the model.

Diffusion Chamber

The most basic measurement of the diffusivity of solutes within a tissue specimen is through a diffusion chamber. The chamber is designed to hold a tissue specimen between an upstream and downstream well containing different concentrations of solute. The diffusivity is measured by keeping the upstream concentration constant while measuring the concentration change over time in the downstream well. In cartilage, the diffusivity of solutes is very low and the time needed to reach steady state would take days, so more effective techniques have been made available.

Electrical Conductivity

Kuo et al. 2010 investigated porcine TMJ discs by using the electrical conductivity method [61]. The TMJ disc has been found to have a very low proteoglycan content, which would indicate a very low fixed charged density. In the case of uncharged tissues, the diffusivity of small solutes in the tissue is proportional to the electrical

conductivity. Instead of using a concentration gradient to drive the flux of solutes through the tissue, an electric potential was used as the source flux for the small ions of sodium and chloride in PBS. The measurement of electrical conductivity for the sample was based on the 4-wire resistance method. A cylindrical sample (~5mm diameter) was placed in a sealed chamber with PBS. The sample was enclosed by two source cylindrical electrodes on each face of the sample, with coaxial Ag/AgCl sintered wires through the electrodes. The cylindrical electrodes sourced a very low current density while the sensing Ag/AgCl wires measure the voltage drop across the tissue. The resistance (Ω) values across the specimens were measured at a very low, constant current density of 0.015 mA/cm^2. The height of the specimen was measured with an electrical current sensing micrometer. The electrical conductivity (χ) values of the specimens were calculated by:

$$\chi = \frac{h}{\Omega A} \qquad \mathbf{1}$$

where h and A are the height and cross-sectional areas of the specimens, respectively.

The electrical conductivity of the specimen was measured at 0%, 10%, and 20% compression levels. For uncharged tissue in NaCl, the relative diffusivity (D/D_0) of NaCl is simply related to the relative conductivity by (Gu and Yao et al., 2002) [153]:

$$\frac{D}{D_0} = \frac{\chi}{\phi^w \chi_0}$$

2

where D is the mean ion diffusivity of Na^+ and Cl^- in tissue, D_0 is the mean ion diffusivity in the bathing solution, χ is the electrical conductivity of the tissue, and χ_0 is the conductivity of the bathing solution. In our analysis, Na^+ and Cl^- were assumed to carry the electrical current because these ions are the primary ionic components of PBS. The conductivity of porcine TMJ discs and human TMJ discs have been studied using this method [152].

FRAP

Shi et al used fluorescence recovery after photobleaching (FRAP) to measure the TMJ disc diffusivity tensor across regions porcine TMJ discs [58]. FITC dextran was allowed to diffuse into the TMJ disc sample until a uniform concentration was reached (48 hour period). An argon laser (488nm) was used to bleach a fluorescent probe. Images of the fluorescence recovery after photobleaching were collected through a microscope with high speed camera. The frames were then analyzed to reconstruct the recovery profile and calculate the anisotropic diffusivities in two directions for each sample. Results were then analyzed for noise and a comparison was made for diffusivities between regions [58].

Regional Variation, Differences Between Species, and Gender differences

In the electrical conductivity study, the anterior region was found to have a significantly higher diffusivity than the posterior region in porcine TMJ discs. However, no regional differences were detected in human TMJ discs. Using the FRAP method, the anterior region again was found to have a higher diffusivity than the posterior region for porcine TMJ discs. One possible reason regional differences were detected in the porcine and not in human disc, could be related to the age of the sample. Samples were tested from relatively young adult pigs (8-10 months) and relatively older human subjects (76-92 years) due to the availability of samples. Previous studies have shown that proteoglycan content increases with age. The presence of charged tissue in human samples may have outweighed regional response.

Using the electrical conductivity method, the samples were tested under physiologic mechanical strains (0%, 10%, and 20%). Increasing strain rates caused the diffusivity of samples to drop significantly. This may indicate that mechanical load has a significant detrimental effect on diffusivity. In the human conductivity study by Wright et al., male and female groups were tested. The study found that female conductivity was higher than male conductivity, indicating a difference in transport material properties between the two groups. The study also found that female conductivity decrease more under mechanical load than male conductivity [62].

2.5 Modeling the TMJ Disc

In vivo TMJ disc measurements of stress and effects on tissue remodeling are impractical due to spatial placement of measuring instruments [28, 33]. A few studies

have been completed on animals through placement of strain gauges, but well controlled data are difficult to obtain. Due to the limitations, models can be constructed using anatomy and joint kinetics. These multibody models investigate joint motion which can be combined with solid anatomy to form finite element models (FEM) that help researchers simulate how tissue responds to various loading conditions. These models can be constructed with *in vitro* data such as material properties from biomechanical characterization combined with parameters the researcher could measure *ex vivo* such as anatomy from MRI/CT imaging and motion from tracking markers attached to the patient. Previous studies have constructed viscoelastic models of the TMJ disc based on the biphasic theory, using different mathematical basis for materials those models. However, as with any model, the model must be validated with real experimental tests to verify model predictions [41].

A proven finite element model that predicts tissue adaptation to load as well as the diffusion of nutrients under different pathological loading environments can have tremendous value in the clinic. Not only can they distinguish between normal and pathologic tissue, but they could lead to the understanding of the etiology of the disorder by providing a theoretical framework [154]. Accurate FE models could have significant impact on monitoring TMD progression, and provide clinicians a quantitative tool for assessing replacement surgery and success of treatments [155]. Finally, FEMs could allow better understanding of the loading and nutrient environment on a patient specific basis as a tool for monitoring progression, while providing an anatomical system by

which to design implants [28]. But before beginning the merits of a model of the TMJ disc, the theoretical background must be examined first.

Biphasic Theory

In biphasic mixture theory, soft tissues can be assumed to be a mixture with a solid phase consisting of ECM components collagen and PG and a fluid phase consisting of the interstitial fluid within the solid matrix.

The compressive response to loading is related to fluid flow within the tissue. If the tissue has low permeability high frictional drag forces could occur, additionally the solid matrix responds relative to Hooke's generalized law. The fluid phase is assumed to carry a major portion of loading in the TMJ disc due to low permeability $\sim 10^{-16}$ $m^4 \cdot N^{-1} \cdot s^{-1}$. As a result, biomechanical tests typically apply a stress (stress-relaxation) or strain (creep test) over time to measure the time-dependent response of the tissue [56, 156].

Triphasic Theory

The triphasic theory builds upon the biphasic theory by adding an ion phase to the mixture of solid and fluid phase [157]. The ion phase stems from the charged sulfate (SO_3^-) and carboxyl (COO^-) groups on the GAGs in the ECM. The highly negatively charged side chains give cartilage a fixed charge density (FCD), which is the charge of the solid matrix (0.04 to 0.2 $mEq \cdot mL^{-1}$ in normal cartilage) [66, 67, 157]. The negative charges due to the solid matrix must be balanced by mobile positive charges (e.g., Na^+) to maintain electroneutrality [66]. An imbalance in ion concentration is caused by the mobile ions and fixed negative charges inside the tissue becoming greater than the ion

concentration outside the tissue. The resulting osmotic pressure caused by the imbalance of ion concentration inside and outside the tissue is known as the Donnan osmotic pressure. Donnan osmotic pressure gives cartilage the unique swelling pressure responsible for as much as 30-50% of tissue response to loading, nearly 0.2 MPa. Further as the tissue is compressed the tissue hydration decreases, increasing fixed charge density and increasing Donnan osmotic pressure [67, 157].

The addition of a charged solid phase generates load support by 1) Donnan osmotic swelling pressure 2) the charged hydrophilic GAG chains further resist fluid flow through the solid matrix, and 3) as the tissue is compressed, the negative side chains resist load through steric repulsion. The triphasic theory has been used to model viscoelasticity, swelling, and electrokinetic behavior found in various charged, hydrated soft tissues [156-158].

Finite Element Models

Finite element models (FEM) have been used by a variety of research groups to predict mechanical reactions *in vivo*. The FE models make fundamental assumptions about the behavior of joint tissues under mechanical stress (linear/non-linear elastic) and about the boundary conditions between anatomical structures. Static three dimensional FE models have been used to evaluate condyle position relative to the mandible at multiple static occlusal positions. A static 3D linear-elastic FE model used by Beek et al. found TMJ disc deformation prevented small contact areas and high peak stresses between articular surfaces of the joint [33]. A 3D model proposed by Tanaka et al. examined variation in stress profiles between the TMJ disc and condyle with and without

displacement. The model analyzed stress profiles upon jaw opening and closing, finding higher stress profiles between the TMJ disc and condyle in models with TMJ disc displacement [42, 44]. Further Tanaka et al. used MRI and joint motion to examine friction between articulating surfaces, discovering that friction concentrations between articulating surfaces may result in injury to the disc and could be a primary cause of disc displacement [115]. Tanaka et al. along with Gallo et al. used the FE models to examine not only peak principal stresses on the disc but the direction of the stresses in relation to collagen fiber alignment found previously in the disc. The FE model has allowed Gallo et al. to simulate and understand condyle translation and the effect of condyle loading on the TMJ disc, such as mediolateral shear stress across the intermediate region of the disc with anterorposterior collagen alignment [44, 73].

In a similar model to Gallo's, Koolstra and van Eijden investigated the effect of stress distribution from the TMJ disc upon articulating surfaces [38]. The FE models showed the TMJ disc distributed local contact stresses over a large area of incongruent surfaces, therefore reducing high stress concentrations between articular surfaces. The study also showed the disc transfers compressive principle stresses into shear stresses across the disc [38].

Another model by Tanaka et al. and more recent model developed by Palomar et al. added the main connective ligaments and major masticatory muscles to generate biomechanical behavior of soft tissues during nonsymmetrical movement [44, 159]. In an associated model Koolstra et al. used human anatomic information retrieved from a cadaver with mechanical properties input into the model from previous porcine studies

[38]. Both models used electromyography (EMG) data to verify muscle forces. Palomar el al found higher shear stresses in the lateral portion of the posterior band. In addition Palomar et al. predicted from the FEM that asymmetric bruxism may affect lateral regions of both discs, and both discs are more prone to higher loads and more likely to suffer perforations [42, 44, 137].

Jaw Tracking

The motivation for jaw tracking originated from the desire to move beyond joint range of motion measurements to understand the complete mechanics of mandibular motion. Motion measuring tools have been used for a considerable amount of time in dental practice from pantographs to photographics, along with articulators which measure maximum incisional opening, Bennet's angle and Posselt's curve [160]. Earlier efforts sought to identify TMD risk factors associated with the morphology of the condyle and articulating surfaces through radiographs [161]. But advances in jaw tracking have sought not only to describe articulating surfaces but to define joint motion and stress profiles through the use of instantaneous accelerations combined with joint morphology to make assessments on patient's risk toward TMD symptoms. Jaw tracking has a variety of levels based on the technological system. Most systems track one point on the mandible, relating jaw motion to one index range of motion, much like Posselt's envelope of motion. However, six degrees of freedom (6 DOF) jaw tracking has been used by several research groups to track the mandible as a rigid body relative to the temporal bone and retrieve patient specific anatomy based on MRI to fit with the tracking data.

Ultrasound system

Ultra-sonic systems such as the Jaw Motion Analyzer (JMA) from Zebris use ultrasound signals to track jaw motion. An ultrasound emitter array is set to the labial surfaces of mandibular teeth, while an array sensor is mounted to the head bow see Figure 10 below [162]. The spatial coordinates tracked by the system are the mandibular signal generator and two points manually selected to represent condylar points. The three points define a plane tracked by the system in 6 DOF with an accuracy of 100 μm.

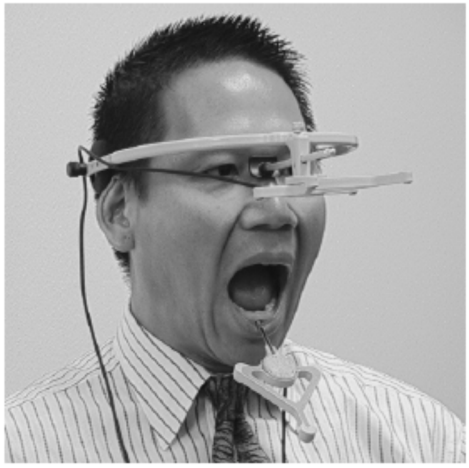

Figure 10 Ultra sonic jaw motion analyzer
The figure shows the ultrasound emitter array attached to the mandible below the sensor array on the head bow [162].

Opto-Electronic tracking system

In an optioelectric tracking system, target frames contain 3 infrared/active markers are attached to the mandible and maxilla. Each target frame contains 3 infrared/active markers that define a rigid body. The system is then able to track the target frame in 6 DOF. Three charged coupled device (CCD) or high speed CMOS cameras are used to define a global coordinate system that allows the rigid bodies to be

tracked in three dimensional space. This tracking system retrieves data in *x, y, z*, coordinates along with instantaneous velocity and acceleration, along with the pitch, yaw, motion of the rigid body; a 6 DOF tracking system. The maxilla target frame is used to cancel any relative head motion, so that only the mandible motion relative to the cranium is tracked. Spatial resolutions range from 10-100μm, while temporal resolution ranges from 60 -1000 frames per second depending on the motion tracking camera. A data file is exported to MatLab or excel or other 3D motion compilation software. The data file is used to generate a trace of the mandible relative to the maxilla in real time with correction position and velocity vectors. This motion data can be attached to the anatomy through a linked CAD based software discussed later [6, 73, 74, 163, 164].

Motion Combined with patient anatomy

A static MRI is the standard imaging technique for gathering patient anatomy specific to the TM joint. Efforts at dynamic MRI's have not produced sufficient quality in both spatial and temporal resolution categories. Current Cine MRI (as in cinema or dynamic series of images) has been investigated to track the disc motion during jaw function. The Cine MRI is not a true dynamic MRI [165]. The technique uses MRI images similar to stop animation to analyze the path of the condyle and disc during jaw opening. The mouth opening is stopped at increments using a Burnett device. However, a study comparing Cine MRI jaw motion to natural jaw motion tracked through opto-electronic methods found that that the use of Burnett device to maintain pauses caused the motion to deviate from natural motion [165]. Therefore the most sophisticated, physiologically accurate motion tracking system is the opto-electronic system combined

with MRI based on the work of Gallo et al. referred to by his group as "dynamic stereometry" [6, 163]. Figure 11 shows stresses on the TMJ disc through dynamic stereometry.

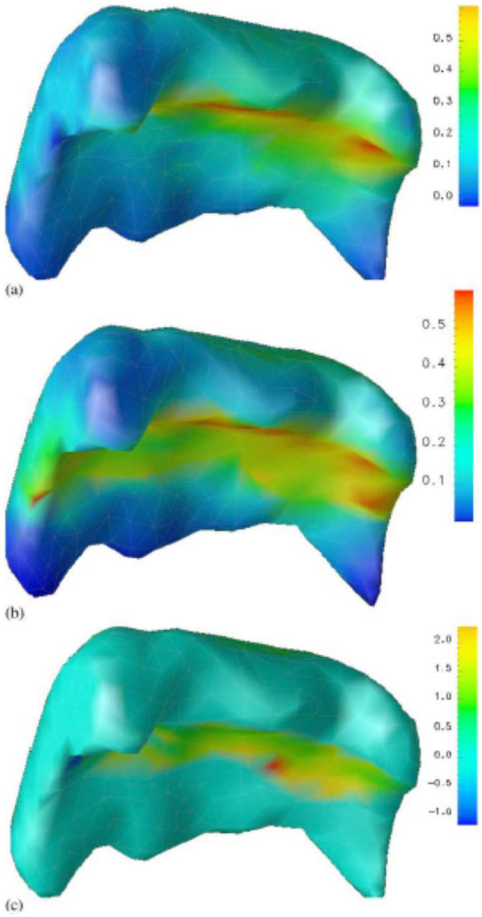

Figure 11 Maximum principal stresses on the inferior surface of the human TMJ disc.
The maximum principal stresses were determined using finite element models of patient specific TMJ discs combined with recorded jaw motion [142].

The first step in dynamic stereometry is to obtain patient data from an MRI. During the MRI, a target frame with contrast medium is fixed to the craniofacial MRI

arm to establish a coordinate basis for transfer between MRI and jaw motion tracking. After the MRI, the contrast agent target frame is measured to the maxilla jaw tracking target frame. Now the coordinate systems can be merged when the MRI is imported to a CAD/CAM software such as SolidWorks. The MRI anatomy file is meshed and imported into a finite element program. The motion tracking data is recorded by software developed by Gallo et al. and processed into a rigid body trace of the motion of the mandible. The motion tracking data is transferred to the patient specific finite element model for analysis, where the data can be analyzed. Gallo et al. performed stress profile analysis using material properties gathered from animal studies. With the combined MRI anatomy of the disc, material properties, and motion data, many finite element models were constructed to simulate joint loading conditions and TMJ disc damage that mimicked the in vivo environment [74, 163, 164, 166].

Gallo et al. used the MRI combined with jaw tracking to determine aspect ratios, instantaneous velocities and distances of stress field translations. These data were used to evaluate the amount of work the TMJ disc was subjected to during opening/closing along with laterotrusive movements. The studies show laterotrusive movement generated over fifty percent more work than previously thought to the contralateral side, while results in opening and closing set a baseline exposure for work during cyclic loading that could potentially lead to fatigue failure. In a similar study Nickel and Iwasaki et al. compared patients with TMD to patients without history of the disorder. The study found that patients with TMD sustained TMJ loads 9.5-65% higher than subjects with normal disc position. A range of biting forces were compared during the study, with TMD patients

experiencing higher joint loads, indicating that pathological loading to the TMJ disc is present in TMD patient and that continued overloading could lead to progression [144].

Proposed Research and Scope of Project

Recent studies in our lab have shown that levels of oxygen and glucose significantly affect cell proliferation and matrix synthesis of porcine TMJ disc cells *in vitro*. This suggests that transport of nutrients through the extracellular matrix (ECM) plays a key role in maintaining the physiological concentration of nutrients, further implying that deviations from physiological levels of nutrient or mechanical loading may initiate tissue remodeling and matrix degradation. We have also found that the human TMJ disc has very low diffusivity compared to other fibrocartilages (hyaline and IVD). Our preliminary data suggest that a steep nutrient concentration gradient might exist in the TMJ disc and that this nutrient environment is uniquely vulnerable to pathological mechanical loadings. Therefore, the ***goal of this research study*** is to characterize the **human mechanical properties** of the TMJ disc and determine the **human transport properties** of the disc under mechanical strain.

Hypothesis

Our central hypothesis is that mechanical properties will vary regionally across the TMJ disc and that sustained mechanical loading can alter solute transport and nutrient levels in the TMJ disc as well as mechanical function resulting in disc derangement and degeneration.

3 TRANSPORT PROPERTIES IN HUMAN TMJ DISCS

3.1 Abstract

This study investigated the effect of mechanical strain on solute diffusion in human TMJ discs (mean cadaver age 77.8) using the electrical conductivity method. The electrical conductivity, as well as small ion diffusivity, of male and female TMJ discs was determined under three compressive strains. In the male group, the average disc electrical conductivity (mean ± sd) at 0% strain was 5.14±0.97 mS/cm, decreased to 4.50±0.91 mS/cm (-12.3%) at 10% strain, and 3.93±0.81 mS/cm (-23.5%) at 20% compressive strain. Correspondingly, the average disc relative ion diffusivity at 0% strain was 0.44±0.08, decreased to 0.40±0.08 (-8.9%) at 10% strain, and 0.36±0.08 (-16.7%) at 20% compressive strain. In the female group, the average disc electrical conductivity at 0% strain was 5.84±0.59 mS/cm, decreased to 5.01±0.50 mS/cm (-14.2%) at 10% strain, and 4.33±0.46 mS/cm (-25.8%) at 20% compressive strain. Correspondingly, the average disc relative ion diffusivity at 0% strain was 0.49±0.05, decreased to 0.43±0.04 (-11.3%) at 10% strain, and 0.39±0.04 (-19.9%) at 20% compressive strain. The results indicated that mechanical strain significantly impeded solute diffusion through the disc. This mechanical strain effect was larger in the female than in the male human TMJ disc. This study may provide new insights into TMJ pathophysiology.

3.2 Introduction

Temporomandibular joint (TMJ) disorders exert significant impact with estimated minimum annual health care and societal costs of $4 billion [167]. Women are about 3 times more likely to be afflicted than men based on the recent OPPERA study [168]. The TMJ is a load bearing joint with a unique articular structure and function [169]. The TMJ disc, a dense fibrocartilaginous tissue, distributes stress and aids in lubrication of the joint [170]. In approximately 30% of TMJ disorder patients, mechanical dysfunction of the TMJ disc, especially displacement due to tissue degeneration, is a common event [171, 172]. Degenerative changes generally occur more than a decade earlier in the TMJ than other human joints (e.g., knee and hip) [173, 174]. It is generally believed that pathological mechanical loading (e.g. sustained jaw clenching or traumatic impact) triggers a cascade of molecular events leading to TMJ disc degeneration [175]. However, the link between pathologic mechanical loading at the tissue level and the resulting biological response at the cellular/molecular level remains poorly understood.

The normal adult human TMJ disc is a large avascular structure and the nutrients required by the disc cells are supplied through diffusion by blood vessels and synovial fluid at the margins of the disc [176, 177]. A nutrient concentration gradient is established across the TMJ disc based on diffusion from the nutrient rich periphery to the interior of the disc and is balanced by the rate of nutrient consumption from the disc cells. The concentration gradient has been shown to impact disc cell viability, matrix synthesis and composition, along with response to inflammatory factors [178, 179]. This suggests deviations from physiological levels may initiate tissue remodeling and matrix

degeneration. The rate of solute diffusion in tissue is governed by solute diffusivities which are affected by the composition and structure of the matrix, as well as mechanical strains on the tissue. Recently, we examined the effect of mechanical loading on small ion diffusivity in porcine TMJ discs using the electrical conductivity method. The results indicated that solute diffusivities in the TMJ disc are much lower than the values in other cartilaginous tissues, and compressive strain significantly impeded solute transport in the porcine TMJ disc [61]. Moreover, our cell metabolic studies have shown that porcine TMJ discs have higher cell densities and nutrient consumption rates than articular cartilage and the intervertebral disc (IVD) [180]. Therefore, it is likely that a steeper nutrient gradient may exist in TMJ discs and is vulnerable to pathological events which impede nutrient supply, including sustained joint loading due to jaw clenching. Although pigs have been considered the best TMJ biomechanical experimental model [181, 182], the mechanical and transport properties of TMJ discs have not been fully compared due to the lack of human material property data. Especially, to our knowledge, the transport properties (e.g., solute diffusivity) and the effect of mechanical loading on these properties, in the human TMJ disc have not been determined. Such knowledge is important for translating the research findings from an animal model to human.

The electrical conductivity method has been employed to determine the effect of mechanical strains on ion diffusivities in hydrogels, IVD, and porcine TMJ discs [61, 183, 184]. In these studies, a relationship between ion diffusivities and the porosity of the material were also determined. In this study, we adopted this method to study the impact of mechanical loading on the solute transport in human TMJ discs. We

hypothesized that the electrical conductivity of the human TMJ disc was mechanical strain-dependent due to changes in tissue porosity caused by tissue compression. In addition, we sought to determine the electrical conductivity in both male and female subjects to investigate if there were sex differences. Therefore, the objective of this study was to measure the electrical conductivity of male and female human TMJ discs under three compressive strains in five disc regions.

3.3 Materials and Methods

Specimen preparation

Human TMJ discs were harvested from the left TMJ of fresh cadavers in the MUSC gross anatomy laboratory with institutional approval. Discs with visible signs of degeneration or trauma were removed, leaving 12 male and 12 female discs for the study. The mean cadaver age was 76.0±7.0 for males and 79.6±10.5 for females. The extracted TMJ disc was wrapped in cellophane and placed into plastic bags. Saline moistened gauze was added to the bag to maintain humidity and prevent specimen dehydration. The disc sample was immediately used for porosity and conductivity measurement. Care was taken to prevent specimen dehydration during specimen preparation. Cylindrical plugs were punched from five disc regions (anterior, lateral, intermediate, medial, and posterior) using a 5mm corneal trephine (Figure 12a below). The plugs were microtomed on a freezing stage to remove the natural concave tissue shape and to allow for a flat surface during electrical conductivity measurements. Each time, one plug was punched and microtomed in a moisture-controlled dissection hood. The rest of the disc was

wrapped and placed in the same sealed plastic bag. Prior to the water content measurement, the specimen was thawed at room temperature for 20 minutes in a sealed plastic vial. The initial height of the specimen was measured by a custom-designed electrical current sensing micrometer to avoid sample compression. The prepared specimens (n=60 for male, n=60 for female) had an average height of 1.49±0.46 mm. Three conductivity measurements were made on each specimen corresponding to the three levels of compressive strain (0%, 10%, and 20%) based on the initial height. Both finite element analysis and MRI imaging data have shown that the change of human TMJ disc thickness during normal joint motion is about 15-20% [185]. The sustained mechanical loading, such as bruxism, may induce 20-30% change of the disc thickness.

Porosity (water volume fraction) measurement

The porosity or water volume fraction of specimens at the undeformed state (ϕ_0^w) was determined using a buoyancy method [186]. Briefly, the weight of the specimens in air (W_{wet}) and the weight in phosphate buffered saline (PBS) solution (W_{PBS}) were measured using the density-determination kit of a Sartorius analytical balance (Sartorius YDK01, Germany). After measuring electrical conductivity, specimens were lyophilized and the dry weights (W_{dry}) were recorded. According to Archimedes' principle and the biphasic assumption, the water volume fraction was determined by:

$$\phi_0^w = \frac{W_{wet} - W_{dry}}{W_{wet} - W_{PBS}} \frac{\rho_{PBS}}{\rho_w}$$

3

where ρ_{PBS} is the mass density of PBS (1.005 g/ml), and ρ_w is the mass density of water. The TMJ disc tissue was considered as a biphasic mixture, consisting of solid phase and free water phase. Both phases are assumed to be incompressible. Thus, the water volume fraction of the specimen at different compression levels (ϕ^w) can be calculated by [157]:

$$\phi^w = \frac{\phi_0^w + e}{1 + e}$$

4

where *e* is the tissue dilatation. Considering one-dimensional confined compression in this study, the tissue dilatation is equal to the compressive strain.

Electrical conductivity measurement

In this study, the impact of mechanical strain on electrical conductivity of human TMJ disc was examined in the superior-inferior direction only. This was achieved by using a confined chamber to ensure that the applied mechanical strain and measured electrical conductivity were aligned in the same direction see Figure 12b below. The superior-inferior direction is the main transport route in the TMJ disc due to its short diffusion distance compared to the anterior-posterior and medial-lateral directions. The electrical conductivity was measured based on the principle of a four wire resistance test using a Keithley Sourcemeter (Model 2400, Keithley Instruments, Inc., Cleveland, OH)

and a custom designed conductivity chamber reported previously [61, 187]. Briefly, the conductivity apparatus consists of two stainless steel current electrodes coaxial to two Teflon-coated Ag/AgCl voltage electrodes placed on the top and bottom of a cylindrical nonconductive Plexiglass chamber (5mm diameter). The specimen was placed inside the chamber for measurement and compression (Figure 12b below).

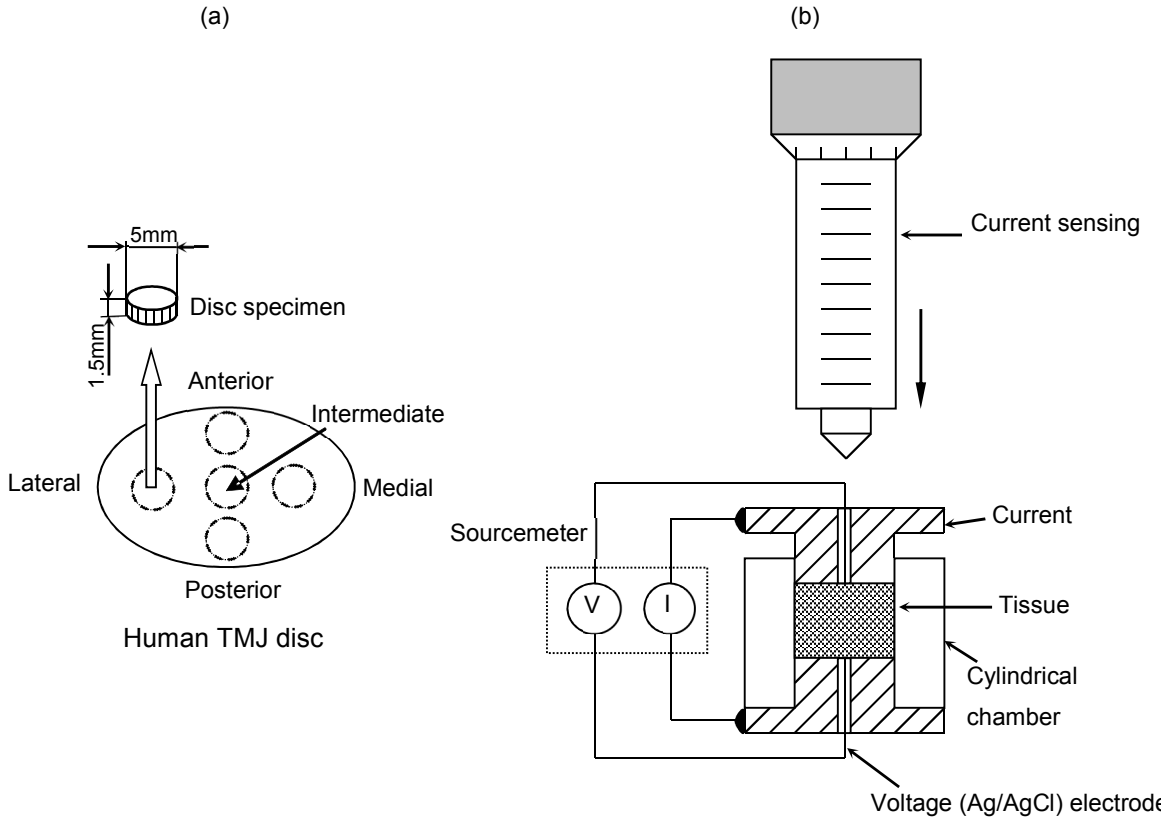

Figure 12 (a) Schematic of specimen preparation. (b) Schematic of apparatus for measuring electrical conductivity

The region and size of test specimens were removed from five regions of each disc, see Figure 11 (a). The conductivity meter shown in Figure 11 (b) consisted of two stainless steel current electrodes, two Ag/AgCl voltage-sensing electrodes, a nonconductive Plexiglass chamber, a current sensing micrometer, and a sourcemeter.

The resistance (R) values across the specimens were measured at a low, constant current density of 0.015 mA/cm^2. The height of the specimen was measured with an electrical current sensing micrometer. The electrical conductivity (χ) values of the specimens were calculated by:

$$\chi = \frac{h}{R \cdot A} \qquad \textbf{5}$$

where h and A are the height and cross-sectional area of the specimens, respectively. The precision for the resistance measurements was 0.5 Ω while the height measured with an accuracy of ±1.0 μm. The electrical conductivity of the specimen was measured at 0%, 10%, and 20% compression levels. The confined compression of the tissue specimen was achieved by lowering the micrometer to the desired height (Figure 12b above) and fluid was allowed to exude from the sample through a small clearance between the chamber and the current electrodes. A resistance measurement was taken at a 15 minute interval after the specimen was compressed to ensure the sample had reached equilibrium with no fluid exudation. The influence of the order of the strain level on the electrical conductivity was not examined in this study, since the order of the strain level is not expected to affect the equilibrium response. All conductivity tests were performed in a bathing solution of PBS at a physiological concentration of 0.15M (pH 7.4) at room temperature (22°C).

Ion diffusivity calculation

Under a zero fluid flow condition, the measured electrical conductivity (χ) of a tissue in NaCl solution is related to intrinsic cation and anion diffusivities (D^i, i = +, -) by [188, 189]:

$$\chi = F_c^2 \phi^w (c^+ D^+ + c^- D^-) / RT \quad \textbf{6}$$

where F_c is the Faraday constant, R is the gas constant, T is the temperature, c^+ is the cation ion concentration, and c^- is the anion concentration. The TMJ disc was considered as uncharged in this study, since biochemical studies have shown that the GAG content of human and porcine TMJ discs is very low (< 4% dry weight) compared to hyaline cartilage and the IVD [190, 191]. More importantly, the high ionic concentration of bathing solution (0.15 M) assured a small osmotic effect on the diffusion process. For uncharged tissues in NaCl solution, the relative diffusivity (D/D_0) of NaCl is simply related to the relative conductivity by [183]:

$$\frac{D}{D_0} = \frac{\chi}{\phi^w \chi_0} \quad \textbf{7}$$

where D is the mean ion diffusivity of Na^+ and Cl^- in tissue, D_0 is the mean ion diffusivity in the bathing solution, χ is the electrical conductivity of the tissue, and χ_0 is the conductivity of the bathing solution. In our analysis, Na^+ and Cl^- were assumed to carry the electrical current because these ions are the primary ionic components of PBS.

Statistical analysis

The electrical conductivity, porosity, and relative ion diffusivity were determined for each specimen (5 regions per disc) under three compressive strains. Mixed effects analysis of variance (ANOVA) was used to investigate the main and interaction effects on each outcome of disc region, strain, sex, and age. The models accommodated correlations among measurements from the same disc both within and between the three strains, allowing that measurements on a disc from the same region may be more highly correlated than measurements from different regions. SAS/STAT® software version 9.3 (SAS Institute Inc., Cary, NC) was used for statistical analyses and statistical significance was determined at p-values < 0.05. Pilot data analyses showed that none of the main and interaction effects involving region or age emerged as statistically significant. Hence subsequent analyses were performed using the average response among the 5 regions for each disc at each strain. Two-way mixed effects ANOVA incorporating a random effect for disc was used to assess the effects of strain and sex on this average outcome.

3.4 Results

Electrical conductivity

The effects of compressive strain on electrical conductivity in the five disc regions are shown in Figure 13 below. No significant regional variation was detected at all strain levels in both the male and female groups. However, there was a significant decrease in electrical conductivity with increases of compressive strain in all five disc regions in both the male and female groups ($p<0.0001$). In the male group, the average

disc electrical conductivity (mean ± sd) at 0% strain was 5.14±0.97 mS/cm, decreased to 4.50±0.91 mS/cm (-12.3%) at 10% strain, and 3.93±0.81 mS/cm (-23.5%) at 20% strain (Figure 13 below).

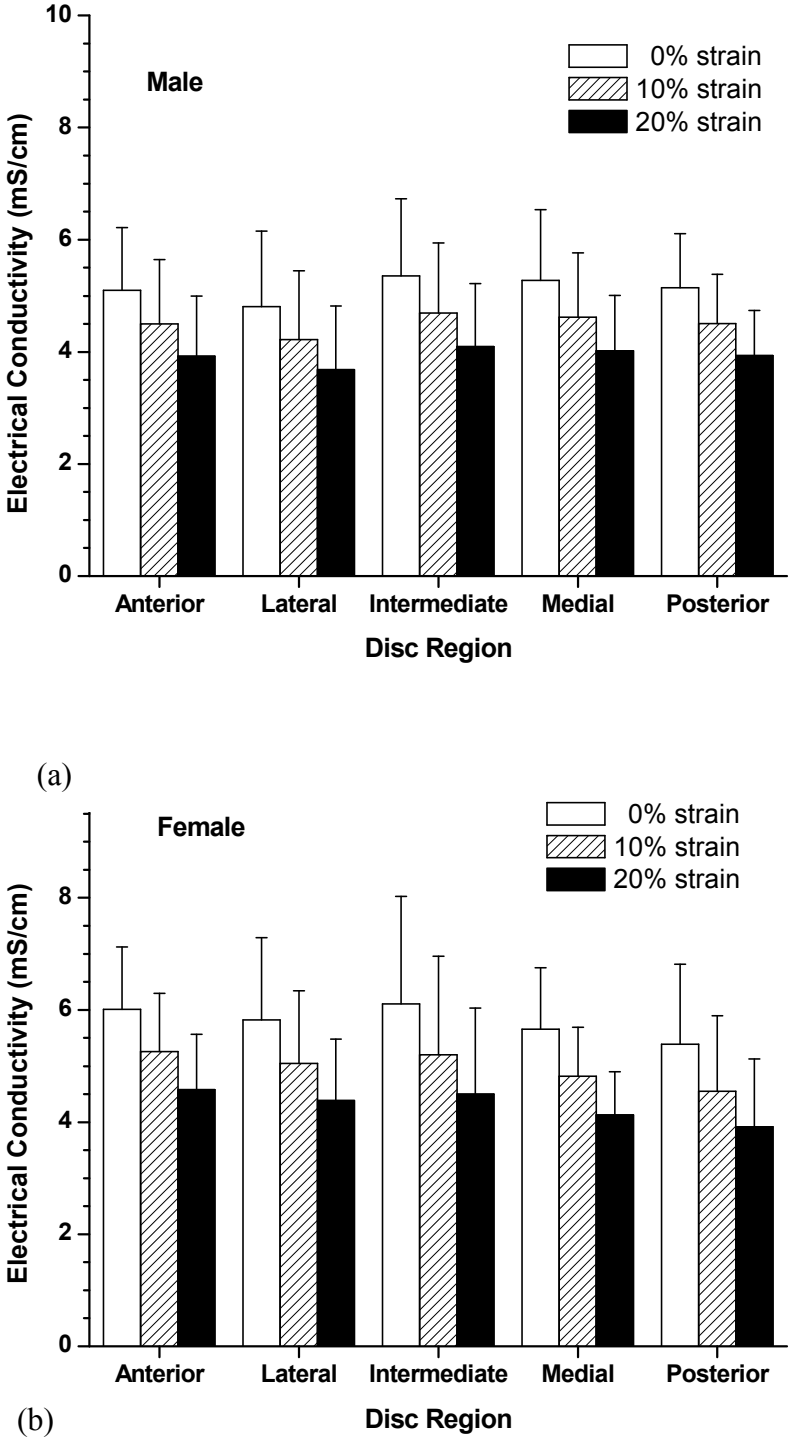

Figure 13 Effect of compressive strains on regional distribution of electrical

conductivity by gender

(a) Male electrical conductivity by region (b), Female electrical conductivity by region. Mixed effects ANOVA as described in the Statistical Analysis section confirmed the lack of significant difference in outcomes among the disc regions and among two-factor interactions between disc region and strain or sex or age of disc donor.

In the female group, the average disc electrical conductivity at 0% strain was 5.84±0.59 mS/cm, decreased to 5.01±0.50 mS/cm (-14.2%) at 10% strain, and 4.33±0.46 mS/cm (-25.8%) at 20% strain (Figure 13 above). The electrical conductivity was higher in the female than in the male TMJ disc, although the differences were not statistically significant ($p=0.08$). Interestingly, the interaction between strain and gender was found to be statistically significant ($p=0.0004$). The impact of the mechanical strain on the electrical conductivity was higher in the female TMJ disc compared to the male.

Porosity (water volume fraction)

The effect of compressive strain on tissue porosity (water volume fraction) in the five disc regions is shown in Figure 14 below. No significant regional variation was detected at all strain levels in both the male and female groups. However, there was a significant decrease in tissue porosity with increases of compressive strain in all five disc regions in both the male and female groups ($p<0.0001$).

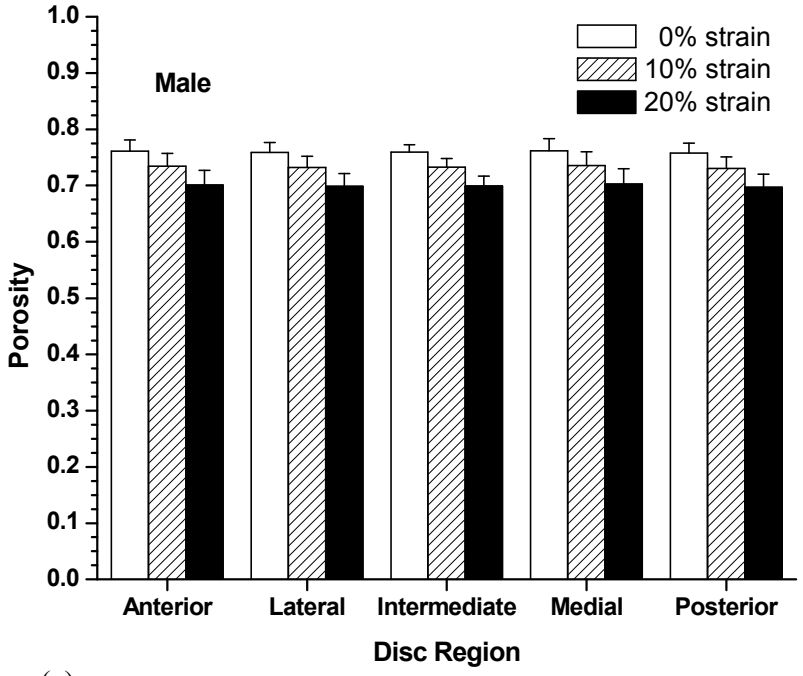
Male
0% strain
10% strain
20% strain
Porosity
1.0
0.9
0.8
0.7
0.6
0.5
0.4
0.3
0.2
0.1
0.0
Anterior
Lateral
Intermediate
Medial
Posterior
Disc Region

(a)

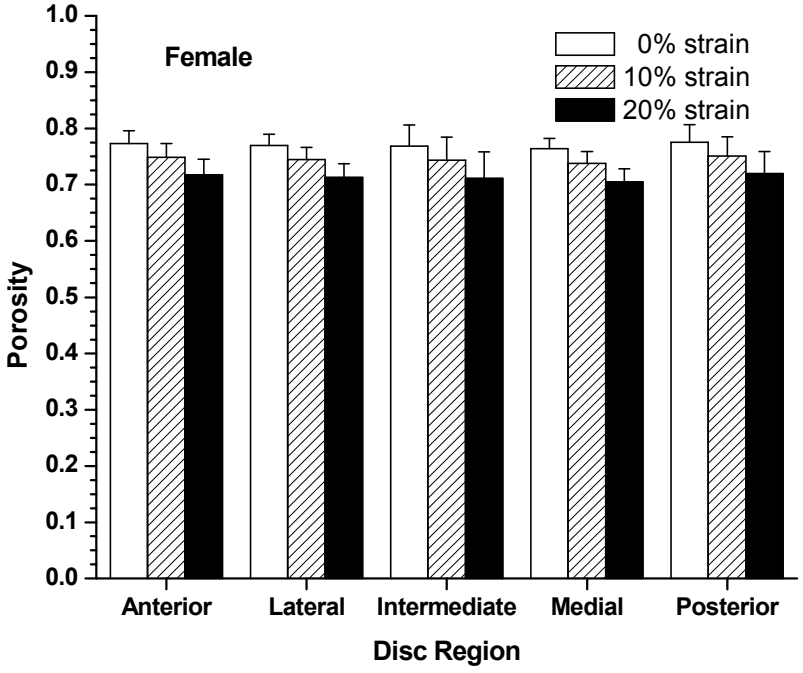
Female
0% strain
10% strain
20% strain
Porosity
1.0
0.9
0.8
0.7
0.6
0.5
0.4
0.3
0.2
0.1
0.0
Anterior
Lateral
Intermediate
Medial
Posterior
Disc Region

(b)

Figure 14 Effect of compressive strains on regional distribution of porosity by gender

(a),Male porosity by region (b), Female porosity by region. Mixed effects ANOVA as described in the Statistical Analysis section confirmed the lack of significant difference in outcomes among the disc regions and among two-factor interactions between disc region and strain or sex or age of disc donor.

In the male group, the average disc porosity at 0% strain was 0.760±0.011, decreased to 0.733±0.012 (-3.6%) at 10% strain, and 0.700±0.014 (-7.9%) at 20% strain (Figure 14 above). In the female group, the average disc porosity at 0% strain was 0.770±0.014, decreased to 0.745±0.016 (-3.2%) at 10% strain, and 0.713±0.018 (-7.4%) at 20% strain (Figure 14 above). The porosity was higher in the female than in the male TMJ disc, although the differences were not statistically significant ($p=0.0533$). The interaction between strain and sex was found statistically significant ($p=0.0218$), even though the magnitude of this effect appears very small.

Ion diffusivity

Electrical conductivities of PBS at 22°C were measured using an Orion conductivity meter (Model 150Aplus, Beverly, MA). The value of 15.5 mS/cm for solution conductivity was used to normalize the measured conductivity data of tissues to calculate the relative ion diffusivity. The effect of compressive strain on relative ion diffusivity in the five disc regions is shown in Figure 15 below. No significant regional variation was detected at all strain levels in both the male and female groups. However, there was a significant decrease in ion diffusivity with increases of compressive strain in all five disc regions ($p<0.0001$).

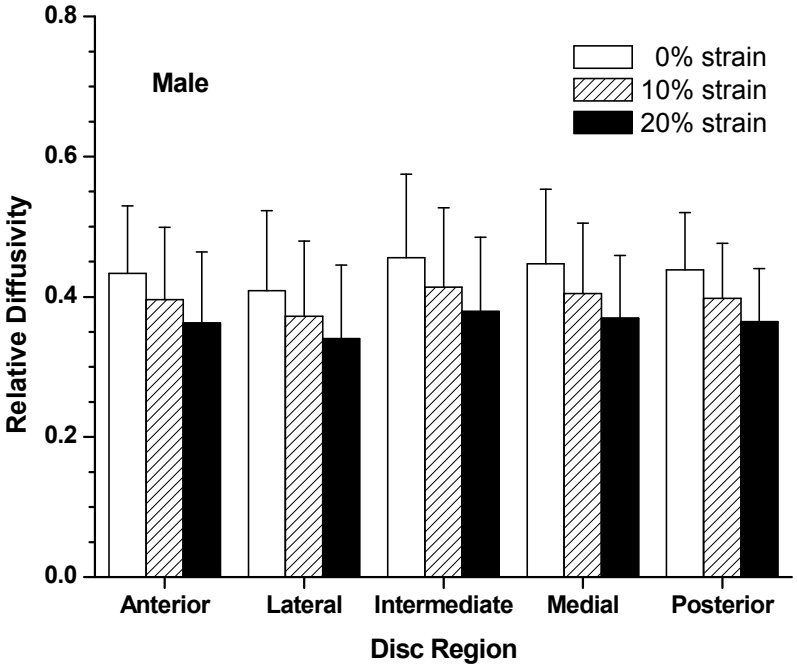
Male
0% strain
10% strain
20% strain
Relative Diffusivity
0.0
0.2
0.4
0.6
0.8
Anterior
Lateral
Intermediate
Medial
Posterior
Disc Region

(a)

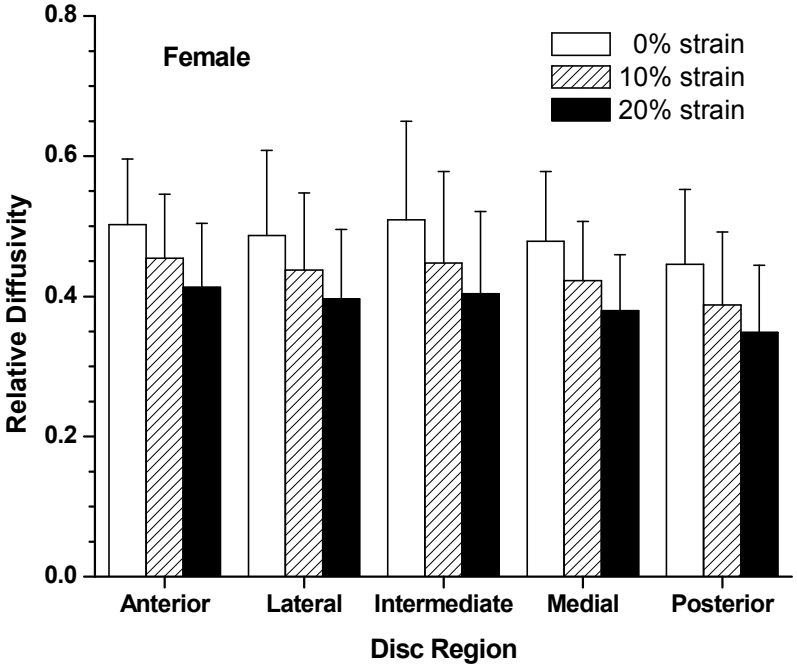
Female
0% strain
10% strain
20% strain
Relative Diffusivity
0.0
0.2
0.4
0.6
0.8
Anterior
Lateral
Intermediate
Medial
Posterior
Disc Region

(b)

Figure 15 Effect of compressive strains on regional distribution of ion diffusivity by sex

(a), Male ion diffusivity by region (b), Female ion diffusivity by region. Mixed effects ANOVA as described in the Statistical Analysis section confirmed the lack of significant difference in outcomes among the disc regions and among two-factor interactions between disc region and strain or sex or age of disc donor.

In the male group, the average disc relative ion diffusivity at 0% strain was 0.44±0.08, decreased to 0.40±0.08 (-8.9%) at 10% strain, and 0.36±0.08 (-16.7%) at 20% strain (Figure 15 above). In the female group, the average disc relative ion diffusivity at 0% strain was 0.49±0.05, decreased to 0.43±0.04 (-11.3%) at 10% strain, and 0.39±0.04 (-19.9%) at 20% strain (Figure 15 above). The relative ion diffusivity was higher in the female than in the male TMJ disc, although the differences were not statistically significant ($p=0.1502$). The interaction between strain and sex was found statistically significant ($p=0.0004$). The impact of the mechanical strain on the relative ion diffusivity was higher in the female TMJ disc compared to the male.

Finally conductivity, porosity and diffusivity were analyzed with respect to % stran compression as shown in Figure 16 below. Mechanical strain is shown to decrease electrical conductivity and porosity. The association between conductivity and porosity is shown in Figure 17 below.

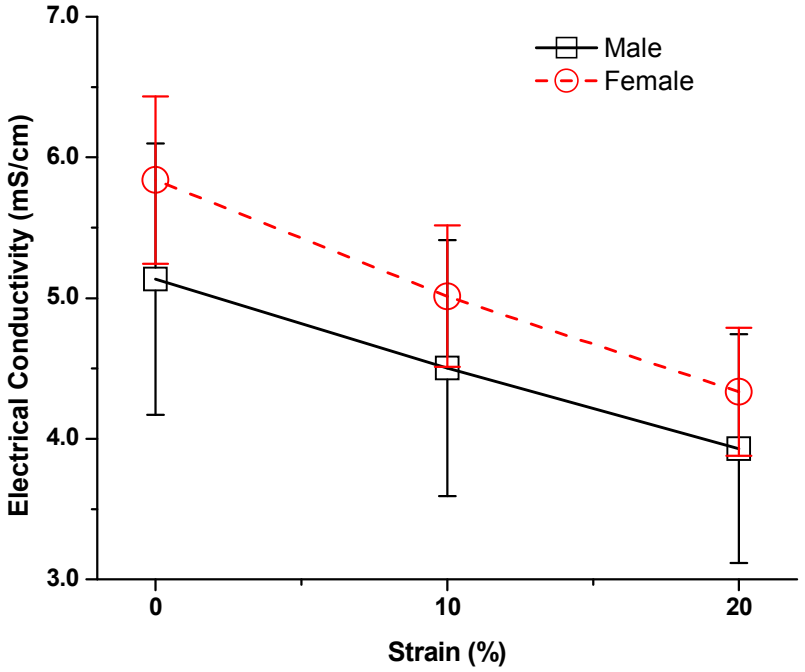
7.0
6.0
5.0
4.0
3.0
Electrical Conductivity (mS/cm)
Male
Female
0
10
20
Strain (%)

(a)

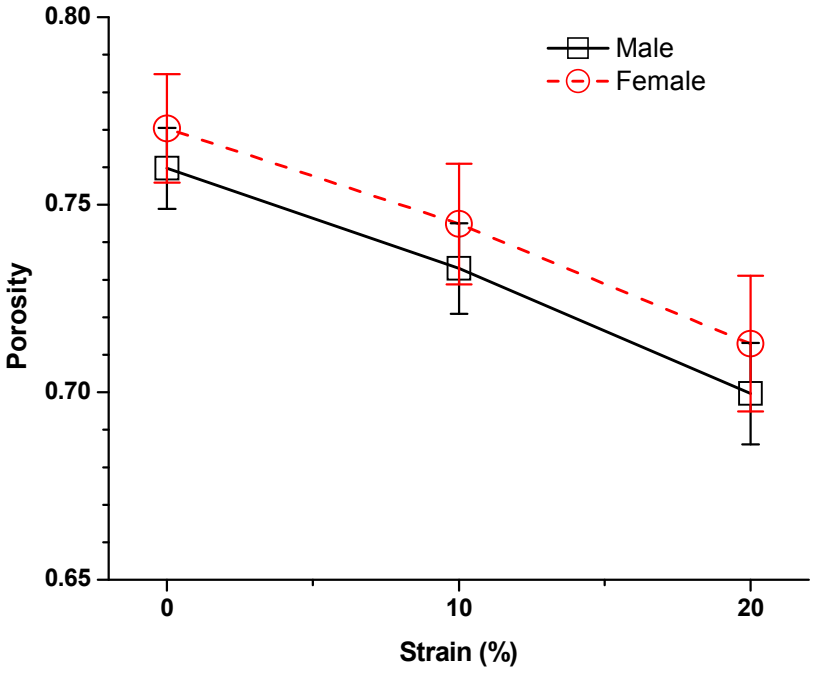
0.80
0.75
0.70
0.65
Porosity
Male
Female
0
10
20
Strain (%)

(b)

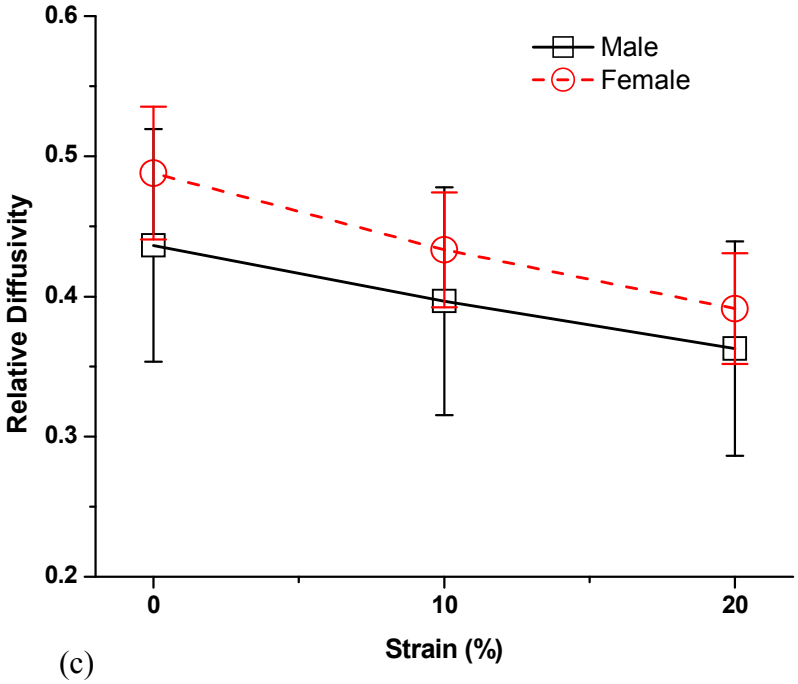

(c)

Figure 16 The effect of sex on the strain-dependent electrical conductivity (a), porosity (water volume fraction) (b), and relative ion diffusivity of human TMJ disc (c). Note that the average value of the five regions from the same disc (male n=12, female n=12) were used to represent the outcomes of that disc since the regional variations were found not statistically significant in this study.

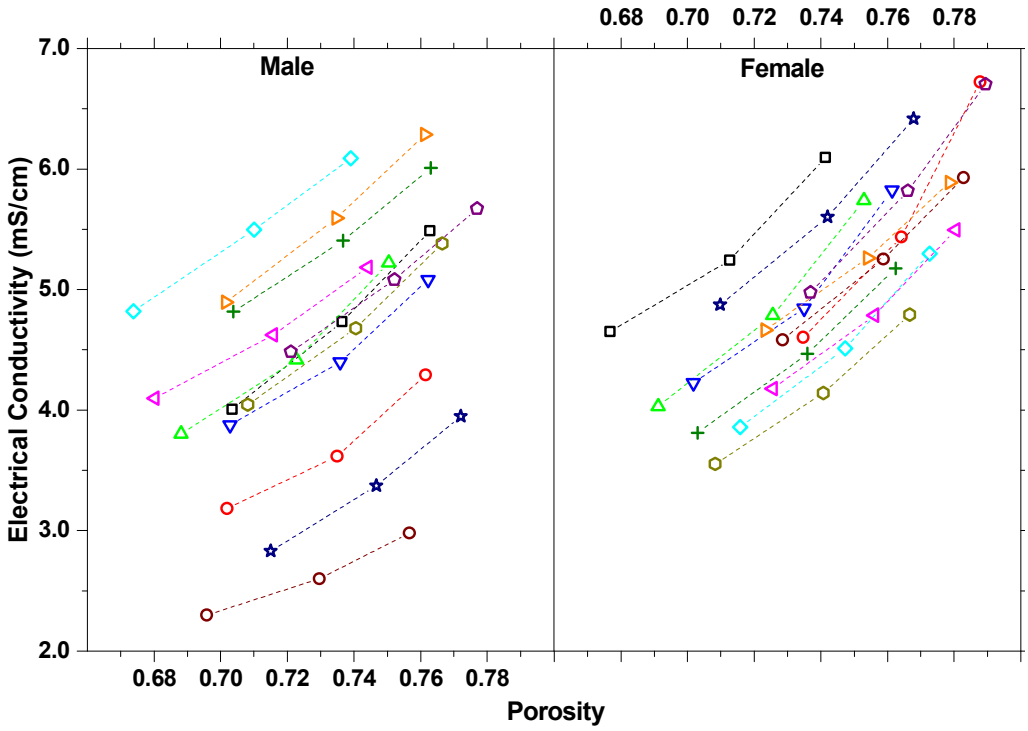

Figure 17 Association between the electrical conductivity and the porosity (water volume fraction).
Each dashed line depicts the data for one disc.

3.5 Discussion

The objective of this study was to investigate the effect of mechanical strain on small ion diffusivity in human TMJ discs using the electrical conductivity method. The measured electrical conductivity and calculated ion diffusivity from this study indicated that compressive mechanical strain significantly impeded solute diffusion through the disc. Our results further indicated that this mechanical strain effect was larger in the female than in the male human TMJ disc.

The decrease in electrical conductivity with increasing mechanical strain in the human TMJ disc was mainly due to the porosity (water volume fraction) reduction caused by increasing compression (see Figure 14 and Figure 16b above). Tissue compression caused fluid exudation and a corresponding decrease in tissue porosity. The reduction in porosity resulted in decreased ion diffusivity in the tissue and subsequently decreased electrical conductivity [183, 184]. This is in agreement with previous studies reporting decreasing diffusivity of solutes with increasing static compressive strain in articular cartilage [192, 193], IVD tissues [194, 195], and porcine TMJ discs [61]. The strain-dependent electrical conductivity and ion diffusivity indicated that mechanical strain impeded solute transport in human TMJ discs. Moreover, the impact of mechanical strain on ion diffusivity was larger in the female than in the male TMJ disc. Figure 17 above showed the association between the electrical conductivity and the porosity for the male and female human TMJ discs. It seems that the electrical conductivity of the female disc is more sensitive to the change of the tissue porosity due to the mechanical strain. This suggested that a subtle tissue structure difference might exist between the male and female TMJ discs. However, to our knowledge, there is no study to quantitatively compare the biochemical composition (e.g., water, GAG, and collagen contents) and tissue structure (e.g., fiber density and orientation) in human male and female TMJ discs. This will be a very interesting thing to look at in our next study. The pathological implication of this finding needs to be further explored. Although the recent OPPERA study confirmed a long standing report of 3 to1 incidence of females to

males for TMJ disorders [168], the causes of such a sex disparity are still poorly understood.

In our previous study of porcine TMJ discs, transport properties were region-dependent with the electrical conductivity and ion diffusivity in the anterior region significantly higher than in the posterior region. This regional difference is likely due to the significant differences of tissue porosity between these two regions in the porcine TMJ disc. In contrast, no significant regional variation of tissue porosity was found in the human TMJ disc. The diffusive transport in both porcine and human TMJ discs was dependent upon tissue composition. Consequently, the electrical conductivity and ion diffusivity were not region-dependent in the human TMJ disc.

The electrical conductivity and tissue porosity of cartilaginous tissues were compared and are listed in Table 2 below. The electrical conductivity in human TMJ discs was the lowest compared with human articular cartilage and human annulus fibrosis. The lower solute diffusion in the human TMJ disc is likely due to a lower tissue porosity compared to other human cartilaginous tissues. The normal adult TMJ disc is a large avascular structure [176, 177], so the nutrients required by disc cells are supplied through diffusion. This study showed that solute diffusivities in the human TMJ disc are lower than the values in other human cartilaginous tissues, and compressive mechanical strain can further impede solute diffusion in the human TMJ disc. Moreover, the TMJ disc has a higher cell density and nutrient consumption rates than in articular cartilage and the IVD [180]. Therefore, it is likely that a steeper nutrient gradient may exist in human TMJ discs and might be vulnerable to pathological events which impede nutrient

supply, including sustained joint loading due to jaw clenching. The strain distribution in the TMJ disc *in vivo* is complex and can be determined through finite element analysis [185]. The strain-dependent diffusivity established in this study needs to be incorporated into finite element models to assess the overall impact of physiological/pathological loading on solute transport in human TMJ discs.

Table 2 Comparison of electrical conductivity and tissue porosity in an unstrained state between the TMJ disc and other cartilaginous tissues (mean±sd).

	Electrical conductivity (mS/cm)	**Water volume fraction** (porosity)	**Reference**
Human TMJ disc (male)	5.14±0.97	0.760±0.011	Present study
Human TMJ disc (female)	5.84±0.59	0.770±0.014	Present study
Porcine TMJ disc	2.97±0.90	0.726±0.038	Reference [13]
Human articular cartilage	6-10	~0.8	Reference [7]
Porcine annulus fibrosis	5.60±0.89	0.74±0.03	Reference [5]
Human annulus fibrosis	7.5±0.8	0.80±0.02	Reference [9]

The electrical conductivity and tissue porosity of the human TMJ disc in this study were much higher than the values of porcine TMJ discs (Table 2 above). It is unclear whether this difference is an intrinsic difference between the species, or due to sample ages. The human TMJ discs were harvested from old donors (>70 yr), while the porcine TMJ discs were collected from young pigs (6-8 month) [61]. The donor age may affect the tissue composition and structure of human TMJ disc, resulting in the change of the material properties, such as electrical conductivity. Thus, it is necessary to further

examine the age effect in future studies. In this study, the electrical conductivity was measured in the superior-inferior direction. However, considering the fiber structure of the TMJ disc, the diffusion in the TMJ disc is significantly anisotropic [58]. Although the superior-inferior direction is the main transport route in TMJ disc, the impact of mechanical strain on solute diffusion in the anterior-posterior and medial-lateral directions still needs to be examined. It is also necessary to determine the impact of mechanical strain on the diffusivities of other essential solutes, such as oxygen and glucose. In summary, the effect of mechanical strain on small ion diffusivity in human TMJ discs was investigated using electrical conductivity methods. The results indicated that mechanical strain significantly impeded solute diffusion through the disc. This mechanical strain effect was larger in the female than in the male human TMJ disc. Although pigs have been considered as a good animal model to study human TMJ disc mechanics, the similarity in terms of tissue material properties still needs further validation.

4 Transport Properties in Porcine Articular Cartilage

4.1 Abstract

Various preservation solutions have been evaluated for longer hypothermic cartilage storage for tissue transplantation, however, the results are mixed. This research was to determine whether phosphate buffered saline (PBS) or organ preservation solutions would preserve both the extracellular matrix and chondrocytes of articular cartilage better than culture medium during refrigerated storage in the time frame that cartilage is stored for clinical use. Porcine cartilage plugs were stored, without the underlying bone, in culture medium with and without fetal bovine serum (FBS), PBS, Belzer's and Unisol solutions for 1 month at 4ºC. Metabolic activity was tested using a resazurin reduction method and matrix permeability was evaluated by measuring electrical conductivity. Storage in culture medium with 10% FBS was shown to provide good cartilage metabolic function for 7 days decreasing to about 36% after 1 month of storage. There was no significant difference between samples stored in culture medium with and without FBS after 1 month of storage ($p=0.5005$). Cartilage plugs assessed after 1 month of storage demonstrated less viability and higher permeability in alternative test solutions (PBS, Belzer's and Unisol) compared with culture medium ($p<0.05$). Refrigerated storage of cartilage in PBS and two solutions (Belzer's and Unisol) designed for optimal refrigerated tissue and organ storage results in loss of chondrocyte function and retention of matrix permeability. In contrast, significantly better retention of chondrocyte function and loss of matrix permeability was observed in culture medium.

Future research is focused on combining retention of chondrocyte function and matrix permeability by storage solution formulation.

List of Abbreviations

DMEM	Dulbecco's modified Eagle's medium
ECM	extracellular matrix
GAG	Glycosaminoglycan
FBS	fetal bovine serum
PBS	phosphate buffered saline

4.2 Introduction

Donated donor-derived osteochondral tissue grafts are typically harvested within 24 hours of donor death and banked at 4ºC for up to 42 days for repair of clinical cartilage defects. Cartilage plugs are employed in mosaicplasty procedures for smaller defects less than 3 cm wide and less than 1cm deep. Osteochondral allograft transplantation has been an effective treatment option with promising long-term clinical outcomes for larger focal posttraumatic defects in the knee for young, active individuals [196]. There were 15,797 allogeneic human articular cartilage procedures performed in the United States of America during 2006 [197]. It is anticipated that many more procedures would be performed if better cartilage preservation methods were available.

The duration of hypothermic refrigerated storage of osteochondral grafts is rather unusual. Although the cells in heart valve leaflets persist for weeks during hypothermic refrigeration in culture medium [198, 199], most tissues are refrigerated for only hours before significant loss of cell viability and tissue function occur. There are, however, reports supporting chondrocyte survival for days or weeks of hypothermic storage in their natural extracellular matrix in humans [200-203] and several animal species [203-212]. Because such survival was considered unusual, compared with other tissue types, we previously initiated research to assess the impact of 4ºC storage in DMEM culture medium on cartilage cell viability and establish whether or not cartilage plugs were an acceptable model compared with bisected femoral heads with both cartilage and bone tissue present [213]. We also included extracellular matrix (ECM) permeability evaluation during storage because prolonged storage of cartilage with viable cells might promote the release of enzymes that impact tissue material properties [213]. We found that storage in DMEM culture medium with 10% FBS provides good cartilage viability for 7 days. In addition, there was a marked tendency for cartilage plugs to demonstrate higher viability values than the femoral heads. However, 1 month storage of cartilage resulted in loss of both chondrocyte viability and ECM permeability [213].

Various preservation solutions have been evaluated for longer hypothermic cartilage storage, however, the results are mixed. Onuma et al. [205] compared DMEM, saline, EuroCollins solution, and UW solution to determine which provided the best hypothermic preservation of rat osteochondral tissues. They concluded that UW solution, an intracellular type solution, was the most suitable. In contrast, Teng et al. [212] clearly

demonstrated the positive impact of more complex culture media formulation upon chondrocyte survival such as DMEM, an extracellular type solution. There are other indications in the literature that media supplementation or modification, such as FBS supplement, might promote chondrocyte survival. However FBS supplement is also an issue for tissue bank products due to FBS batch variation and the associated health risks [212, 214]. To date, extensive research is still needed to determine what type of solution is best for chondrocyte preservation in cartilage and to define the optimal solution composition.

Therefore, the purpose of the research presented in this manuscript was further investigation of cartilage cell and biomaterial properties during storage in a common culture medium, hypothermic solutions designed for cell, tissue and organ storage and a commonly used salt solution. Moreover, the effect of FBS supplement on cartilage cell viability was examined during storage in common culture medium. Improved storage solutions could result in increased utilization of banked allogeneic cartilage for reconstruction of articular cartilage defects and possibly storage and distribution of tissue engineered cartilage.

4.3 Materials and Methods

Specimen Preparation

Articular cartilage, 2-3 mm thick, was obtained from the femoral weight bearing condyles of animals after they were sacrificed for other experimental studies (bona fide excess tissues). Bona fide excess tissue is a term used to describe animal-derived

materials obtained from animals after they have been sacrificed for other uses. Pig knees were procured from skeletally immature domestic Yorkshire cross farm pigs (30-60 Kg, aged 4-8 months) at the conclusion of other Institutional Animal Care and Use Committee approved research projects at the Medical University of South Carolina. These pigs were skeletally immature, and maturity is achieved at weights >200 kg and 2 years of age. The knees were placed in zip lock bags with an iodine solution and transported on ice to our laboratory for aseptic dissection.

Study 1: Effect of FBS Supplement

In the first set of experiments porcine femoral cartilage consisting of 6mm cartilage plugs without the underlying bone were stored in high glucose (25mM) Dulbecco's Modified Eagle Medium (DMEM, Cat. #01-017 without sodium pyruvate, Mediatech, Manassas, VA) with and without 10% fetal bovine serum (FBS, JR Scientific, Woodland, CA) for 0 (fresh untreated control), 1 week or 1 month at 4ºC. Cell viability was examined at each storage time. Cartilage plugs from two donor pigs were harvested for this study. There were six cartilage plugs for each tested group.

Study 2: Effect of Storage Solution

In the second set of experiments, 6mm cartilage plugs were stored in DMEM with 10% FBS, Belzer's Solution (SPS-1, Organ Recovery Systems, Inc., Itasca, IL), Unisol (Cell & Tissue Systems, Charleston, SC), and phosphate buffered saline (PBS) for 1 month at 4ºC. Formulations of the SPS-1 and Unisol solutions are listed in Table 1. The media were changed weekly. Cartilage plugs from four donor pigs were used in this

study and were mixed and randomly assigned to each tested group. The cell viability of cartilage plugs was examined during a 4-day recovery period after 1 month of hypothermic storage. The cartilage plugs were recovered in DMEM with 10% FBS at 37 ºC. There were twenty cartilage plugs for each tested group in each experiment. The tissue matrix permeability before and after 1 month hypothermic storage was examined using the electrical conductivity method. There were twenty cartilage plugs for each tested group.

Viability Assessment

Chondrocyte metabolic activity was assessed using the resazurin reduction method. The resazurin reduction assay incorporates a water soluble fluorometric viability oxidation-reduction (REDOX) indicator which detects metabolic activity by both fluorescing and changing color in response to chemical reduction of the growth medium. Metabolically active cells reduce resazurin to fluorescing resorufin [215]. Fresh control and hypothermically stored tissue samples were placed in 37°C culture conditions for 1 hour to permit adjustment to tissue culture conditions in DMEM plus 10% FBS. The tissues were then incubated for three hours with resazurin working solution, after which aliquots of medium were placed in microtiter plate wells and read on a microtiter plate spectrofluorometer at a wavelength of 590 nm. The data is expressed as the mean ± standard deviation relative fluorescent units after subtraction of baseline florescence from incubation controls containing the same amount of culture medium and resazurin reagent without tissue.

Biomaterial Testing

Cartilage plugs were also evaluated for permeability by measuring their electrical conductivity to determine if cartilage matrix characteristics were being altered during storage. Specimens were prepared by cutting a 5mm cylindrical plug using a corneal trephine from the stored 8mm diameter cartilage discs. The samples were tested after 0 and 1 month of storage, the cartilage surfaces were trimmed manually using a sharp blade. The average height after trimming was 1.53 ± 0.27 mm. Then conductivity was tested, first in isotonic PBS and then after swelling in hypotonic saline (0.2xPBS). The electrical conductivity was measured based on the principle of a four wire resistance test using a Keithley Sourcemeter (Model 2400, Keithley Instruments, Inc., Cleveland, OH) and a custom designed conductivity chamber reported previously [153, 213]. Briefly, the conductivity apparatus consists of two stainless steel current electrodes coaxial to two Teflon-coated Ag/AgCl voltage electrodes placed on the top and bottom of a cylindrical nonconductive Plexiglass chamber (5mm diameter). The specimen was placed inside the chamber for measurement. The resistance (R) values across the specimens were measured at a low, constant DC current density of 0.015 mA/cm^2. The height of the specimen was measured with an electrical current sensing micrometer. The electrical conductivity (χ) values of the specimens were calculated by:

$$\chi = \frac{h}{R \cdot A}$$

8

where h and A are the height and cross-sectional area of the specimens, respectively. The precision for the resistance measurements was 0.5 Ω while the height measured with an accuracy of ±1.0 μm. All electrical conductivity measurements were performed at room temperature (22°C).

Electrical conductivity is a material property of biological tissues. Its value is related to the diffusivity of small ions in the tissue, which depend upon tissue composition and structure [216, 217]. Using an electrical conductivity method, the effect of matrix composition on solute permeability has previously been studied in hydrogels and cartilaginous tissues [218, 219]. In this study, we adopted this method to study the impact of 4ºC storage on cartilage ECM solute permeability. It could be considered that the measured electrical conductivity mainly represents the tissue property since chondrocytes normally occupy 1-10% volume of articular cartilage [220]. Moreover, the transport of small solutes (e.g., ions, oxygen, and glucose) within avascular cartilage tissues mainly depends on diffusion [221]. Therefore, electrical conductivity was selected in addition to cell viability in order to evaluate tissue ECM changes that may affect nutrient transport ability as well as mechanical function *in vivo*.

Statistical Analysis

The measurements were presented as mean ± standard deviation. One-way ANOVA with Tukey's post hoc analysis ($p<0.05$) was conducted to determine

differences in mean values of cell fluorescence units and electrical conductivity. In Study 1, the effect of FBS supplementation on cell viability (n=6) was examined. In Study 2, the effect of storage solution on cell viability (n=20), as well as on electrical conductivity (n=20), were examined. SPSS 16.0 software (SPSS Inc., Chicago, IL) was used for all statistical analyses and significant differences were reported at p-values < 0.05.

4.4 Results

In Study 1, the effect of FBS supplementation on chondrocyte metabolic activity was assessed using the resazurin reduction method and results are shown in Figure 18 below. After 7 days storage, the chondrocyte metabolic activity of cartilage plugs stored in DMEM medium with 10% FBS was not significantly different from the value of fresh controls (p=0.3879), while the metabolic activity of cartilage plugs stored in DMEM medium without 10% FBS was significantly lower than the value of fresh controls (p=0.0339). Extended storage reduced the cartilage metabolic activity. The metabolic activity of cartilage samples dropped to about 36% of the value of the fresh controls after 1 month of storage. There was no significant difference between samples stored with and without FBS after 1 month of storage (p=0.5005).

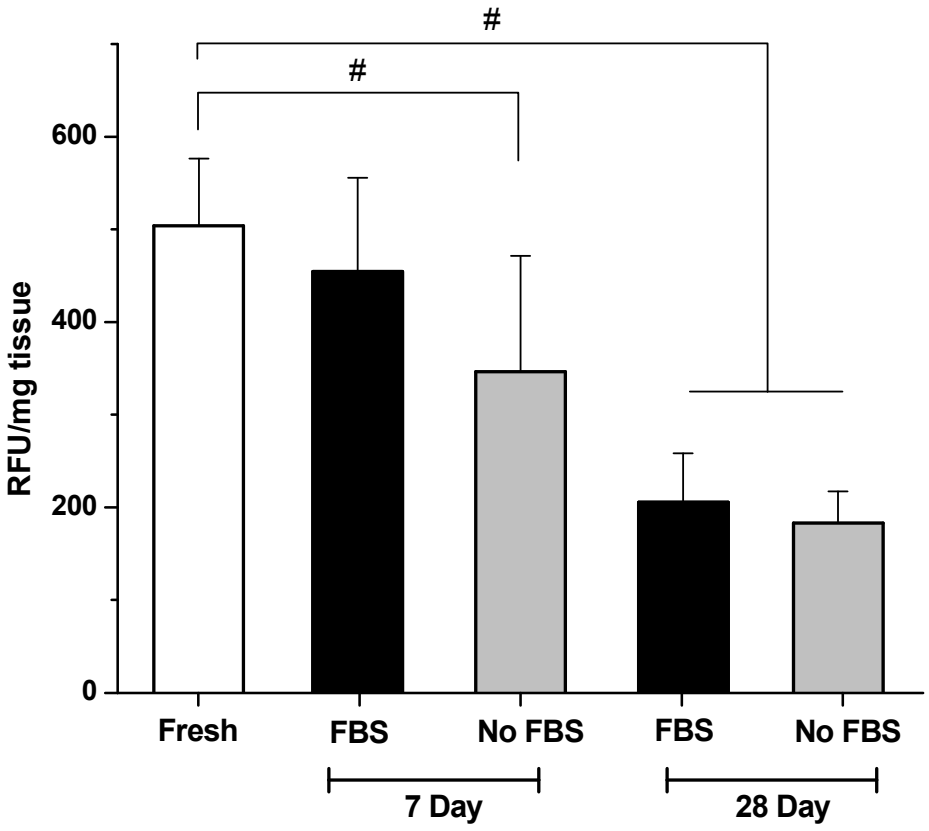

Figure 18 Chondrocyte viability assessed by resazurin reduction reaction Chondrocyte viability during cartilage plug hypothermic storage in culture medium with (open bars) and without FBS (cross hatched bars) assessed by the resazurin reduction metabolic assay (n=6). The data shown are means ± standard deviations. # indicates significant difference compared to fresh controls at $p<0.05$.

In Study 2, cartilage samples were stored at 4ºC for 1 month in three solutions and culture medium with 10% FBS followed by cell metabolic activity and matrix permeability evaluations. All solutions resulted in decreased chondrocyte viability after 1 month of storage (<21% of fresh controls), however, during 4-day follow-up evaluations under cell culture conditions culture medium supplemented with 10% FBS resulted in

significantly higher viability compared with the three alternative solutions starting at day-2 ($p<0.0081$) reaching fresh control viability values on day 4 (Figure 19 below).

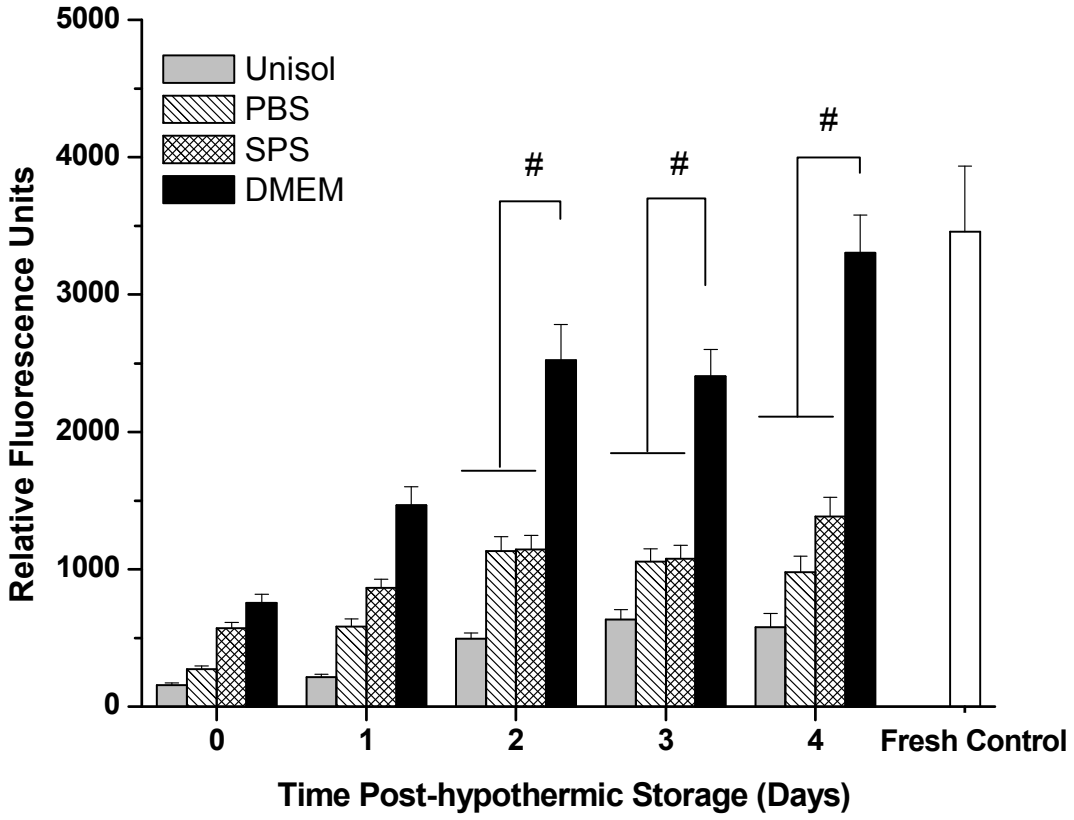

Figure 19 Comparison of chondrocyte metabolic function by resazurin reduction during 4-day recovery period after 1 month of hypothermic storage Comparison of chondrocyte metabolic functions after storage in intracellular-type and extracellular-type solutions (n=20). Function was assessed by the resazurin reduction metabolic assay data expressed as the mean ± standard deviation. # indicates significant difference compared to the DMEM containing 10% FBS group at $p<0.05$. Significant differences were observed between DMEM containing 10% FBS and the other alternative solutions starting at day 2. DMEM containing 10% FBS achieved progressive increases in cell viability reaching control levels at day 4. Fresh control values are shown at the right side of the figure.

Simultaneously, samples were prepared for matrix permeability assessment using the electrical conductivity method. When the plugs were tested in the isotonic saline, significant differences in electrical conductivity were observed between the control and plugs stored in culture medium with FBS ($p=0.0078$), Unisol ($p=0.0034$), and SPS ($p=0.0068$) (Figure 20a below). The differences in isotonic solution were small, however they were statistically significant and were magnified when the samples were subsequently swollen in hypotonic solution for testing (Figure 20b below). The electrical conductivity of samples stored in culture medium was lower than the values of the samples stored in the other storage solutions ($p<0.0001$) and only about 60% of the fresh control (Figure 20b below).

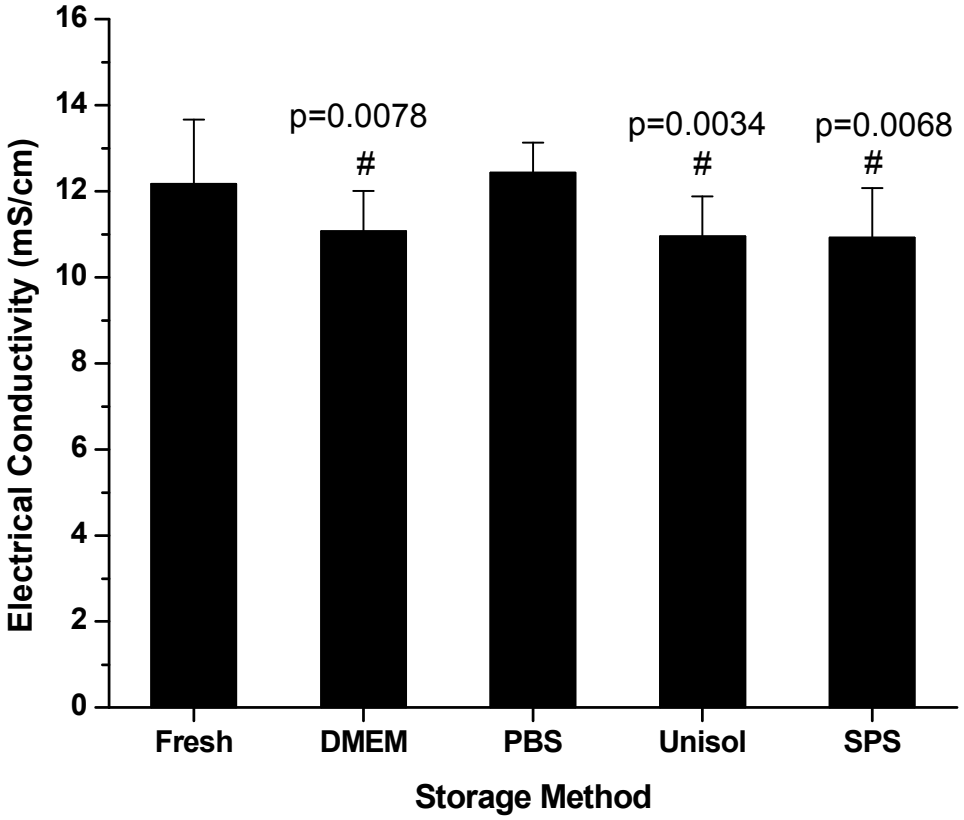

(a) Isotonic conductivity

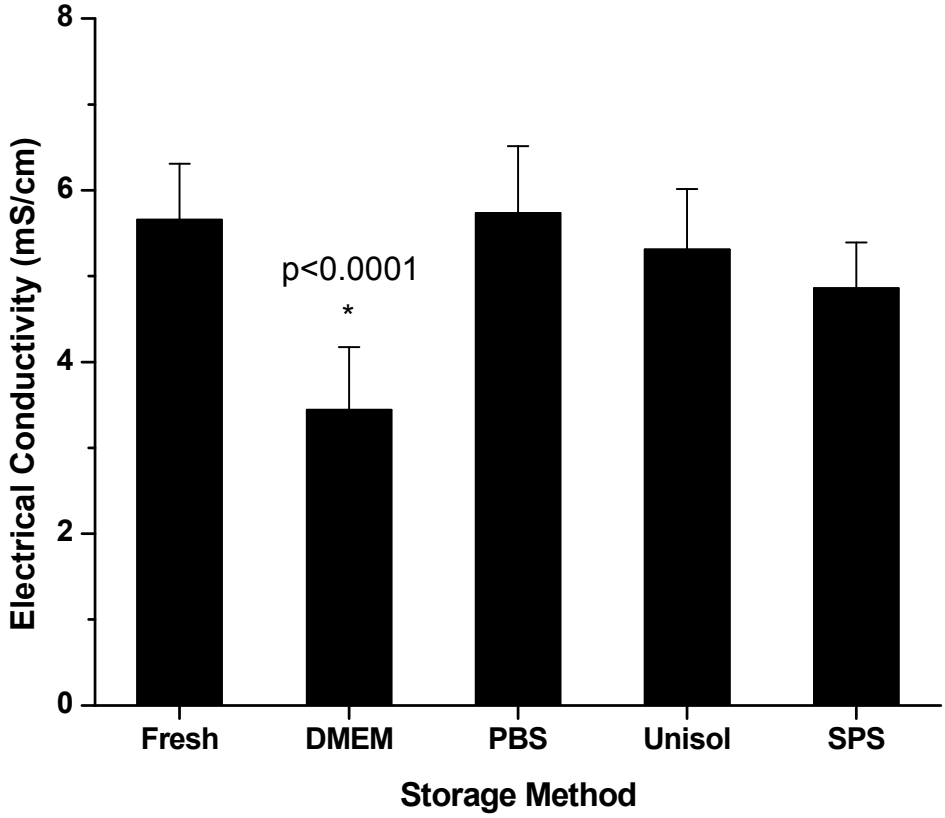

(b) Hypotonic conductivity

Figure 20 Electrical conductivity of cartilage plugs after 30 days based on storage method compared with control fresh samples.
Impact of hypothermic storage of cartilage in intracellular-type and extracellular-type solutions on electrical conductivity in A) isotonic saline and B) hypotonic saline (n=20). The data is expressed as the mean ± standard deviation and # indicates significant differences compared to Fresh Control at $p<0.05$. * indicates significant differences between the DMEM containing 10% FBS group and the other groups at $p<0.05$. In hypotonic saline, the electrical conductivity of samples stored in DMEM containing 10% FBS is lower than the values of the samples stored in the other storage solutions ($p<0.0001$) and only about 60% of the fresh control.

4.5 Discussion

Chondrocyte viability at the time of implantation is an important factor in ensuring long-term allograft survival *in vivo* [222, 223]. Commercially available fresh osteoarticular allografts are stored for at least seventeen days to allow serologic and microbiologic testing prior to implantation because of concerns about potential infection [200, 224]. We found, in agreement with our prior study [213], that storage in DMEM culture medium with 10% FBS provides good cartilage viability for 7 days. In that study [213], we compared the assay employed in the present study with Trypan blue. The metabolic assay provided higher cell viability values at 7 days than Trypan blue, by 28 days the results using the two assays were similar with less than 30% cell viability. Our interpretation of the results was that many of the chondrocytes may have been damaged at 7 days, resulting in loss during the cell isolation procedures employing collagenase required prior to the determination of cell viability using Trypan blue. This may also explain concerns previously expressed regarding the use of fluorescent assays for cartilage storage studies [225]. It is possible that the metabolic assay at this time point is an accurate measure of potential viability if the tissues were implanted rather than subjected to collagenase digestion. The Trypan blue-excluding cells from fresh and both 7- and 28-day-stored tissues were also able to proliferate. Qualitatively similar appearing cultures were obtained after 1 week under physiological conditions provided that consistent numbers of Trypan blue excluding cells were plated.

The presence of FBS improved cell survival after the first week of storage, but there was no difference in cartilage viability between samples stored with and without

FBS after 1 month storage (Figure 18). This last observation leads us to believe that with further culture medium supplementation, it may be possible to remove FBS from osteochondral storage solutions reducing concerns about FBS batch variation and the associated health risks [212, 214].

Comparison of tissue metabolic activity after hypothermic storage in solutions employed for organ and tissue storage (SPS-1 and Unisol), complex DMEM culture media supplemented with FBS, and simple PBS yielded unanticipated results (Figure 19). Belzer's solution (SPS-1) and Unisol are both examples of "intracellular-type" preservation solutions which are typically hypertonic and formulated to restrict the passive exchange of water and ions during hypothermia-induced inhibition of cell membrane pumps (reviewed, [226]). An intracellular-type solution usually includes a non-permeating anion such as lactobionate or gluconate to partially replace chloride ions in the extracellular space. This provides osmotic support to balance the intracellular oncotic pressure generated by cytosolic macromolecules and their associated counter-ions locked inside the cell. In contrast, saline and culture media are "extracellular-type" solutions [226]. They are isotonic with a plasma-like complement of ions that mimics the normal extracellular environment of cells. Culture media contain a more complete complement of ions, amino acids and other metabolites that mimic the extracellular composition of plasma while providing nutritional support. PBS is a simple formulation consisting of salts and a buffer without nutritional components. Prolonged hypothermic storage of cells and tissue in extracellular media usually results in cell swelling, due to cold inactivation of membrane pumps, and cell death [226].

Most published studies on cartilage hypothermic storage have employed extracellular type solutions. However, Onuma et al. [205] compared DMEM, saline, EuroCollins and Belzer's solutions to determine which provided the best hypothermic preservation of rat osteochondral tissues. They concluded on the basis of two assays and histology that Belzer's solution (SPS-1) was the most suitable. In contrast, Teng et al. [212] clearly demonstrated the positive impact of more complex culture media formulation upon chondrocyte survival, such as DMEM, especially when supplemented with insulin growth factor-1 or an apoptosis inhibitor (Z-VAD-fmk). Our results confirm that complex extracellular-type culture media are best for maintenance of chondrocyte functions, which we have previously shown to correlate with cell survival by trypan blue [213]. The three alternative solutions, compared to DMEM, resulted in less metabolic activity after one month that achieved statistical significance during follow-up recovery incubation under physiologic tissue culture conditions. The resazurin metabolic assay has an advantage over other more commonly employed assays of being non-cytotoxic, so the same piece of tissue can be assayed several times as we have done in this study (Figure 19). Single time point use of the resazurin assay may be hard to interpret due to fluxes in metabolic activity during recovery from experimental insults or delayed cell death. This could lead to high readouts compared to assays such as Trypan blue [Brockbank et al., 2011b]. Alternatively, as already discussed, the differences observed could be due to reversibly damaged cells that are being further damaged by the isolation procedure required prior to Trypan blue evaluation. A deficiency of the resazurin assay in contrast with intracellular viability indicators using florescent microscopy methods is

that the assay does not discriminate between cartilage zones, so the results obtained with this assay are the mean of the entire sample. An alternative way to express our data is to measure DNA content, after the tissue digestion, and estimate the number of cells present using the conversion 7.7 pg DNA per cell [Kim et al. 1988] and then extrapolate the relative metabolic activity per cell. We have expressed the resazurin results in relative florescent units per mg dry weight of tissue. Future experiments are planned to determine whether the recovery observed in the culture medium group is due to cells recovering from reversible injuries or proliferation.

However, when cartilage permeability was assessed the three alternative solutions all resulted in better retention of permeability in marked contrast with the significant permeability decrease observed for complex extracellular-type media stored cartilage (Figure 20b) [213]. The values of the electrical conductivity in this study are comparable to those in the literature for articular cartilage [Hasegawa et al. 1983]. The electrical conductivity (11.51±0.73 mS/cm) of porcine articular cartilage measure in this study is higher than the values (6-10 mS/cm) of human articular cartilage [Hasegawa et al. 1983]. The higher electrical conductivity in young porcine articular cartilage is likely due to higher tissue porosity (water content) compared with that in human articular cartilage. The value of electrical conductivity is related to the diffusivity of small ions in the tissue, which depends upon tissue composition and structure [216, 217]. Using an electrical conductivity method, the effect of matrix composition on solute permeability has previously been studied in hydrogels and cartilaginous tissues [152, 218, 219]. These studies show that the electrical conductivity is positively correlated with tissue porosity

(i.e., water volume fraction) in cartilaginous tissues (e.g., articular cartilage, intervertebral disc, and temporomandibular joint disc). This may be attributed to an increase of ion diffusivities with porosity. The hydration/porosity of articular cartilage is maintained by the GAG content through the osmotic swelling mechanism. The fixed negative charge on the GAGs attracts counter-ions and gives rise to Donnan osmotic pressure that favors tissue hydration [216, 217]. This fixed charge induced Donnan osmotic swelling is more significant in hypotonic conditions. A decrease of fixed charge density due to a decrease of GAG content will reduce tissue porosity, resulting in a decrease of electrical conductivity. It has been shown that the trypsin treated porcine annulus fibrosus has a lower porosity and electrical conductivity compared to the control group [Gu et al, 2002]. In this study, for complex extracellular-type media stored cartilage, the decrease of the electrical conductivity may be due to the decrease of the porosity caused by the decrease of the GAG content. Maintenance of living metabolizing cells in this group of cartilage may lead to production of functional enzymes that subsequently degrade the ECM, decreasing its GAG content. In the future, the change of tissue porosity and GAG contents in stored cartilage needs to be further determined.

Cartilage tissue is comprised of a solid and fluid phase and it may be treated as a biphasic material [156]. Cartilage executes its biomechanical role in the body to absorb and distribute joint stresses based on the mechanism of fluid pressurization [227]. Therefore, the permeability characteristic is an important mechanical property of cartilage that is often overlooked in contrast to more commonly studied tensile or compressive parameters. Studies of such biomechanics parameters in the literature have

consistently failed to demonstrate any changes in cold stored cartilage. We previously observed extracellular matrix damage in frozen articular cartilage using laser scanning microscopy [228] and permeability deterioration during hypothermic storage of cartilage [213]. Permeability changes were observed during both isotonic and hypotonic testing, and the differences were greater in hypotonic saline than in isotonic saline. Hypotonic solution made the tests more sensitive due to increased tissue swelling which magnified changes in the highly charged ECM [153].

Our working hypothesis to explain the new permeability data is that maintenance of living metabolizing cells in the cartilage leads to production of functional enzymes that subsequently degrade the ECM, decreasing its permeability. The rationale for this is that none of the three solutions that resulted in retention of permeability supported cell functions to the same degree as culture medium. Experimental enzyme treatment with trypsin has been previously shown to alter the permeability of intervertebral discs [153, 229]. Further experiments designed to determine whether release of endogenous enzymes, metalloproteinases, results in cartilage permeability changes are in progress. Biochemical assays are also included to directly measure biochemical composition (e.g., water, collagen, and GAG content) changes. Laser scanning microscopy [228] and RAMAN spectroscopy [230] may also provide useful information on changes in collagen structure during hypothermic storage.

Table 3 Formulations of intracellular-type solutions used for cartilage storage.

Components (mmol/L)	*Unisol I*[a]	*SPS-1*
Ionic		
Na^+	62.5	30
K^+	70.0	125
Ca^{++}	0.05	-
Mg^{++}	15.0	5.0
Cl^-	30.1	-
SO_4^-	-	5.0
pH buffers		
$H_2PO_4^-$	2.5	25
HCO_3^-	5.0	-
HEPES	35.0	-
Impermeants		
Lactobionate$^-$	30.0	100
Sucrose	25.0	-
Mannitol	25.0	-
Glucose	5.0	-
Gluconate	70.0	-

Raffinose	-	30
Colloids		
Hydroxyethyl Starch	-	50g/L
Pharmacologics		
Adenosine	2.0	5.0
Glutathione	3.0	3.0
Allopurinol	-	0.136g/L
Osmolality (mOsm/Kg)	350	320
pH	7.6	7.4

5 Fixed Charge Density in Human TMJ Discs

5.1 Abstract

The TMJ disc has been found to have roughly 5% ~ glycosaminoglycan (GAG) by dry weight with chondroitin sulfate and dermatan sulfate being the primary GAGs. In cartilage, fixed charge density (FCD) results from the negative charges on the end of GAG chains. It has been shown during tissue degeneration that GAGs are depleted resulting in the loss of mechanical function in cartilage. In the TMJ disorders (TMDs), tissue degeneration causes the disc to become displaced resulting in mechanical dysfunction of the jaw. The aim of this research was to determine the amount of FCD present in the human TMJ disc and compare the significance to other types of cartilage which have been well characterized.

Human postmortem tissues were used for all TMJ disc specimens, six female and six male. The fixed charge density was determined using a two conductivity method developed by Jackson et al. [231]. A blyscan biofluorescence assay was used to determine glycosaminoglycan (GAG) content by dry weight.

The total average FCD (mean ± SD) of the human TMJ disc was 0.050 ± 0.018 (mEq charge/g wet tissue), while male FCD was 0.053 ± 0.017 (mEq/g) and female FCD was 0.046 ± 0.018 (mEq/g) with no significant difference (p=0.325). Even though the intermediate region had the lowest FCD 0.041 ± 0.015 (mEq/g), no significant difference was found between regions (ANOVA with Tukey's Post Hoc, p=0.673). The total GAG content as % dry weight was 1.65% ± 0.64, where male GAG content was 1.66% ± 0.59

and female GAG content was 1.63% ± 0.72 (with no regional significant difference, p=0.91).

Our results were comparable to FCD values of other fibrocartilaginous tissues. Previous reports indicate the value of bovine lumbar annulus fibrosus (AF) FCD as 0.060 mEq/g compared to 0.050 mEq/g for the TMJ disc in this study and 0.09 mEq/g for porcine articular cartilage tested in this study. The corresponding GAG contents by dry weight were 5.4% for annulus fibrosus, 1.65% for TMJ disc and 21.8 % for articular cartilage control sample from the femoral head of porcine knee. The role of FCD in the TMJ disc may not be as significant as many other cartilages such as hyaline which are involved in primarily compressive load support.

5.2 Introduction

TMJ disorders (TMDs) have an age of onset between 25-45 years, much earlier than degenerative changes in other joints (~55 years). In addition, TMDs affect twice as many women as men. Symptoms include clicking and popping of the jaw and pain in the craniofacial region (NIDCR). Severe cases of TMJ disorder can result in disc displacement. In over 70% of these cases, disc displacement arises due to disc degeneration brought on by a change in the material properties of the disc which inhibit the disc from carrying out normal biomechanical function [5, 16]. These changes can involve enzymatic degradation of collagen and glycosaminoglycans (GAGs), major extracellular matrix proteins responsible for mechanical function.

Cartilage has a unique concentration of proteoglycans with long GAG chains containing a high density of negative charges. This is responsible for high fixed charge

density per unit volume of tissue in some types of cartilage, such as articular cartilage and nucleus pulposus (NP) of the intervertebral disc (IVD). The fixed charge density gives cartilage a high osmotic swelling pressure, which allows cartilage to absorb and distribute large forces without injury to cells within cartilage and also the articular surfaces of joints [68, 101, 232, 233]. The fixed charge density is also responsible for electrokinetic effects such as streaming potential. These electrokinetic phenomenon can have significant influence on cartilage behavior from the diffusion of nutrients within the tissue to cell signaling based on physicochemical signals at the cellular level [94-101]. These unique properties have been demonstrated in other types of cartilages. This has led to a better understanding of how articular cartilage maintains its ECM in response to load and while elucidating cell response to macroscopic ECM generation. In some cases, the depletion of FCD has been used as a marker for tissue degeneration [68]. In this study, the FCD is investigated in order to better understand the TMJ disc behavior as cartilage. By understanding the role FCD plays in TMJ disc function and behavior, we can better understand the nature of TMJ disc degeneration in TMJ disorders.

The TMJ disc is a dense, avascular fibrocartilage which receives nutrients by diffusion. Bruxism or other mechanical insult to the tissue could result in a significant reduction of available nutrients within the tissue. In the past, we have measured the diffusivity of small ions and nutrients (Glucose and Oxygen) under mechanical strain within the tissue while considering the TMJ disc to be an uncharged tissue [61, 62]. Recently, however, we have begun to investigate the effect of the charged matrix on disc mechanical behavior as well as response to nutrient diffusion under load. Other types of

cartilage have been shown to contain a highly charged matrix owing to the large proteoglycan content within the tissue. This material property has provided key insights into tissue behavior [96, 101, 234].

The TMJ disc acts to distribute contact stresses between the mandible condyle and glenoid fossa while lubricating the joint. The motion and function of the TMJ disc is unique compared to other joints which give rise to the TMJ disc's unique biochemical composition. The TMJ disc is composed of 85-95% (dry weight) type I collagen with a significant amount of proteoglycan 3-5% (dry weight) [234]. This is significantly different from articular cartilage which has been well characterized and contains mainly Type II collagen ~60% (dry weight) and proteoglycans, 25-35% (dry weight) [69].

In triphasic models of cartilage, the tissue is comprised of a solid (collagen and proteoglycan), fluid and ion phase (fixed charges in the GAG matrix along with small ions suspended in the interstitial fluid). The role of mechanical loading support is not only defined by the solid-interstitial fluid reaction, but must be considered as an ion exchange medium in which fixed negative charges within the matrix resist fluid exudation and support load through high osmotic swelling pressure [59, 68, 95-99, 101, 153, 232, 235]. Collagen fibers retain the proteoglycans and resist the cartilage's natural swelling pressure. Many cartilage degeneration models investigate the loss of proteoglycan content or loss of collagen content and its effect on tissue function and further degeneration. The FCD is responsible for as much as 50% of the loading in the joint, with the loss of fixed charge density being a key bio indicator of degeneration [98].

The FCD is due to proteoglycan proteins which are heavily glycosylated. These large proteins are synthesized by chondrocytes and in the case of TMJ tissue unique fibrochondrocyte-like cells [26]. Proteoglycans are composed of a core protein covalently connected to one or more linear polymers of disaccharides known as glycosaminoglycans (GAGs). The GAG chains have a sulfated end group which gives the proteoglycan the fixed negative charges at the end of the brush like structures. Chondroitin sulfate and dermatan sulfate are the primary sulfated groups that have been measured in the TMJ disc [234]. Research has shown a higher concentration of proteoglycans within the intermediate region of the TMJ disc, where the disc is believed to maintain a role in compressive load support.

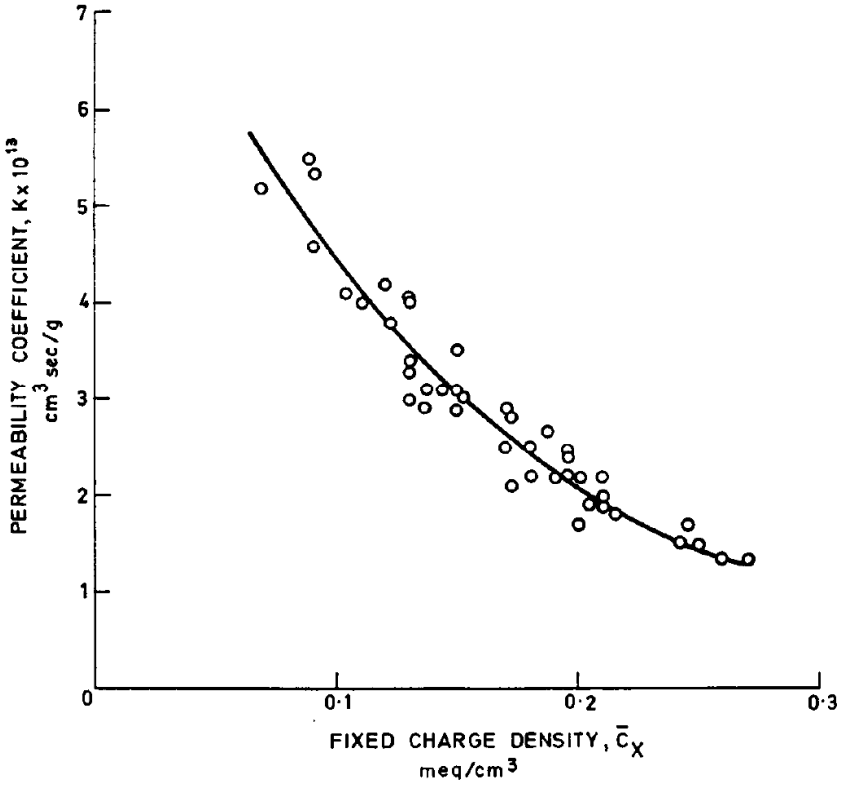

Figure 21 The effect of fixed charge density on the solute permeabilities in cartilage
This figure is taken from Maroudas et al. seminal work investigating cartilage as an ion exchange material where charged ions balance a charged matrix [101].

The interaction between the solid, fluid and charged solid matrix of cartilage has been well studied in hyaline cartilage of the knee, the intervertebral disc IVD in the spine as well many other articular surfaces in the hip and shoulder [101, 232, 235-238]. But to our knowledge, the role that the fixed negative charges play in the TMJ disc has not been investigated. The objective of this study was to determine the fixed charge density of human TMJ disc in order to understand the role the FCD plays in TMJ disc biomechanical function. In addition, the FCD will be used in our triphasic model of the TMJ disc in order to simulate the influence of FCD on mechanical function and transport

behavior of the tissue (see Figure 21 above [94, 97, 232]. This will allow us to predict the in vivo mechanical and nutrient environment within the disc [95, 99].

Theoretical Background:

In the past, a radioisotope method was used to track the attraction of isotopes to the charged proteoglycan matrix. But given the increased accuracy of sintered electrodes and high impedance sourcemeters, a proven conductivity approach was used in place of radioactive materials [231].

An electrical conductivity approach was taken to measure the fixed charge density (FCD) of the human TMJ disc [61, 62, 101, 153, 218, 231, 239, 240]. The method used in this study employed a two point conductivity measurement approach developed by Jackson et al. [231]. This approach used the rationale that the fixed charge density of a tissue specimen will remain constant in two bathing solutions with different salt concentration. The conductivity of the tissue specimen was measured in isotonic bathing solution, then equilibrated in hypotonic solution and measured again in a hypotonic bathing solution. The measured conductivities in each bathing solution along with the known ionic concentrations of bathing solution were used to calculate the FCD described below.

Conductivity of a specimen

The conductivity of a tissue specimen is given by:

$$\chi = \frac{h}{R \cdot A}$$

9

where specimen height and area are given by h and A, respectively and Ω is the measured resistance of the tissue. The conductivity of the tissue (χ) is related to the solute diffusivities (D^i, i= D^+, D^-) within the tissue by (Helfferich, 1962):

$$\chi = F_c^2 \phi^w (c^+ D^+ + c^- D^-) / RT$$

10

where F_c is the Faraday constant, R is the gas constant, c^+ is the cation ion concentration and c^- is the anion ion concentration. For negatively charged tissues to maintain equilibrium with the KCl solution, the following electroneutrality condition must be satisfied within the tissue:

$$c^+ = c^- + c^F$$

11

where c^+ is the cation concentration, c^- is the anion concentration and c^F is the absolute value of the fixed charge density assuming a negatively charged tissue containing proteoglycans. In addition to electroneutrality condition, Donnan equilibrium must be satisfied between charged ions within the tissue (c^+ and c^-) and the external bathing solution ion concentration (c^*):

$$(c^*)^2 = c^+ \cdot c^-$$

12

From electroneutrality and the ideal Donnan equation, the ion concentrations can be calculated by:

$$c^+ = \frac{c^F + \sqrt{(c^F)^2 + 4(c^*)^2}}{2} \qquad c^- = \frac{-c^F + \sqrt{(c^F)^2 + 4(c^*)^2}}{2}$$

13

The equation for the ion concentrations can be substituted in the conductivity equation with respect to diffusivity (Helfferich, Ion Exchange 1962):

$$\chi_2 = \frac{F_c^2 \phi^w}{RT} D\sqrt{(c^F)^2 + 4(c_2^*)^2} \qquad \chi_1 = \frac{F_c^2 \phi^w}{RT} D\sqrt{(c^F)^2 + 4(c_1^*)^2}$$

14

where χ_1 is the conductivity of the specimen in isotonic bathing solution (0.1M KCl) and χ_2 is the conductivity of the specimen in hypotonic bathing solution (0.03M KCl). The bathing solution concentrations are c_1^* for isotonic solution and c_2^* for hypotonic concentration (molar). Although conductivities are different in two bathing solutions, the fixed charge density, c^F, remains the same provided there is no swelling. Using these two equations and D^i, i= D^+, D^- for KCL allowing the diffusivites to cancel, therefore c^F can be expressed as:

$$c^F = 2\sqrt{\frac{\chi_1^2[(c_1^2)-(c_2^2)]}{[\chi_1^2-\chi_2^2]}-(c_1^*)^2}$$

15

The fixed charge density was calculated from Equation 15 above and compared to the GAG content for each region [231].

5.3 Materials and Methods

Sample preparation

Human postmortem tissues were used for all TMJ disc specimens. A total of 6 female and 6 male joints were dissected in accordance to the MUSC anatomy guidelines with IRB approval. The right TM joint was removed while leaving the joint compartments intact. Specimens were wrapped in cellophane with KCL soaked gauze, placed into a zip lock bag, and stored at -20 for later dissection. Discs were visually inspected for signs of trauma or degeneration; only healthy discs were used in the experiments. Each region of the disc (Anterior, Posterior, Lateral, Intermediate and Medial) were sampled from the disc using a 5 mm diameter trephine, see Figure 22. The cylindrical samples were then microtomed (Leica, Germany) to remove natural biconcavity of the sample and to remove the superficial layer of tissue. This ensured flat, concentric surfaces on the ends of the cylindrical specimen for conductivity measurements. After the samples were microtomed, they were immediately measured for height using a custom designed current sensing micrometer to prevent compressing the sample while measuring. The height was recorded before the samples were measured for

water content. In addition to TMJ discs, articular cartilage from the porcine femoral heads (n=6) was used as a control sample

Water Content

The water content was measured as water volume fraction reported previously, (Yao and Gu et al. 2002). The weight of the specimens was recorded in air W_{wet} and then KCl (W_{KCl}) using a density determination kit and analytical balance (Satorious YDK01, Germany). After the electrical conductivity measurement, the specimens were lyophilized and the dry weights were recorded, W_{dry}. Using Archimedes principle and the biphasic assumption, the water volume fraction was determined by (Gu et. al 1996):

$$\phi^w = \frac{W_{wet} - W_{dry}}{W_{wet} - W_{KCL}} \frac{\rho_{KCL}}{\rho_w} \quad \textbf{16}$$

where ρ_{KCl} is the mass density of KCl (1.007 g/ml), and ρ_w is the mass density of water.

Conductivity measurement

Conductivity of the samples was measured using a custom designed conductivity chamber based on the 4-wire method. All samples were equilibrated in 0.15 KCL 4 hours prior to measuring conductivity. The chamber was made of two 5 mm diameter stainless steel reference electrodes and two Ag/AgCl sintered wires (0.52 mm diameter) as measuring electrodes coaxial to the reference electrodes (Figure 22b below). A Keithley 2400vSourcemeter (Kansas City) was used to deliver a 0.015 mA/cm^2 current density while measuring the resistance of the tissue in Ohms. After measurements of the

tissue were recorded in isotonic solution, the samples were placed in hypotonic KCL (0.03M KCL) and allowed to equilibrate for 24 hours. The samples were then measured for height, air and KCL weight to determine if swelling had occurred. Statistical comparison (t-test) indicated no significant swelling. A second conductivity reading was taken under 0.015 mA/cm^2 current density in hypotonic bathing solution (see Table 4 for conductivity steps). Samples were then lyphilized and dry weight was measured for water content calculation.

Biochemistry

A blyscan biofluorescence assay was used to determine glycosaminoglycan (GAG) content by dry weight. A 2 ± 0.1 mg sample was removed from each lyphilized sample. The 2 mg dry tissue was digested in 1.5ml of Papain solution in a 1.5 ml centrifuge tube at $65C^0$ for 48 hours. Blyscan dye was added to the solution to bind with available GAG. The samples were centrifuged at 12,000 rmp to remove GAG from suspension. The supernatant dye was poured off the GAG pellet from the centrifuge tube and 1.0 ml Blyscan reagent was added to suspend the GAG again. A 200μL sample was removed from the centrifuge tube and added to a 96 well plate. The well plate was read using FLUOstar Optima fluorescent plate reader (Isogen, Netherlands) at 660λ. GAG concentrations for each sample were determined using a standard calibration curve to correlate fluorescence units to GAG content (dry weight).

Statistical analysis

A one-way ANOVA statistical analysis was conducted using SPSS statistics software to determine if significant differences existed between regions of the disc, groups (male and female). A Shapiro-Wilk test for normality was run before conducting ANOVA for regional group, with normality being determined. A confidence interval of 95% was used to report significant differences ($p<0.05$). A linear regression was also performed to determine if there was a correlation between FCD, GAG, Age and Water Content.

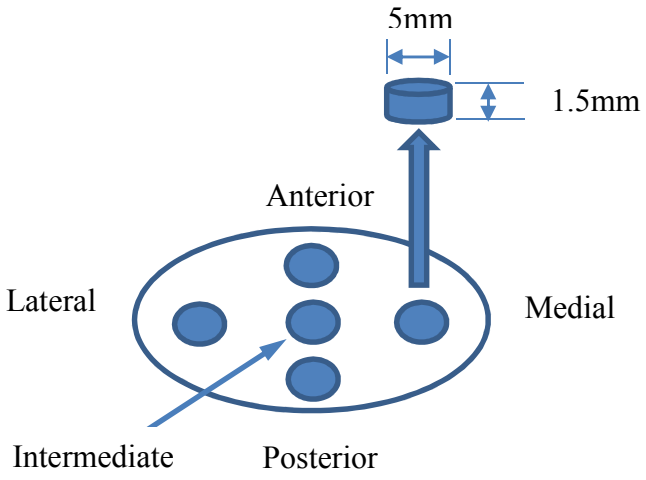

Human TMJ Disc

(a)

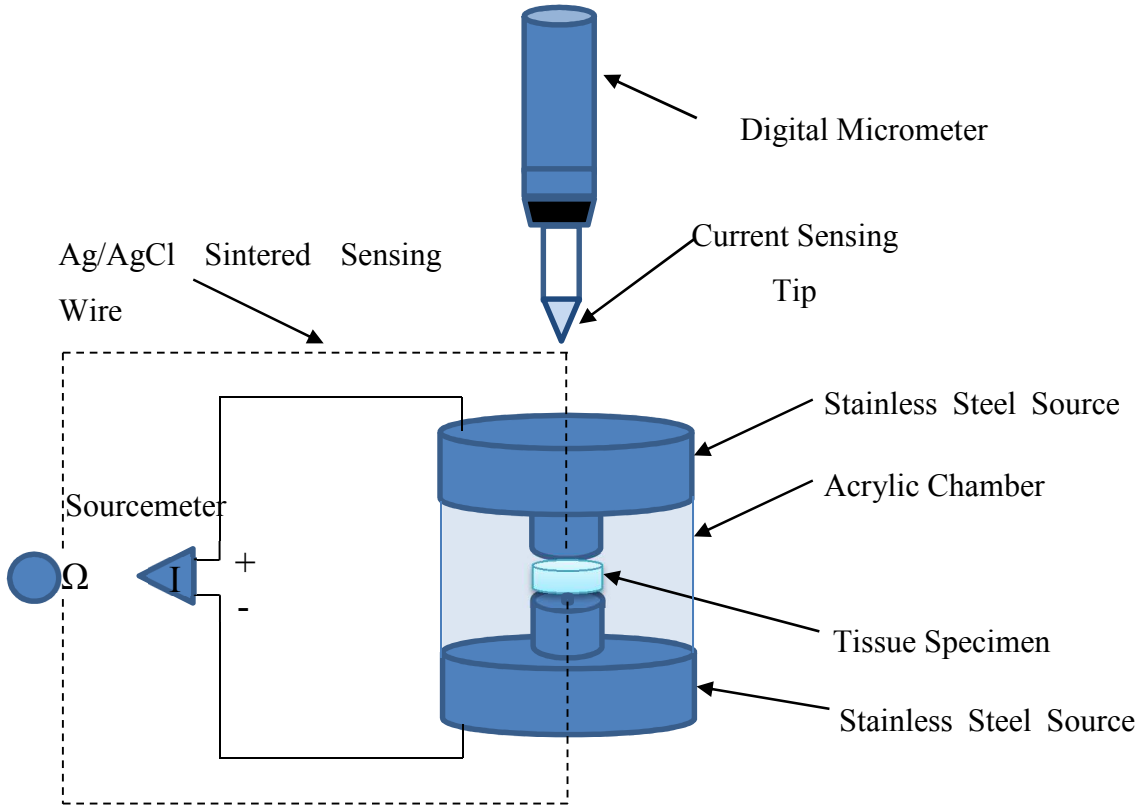

Figure 22 Sample preparation and conductivity chamber using the 4-wire resistance method

Samples were trephined in five regions with a five millimeter diameter shown in Figure 1a. The sample conductivity was measured using a custom chamber based on the 4-wire resistance method. The chamber consisted of 2 current source electrodes and 2 coaxial sense wires shown in Figure 1b. A Keithley 2400 sourcemeter was used with offset compensation to measure the resistance (Ω) using a current source of 3μ ampere. A sample was inserted into the chamber, the micrometer was lowered until the custom circuit made contact (so the sample was not compressed) and the sourcemeter was used to take a resistance measurement.

Table 4 Conductivity measurement steps

Step 1	Sample preparation, height and water content measurement	Isotonic (0.015M PBS)
Step 2	Sample placed in conductivity meter with isotonic (0.15M PBS) bathing solution, resistance read.	Isotonic (0.015M PBS)
Step 3	Sample equilibrated in hypotonic (0.03M PBS) for 24 hrs.	Hypotonic (0.03M PBS)
Step 4	Sample placed in conductivity meter with hypotonic bathing solution, resistance read.	Hypotonic (0.03M PBS)

5.4 Results

Fixed Charge Density

The total average FCD (mean ± SD) of the human TMJ disc was 0.050 ± 0.018 mEq charge/g wet tissue. Regional FCD is shown in Figure 23 below. Even though the intermediate region had the lowest FCD 0.041 ± 0.015 mEq charge/ g wet tissue, no significant difference was found between regions (ANOVA with Tukey's Post Hoc, p=0.673). The FCD content for the articular cartilage (AC) control was 0.09 mEq/g wet tissue with a corresponding GAG content of 21% by dry weight.

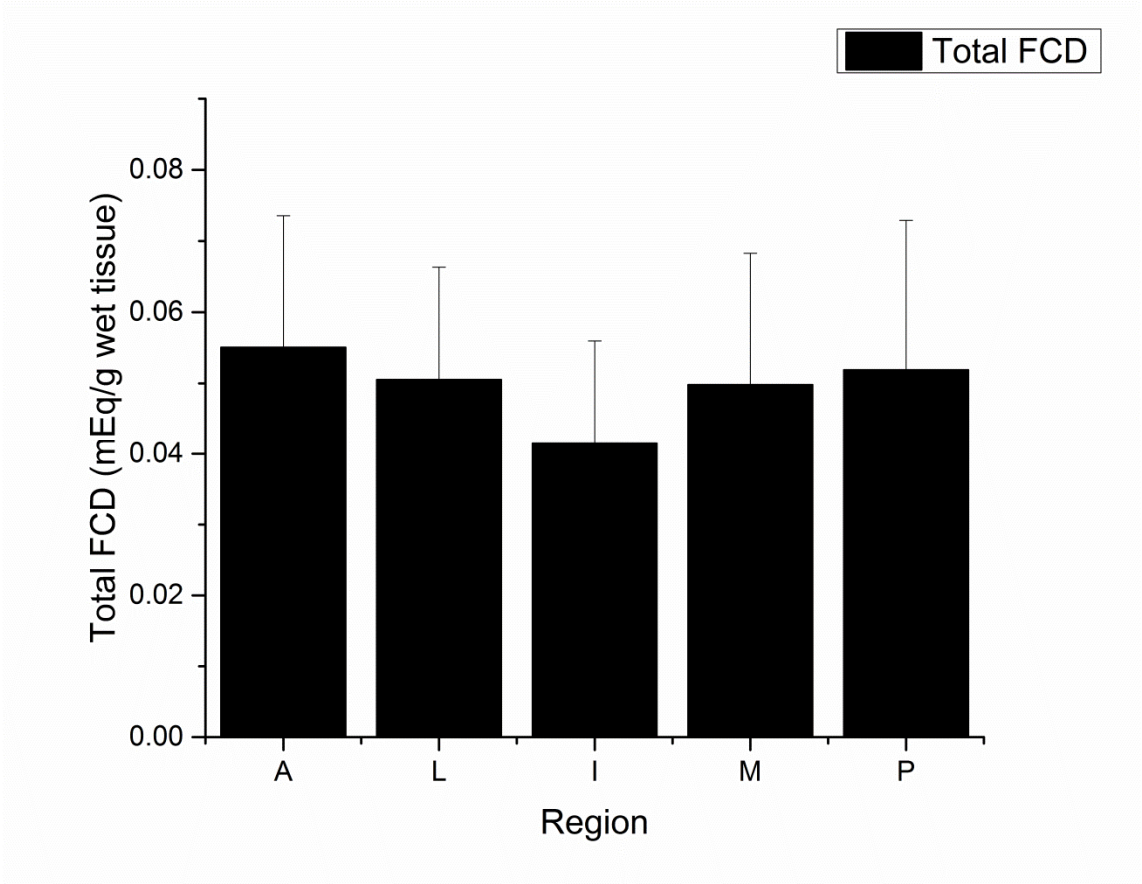

Figure 23 Fixed charge density by region (male and female combined, n=12). The intermediate region had the lowest fixed charge density but this value was not statistically significant.

FCD was then analyzed by gender. Male FCD was 0.053 ± 0.017 mEq/g wet tissue, while female FCD was 0.046 ± 0.018 mEq/g wet tissue with no significant difference (p=0.325). A regional comparison of FCD between male and female TMJ samples is shown in Figure 24 below. There were no regional differences found within male and female groups. A two-way ANOVA was used to investigate gender and regional interaction with no interaction found (p=0.561).

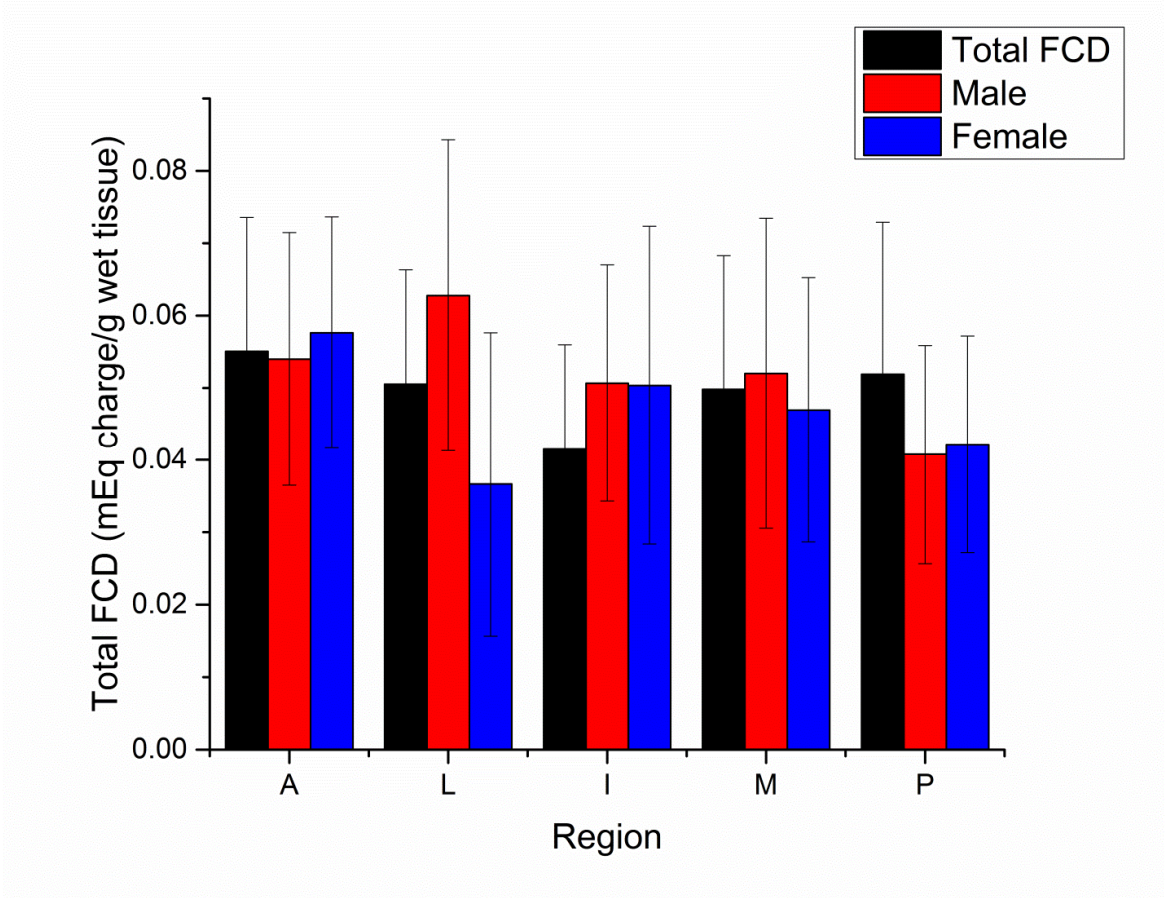

Figure 24 Male and female comparison of FCD by region (n=6).

Biochemical Composition

The total GAG content as % dry weight was 1.65% ± 0.64, where male GAG content was 1.66% ± 0.59 and female GAG content was 1.63% ± 0.72 (with $p<<0.05$). There was no regional significant difference based on GAG content ($p=0.91$). Volume water content was 83.1% ± 2.9% for males and 82.8% ± 3.8% for females, with no statistical significance ($p=0.941$). Mean volume water content did not vary between regions ($p=0.916$).

Linear Correlations Between FCD, GAG, and W_c

A linear regression plot of GAG vs FCD is shown in Figure 25 below. Articular cartilage control samples were also measured in this study and plotted with the TMJ disc samples to further investigate FCD and GAG correlation shown in Figure 26 below. No linear correlation was found between FCD and GAG (R^2 =0.007). Next, a plot of age and FCD is shown in Figure 27 below.

Additionally, there was no linear correlation between FCD and age (R^2 =0.001). Finally, a linear regression plot was conducted between water volume fraction and FCD, shown in Figure 28. Only a slight linear correlation was found between FCD and water content (R^2 =0.208).

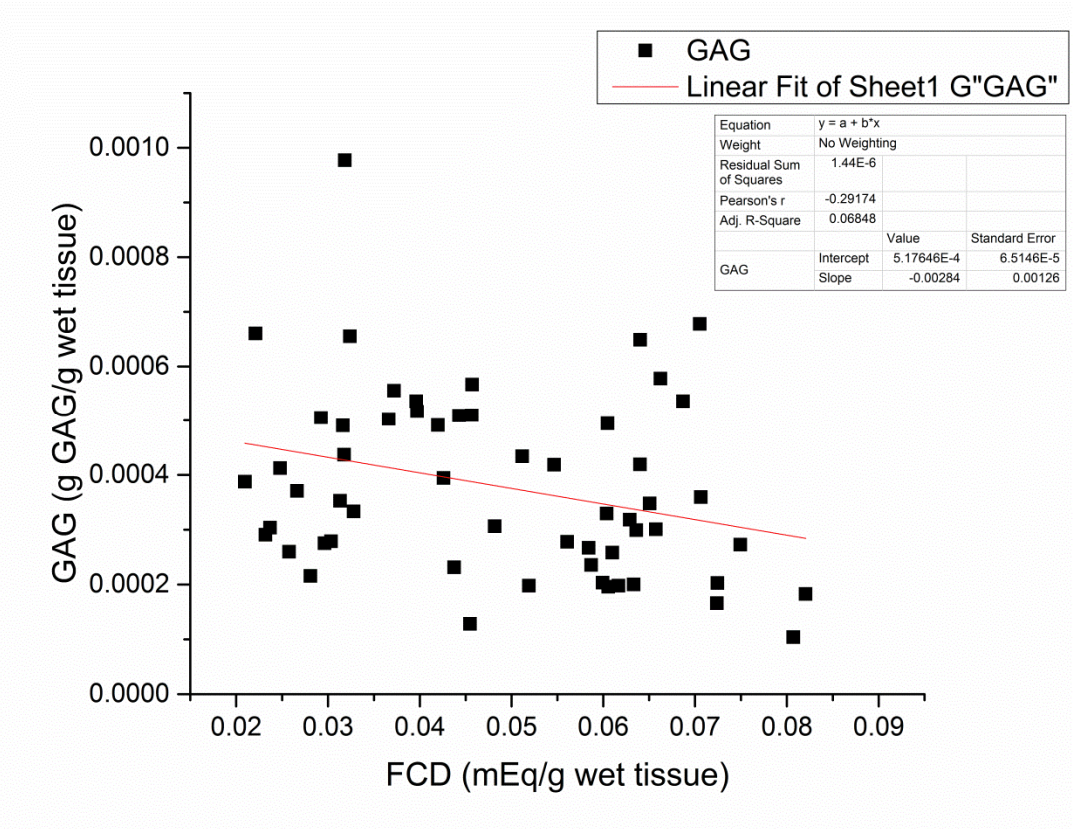

Figure 25 FCD vs GAG weight per wet tissue weight plot for linear regression.

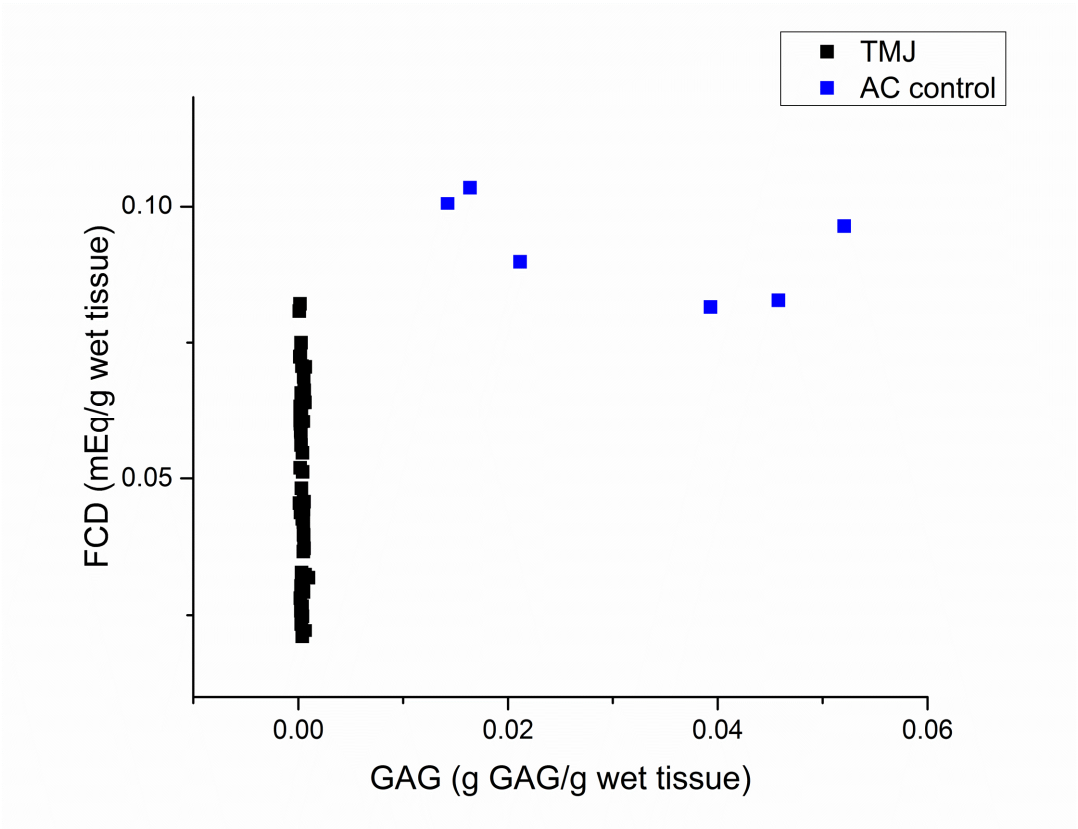

Figure 26 Association between fixed charge density and GAG content per wet weight of tissue.
Articular cartilage samples were plotted with the TMJ sample to investigate a linear correlation between FCD and GAG. Since the TMJ disc sample had low GAG content to FCD signal, they were tightly grouped, whereas the AC control samples had a much larger GAG content and associated FCD signal.

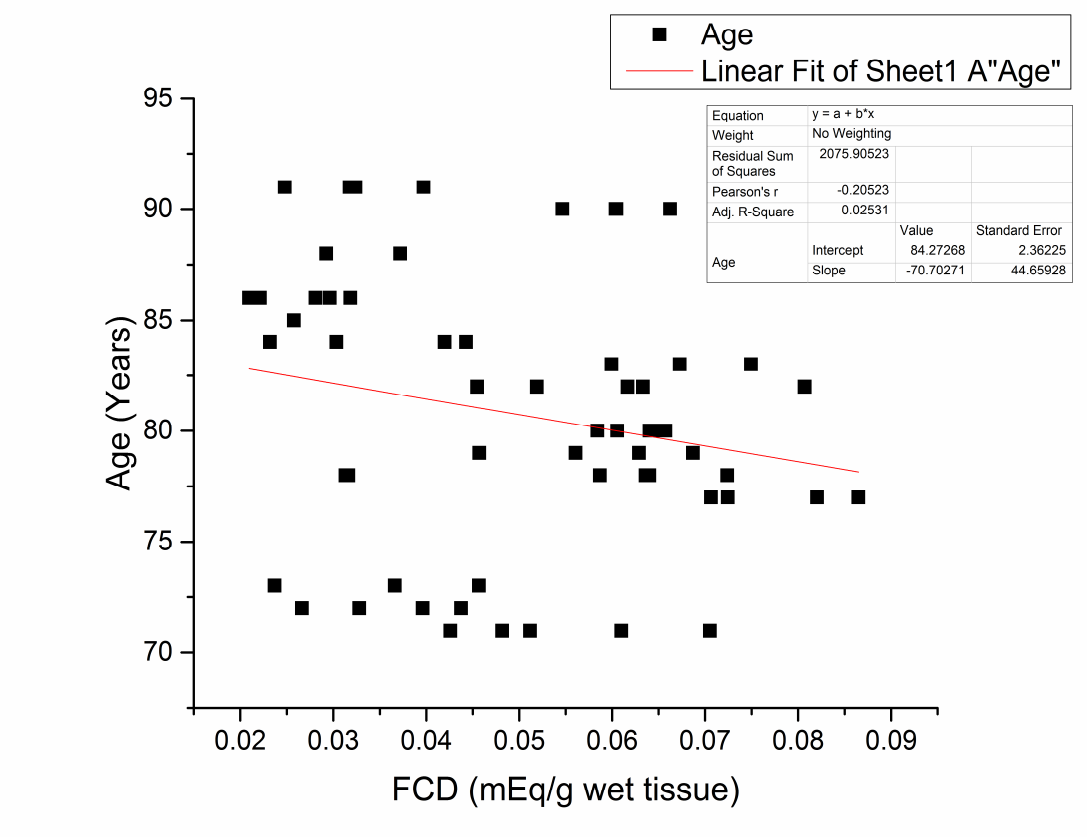

Figure 27 Association between fixed charge density and age
There was no correlation between age and depletion of FCD. The general assumption was as age increased and degeneration likely increased therefore reducing GAG and FCD. But this trend was not shown within the samples and age of this population tested.

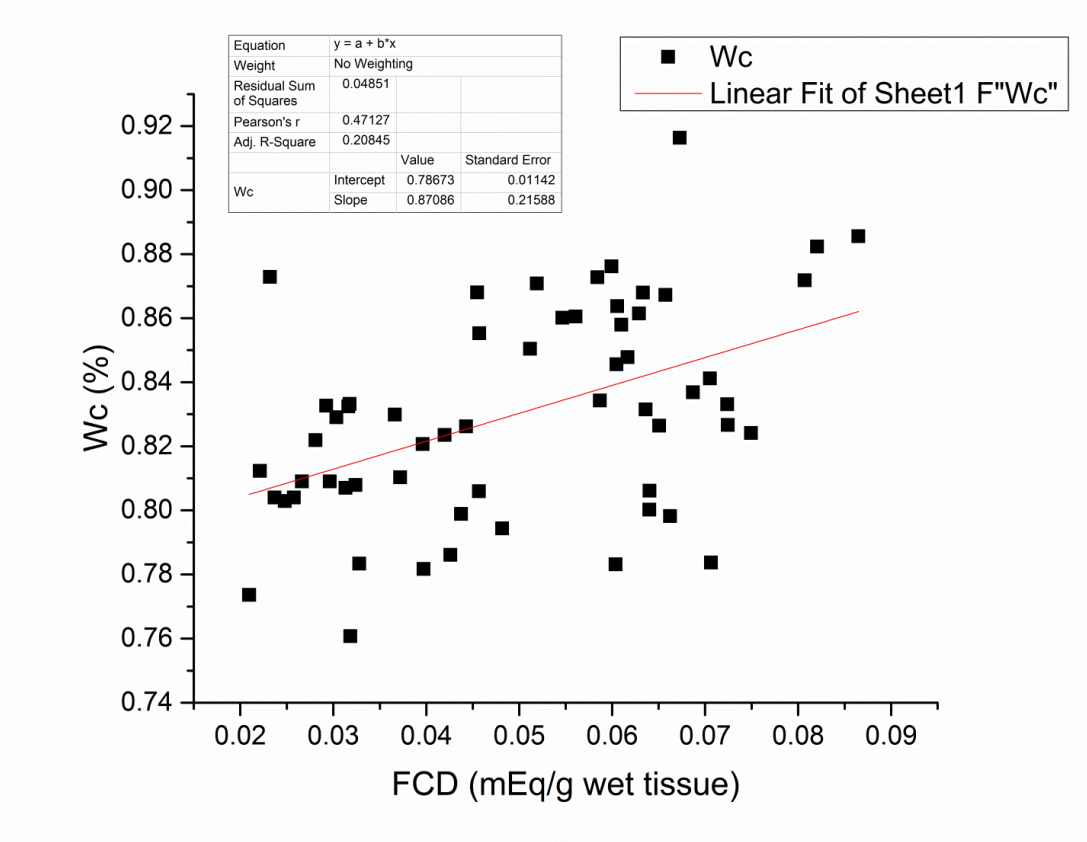

Figure 28 Association between fixed charge density and % water content
The correlation was stronger with water content than GAG content. But the R value of 0.47 was still low likely due to the small range of FCD (.02-0.09) and small range of water content (0.76-0.90).

5.5 Discussion

The purpose of this study was to determine the FCD in human TMJ discs and understand its importance in tissue behavior. The FCD of the samples were measured by a two point conductivity method [231]. Results were first compared with other cartilage types reported previously for both FCD and GAG contents. Finally, FCD values for the TMJ disc were compared by assessing regional variation, male and female FCD, aging effects and the relationship to the tissue's biochemical structure and function. All FCD values are reported as milliequivalent charges per gram of wet tissue (assuming monovalent GAG where 1mEq=1mMol).

Our results were comparable to FCD values of other fibrocartilaginous tissues. Previous reports indicate the value of bovine lumbar annulus fibrosus (AF) FCD as 0.060 mEq/g compared to 0.050 mEq/g for the TMJ disc in this study. The comparison between other cartilage types is shown in Figure 29 below. The FCD value for the TMJ disc is lower than AF tissues. The glycosaminoglycan (GAG) found in the bovine annulus fibrosis was 5.4% compared to the GAG content of 1.65% the for human TMJ disc found in this study. The lower GAG content in the TMJ disc could account for the lower FCD compared to AF tissue [231]. A GAG content comparison between tissues is shown in Figure 30 below.

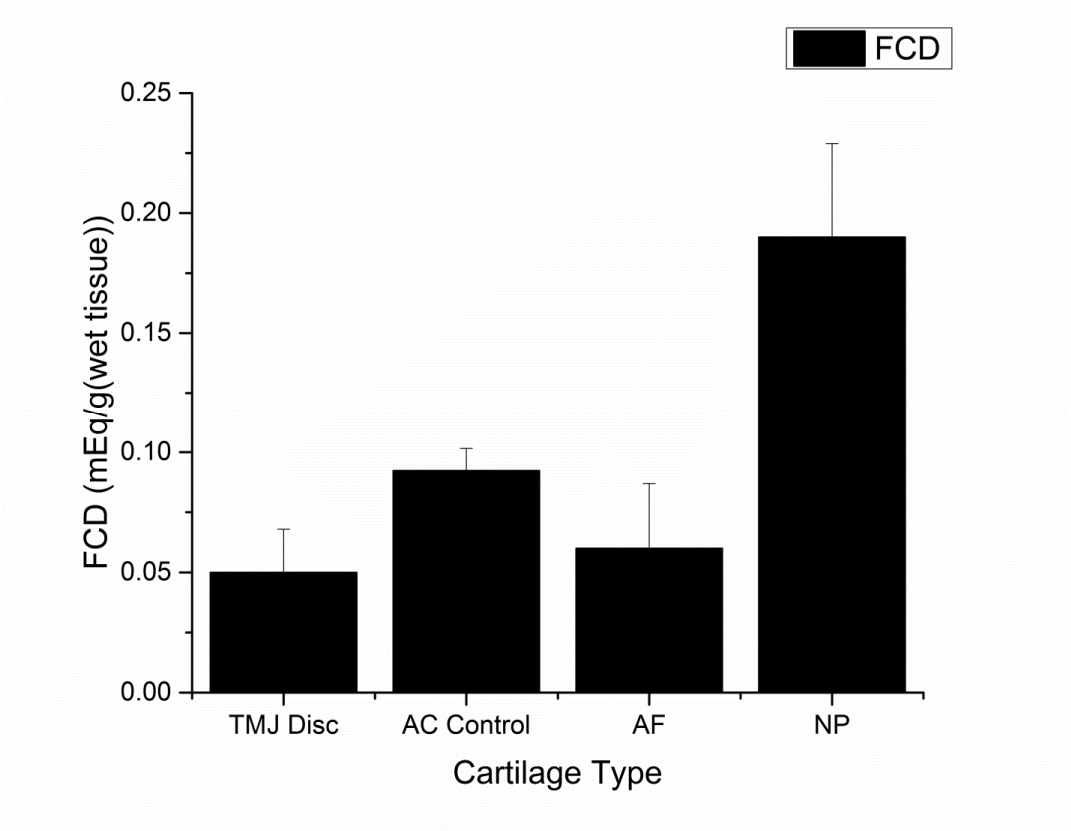

Figure 29 Fixed charge density graphed in comparison to other cartilage types.
The cartilages listed are TMJ disc, Articular Cartilage from porcine femoral head from this study, Annulus Fibrosus from bovine IVD, and Nucleus Pulposus from bovine IVD [231]. The TMJ disc FCD was most similar to the AF tissue of the IVD.

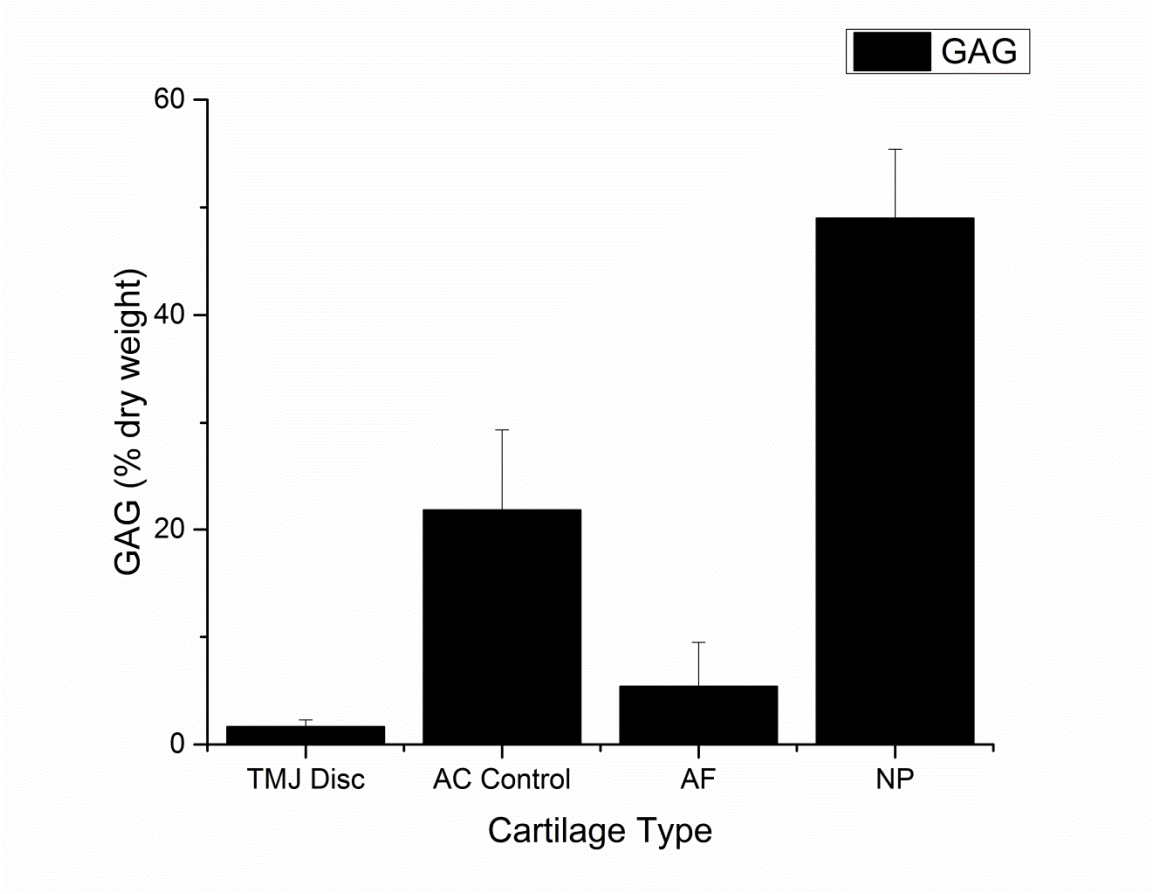

Figure 30 GAG content graphed in comparison to other cartilage types. The cartilages listed are TMJ disc, Articular Cartilage from pig femoral head from this study, Annulus Fibrosus from bovine lumbar IVD, and Nucleus Pulposus from bovine lumbar [231]. The TMJ disc GAG content is again most similar to the AF GAG content of the IVD, which is consistent with the FCD findings.

Also, articular cartilage porcine femoral heads were used as a control for this study. The FCD was found to be 0.09 mEq/g wet tissue with a corresponding GAG content of 21.8% dry weight (both FCD and GAG were statistically significant from TMJ discs (ANOVA $p<<0.05$)). This value was expected to be higher given articular cartilage's higher proteoglycan content. This value also was within a reasonable upper limit for the protocol used to determine TMJ disc FCD and GAG. The value for articular

cartilage is proportional with the nucleus pulposus with a 0.19 mEq/g wet tissue and corresponding GAG content of 49%. The fact that the FCD is lower with respect to other cartilages could indicate a more biphasic loading environment in the disc. This loading environment could be required to support a large amount of tension and shear-traction forces through the dense collagen I matrix, while compressive forces could be supported by fluid pressurization as interstitial fluid tries to exude from the tissue with low hydraulic permeability.

A significant weakness of this study was the age range 72-91 of the discs (overall average 80.75 ± 6.11, female 86.42 ± 3.46 and male 76.85 ± 4.17, $p>0.05$ between female and male). Ideally this study would have included human discs from age of onset 20-25 through old age ~80 but tissues were only available within this age range. In addition, we tried to sample discs with respect to age to keep the average age of male and female similar. The difficulty arose from finding female tissue that had no signs of degeneration. Over twice as many female discs were sampled compared to male to arrive at the same number of healthy discs, yet the age was still statistically higher. It could be possible with older tissues that large matrix proteins such as collagen bundles are preserved through storage, whereas sulfated GAG chains are cleaved by enzymatic degradation. However, other studies have stored tissues in a similar manner with comparable FCD values found in this study [101, 231]. Additionally, when age correlation to GAG and FCD content were investigated for these tissues, no correlation was found. Future work should investigate differences in GAG and FCD in normal compared to degenerated TMJ discs. It may be possible that even though the FCD may not play a large role in

mechanical loading support, the FCD and GAG could play a vital role in the extracellular detection of the loading environment, and therefore crucial for cell response to matrix generation.

As mentioned previously, no GAG to FCD correlation was found in the TMJ samples. This may have been due to the low signal of FCD and corresponding low GAG content. With signals this low, a clear linear correlation was difficult due to the cluster of results at similar levels of GAG~ 1.65% ± 0.64 and FCD 0.050 ± 0.018. When articular cartilage samples were analyzed with the TMJ samples, a linear correlation began to appear (R^2 =0.59). However, TMJ samples had to be removed due to the large sample number disparity (TMJ disc n=60, Articular cartilage n=6).

The proteoglycan content of the TMJ disc is relatively small compared to other cartilages. In effect, the FCD was small but within an order of magnitude. This value was still very important to measure in the human TMJ disc. This material property will allow us to understand the role FCD plays in nutrient transport and function, while helping us understand the similarities and differences to other types of cartilage.

In conclusion, the FCD content of human TMJ discs were most similar to annulus fibrosus tissues, with a FCD value of 0.050 ± 0.018 mEq charge/g wet tissue compared to 0.060 ± 0.027 mEq charge/g wet tissue. The TMJ disc may rely more on the collagen matrix for tensile and traction load support and less on GAG content for a role in compressive loading. The FCD for TMJ disc tissue appears to be significantly lower than knee articular cartilage in porcine femoral heads, which could maintain a different loading environment. However, based solely on the FCD values it is too general to

conclude how the tissue behaves. More research is needed to understand how much the tissue deforms during loading. The loss of water content and high deformation would significantly increase the FCD in the tissue. In addition, finite element models can effectively use the FCD property values to simulate the FCD effect on energy dissipation, material response, and changes in diffusivity under joint loading within a charged tissue environment. Finally, if GAG content and FCD content does not play a major role in mechanical function, it could impact on the physicochemical signaling environment within the disc. More advanced finite element models combined with accurate patient anatomy are needed to bridge these biomaterial properties with biologic processes.

6 Tensile Properties of the Human TMJ Disc

6.1 Abstract

The temporomandibular joint disc is a large fibrocartilage responsible for the stress dissipation and lubrication of the jaw. In over 70% of cases of diagnosed TMD, the TMJ disc has been found to be displaced resulting from disc degeneration. Previous studies have sought to characterize the mechanical properties of the TMJ disc in an effort to determine the disc's mechanical function specifically in tension as it is believed the disc could carry a significant amount of joint loading through tension during opening and closing of the jaw.

Animal models have been used extensively in order to characterize the biomechanical function of the TMJ disc. But few studies have investigated human TMJ disc biomechanical function owing to the scarcity of human tissues. In this research study, TMJ discs were extracted from twelve human cadavers (six male and six female). The tensile properties of the TMJ disc were investigated under incremental stress relaxation. The TMJ disc samples were tested at a rate of 1% per second for physiologic 0-30% strain in a 37º PBS filled chamber.

The initial instantaneous stress response was plotted for each incremental strain while the relaxed modulus was plotted at equilibrium, with the slope yielding the instantaneous and relaxed modulus. The overall instantaneous modulus was 7.59 ± 3.26 MPa and relaxed modulus was 3.27 ±1.39 MPa. Female instantaneous modulus 8.87± 3.34 MPa was greater than male instantaneous modulus 6.46 ± 2.77 MPa (p=0.003, two

sample t-test). Female relaxed modulus 3.94± 1.54 MPa was greater than male relaxed modulus 2.67 ± 0.93 MPa (p=0.002, two sample t-test).

The results indicate the TMJ disc instantaneous and relaxed modulus was lower than previous studies investigating porcine TMJ discs [24]. In addition, anisotropy was not found between the anteroposterior and mediolateral sections of the disc as anisotropy was found in previous studies. The lower modulus could be attributed to the age of the TMJ discs samples.

6.2 Introduction

TMJ disorder is a broad term used to describe many symptoms and pathologies related to craniofacial pain, jaw pain and function (NIDCR). The exact etiology appears to be multifactorial. As many as 20-30% of the population experience clicking, popping, and pain in the TM joint with about 3-4% developing TMDs [7]. However, for those that experience progression of the disorder, symptoms can be debilitating including TMJ disc derangement. In 70% of these cases, the TMJ disc loses biomechanical function resulting in disc displacement [5, 14, 16]. Animal models have been used extensively in order to characterize the biomechanical function of the TMJ disc [24, 26, 30, 130, 134]. But few studies have investigated human TMJ disc biomechanical function owing to the scarcity of human tissues. In this study, human TMJ disc were used to measure the tensile modulus under incremental stress relaxation tests. Studies show the tensile properties of the disc are significant for jaw opening and closing. The results were interpreted with respect to previous pig models. The biomechanical function was also analyzed using current quasilinear viscoelastic theory [14, 24, 114, 241-243].

The large fibrocartilaginous TMJ disc plays a central role in stress dissipation and lubrication between the incongruent surfaces of the glenoid fossa and condyle of the mandible [24, 114]. The disc shields the TM joint from high stress concentrations and dissipates energy throughout the tissue [114]. The dense collagen matrix along with the proteoglycan content absorbs and distributes joint loads [24]. In the event of mechanical injury in cartilage or degeneration of tissue, the cartilage loses its ability to support the mechanical load which further stresses the tissue while cellular function ceases to maintain regeneration of a healthy tissue matrix that can withstand mechanical load [14, 21]. The result is a joint degenerative disease such as osteorarthritis as well as internal derangement of the TMJ disc [241, 244].

The TMJ disc is unique from other types of cartilages because it is made up of 80% to 90% of collagen I [24]. Comparatively, hyaline cartilages of the knee are made up of ~60% collagen II [69]. The disc exhibits a highly biconcave shape in humans and appears to exhibit some anisotropy based on regions within the tissue. The TMJ disc translates with the condyle during function because it is supported by an anterior attachment to the lateral pterygoid and anterior insertion into the condyle and a posterior attachment to the retrodiscal tissue [114]. Through these attachments the disc divides the glenoid fossa and the condyle into the upper and lower compartments. During opening and closing of the jaw the disc translates anteriorly with the condyle [2]. The translation requires the disc to support tension as it is stretched anteriorly and posteriorly over the condyle during motion [37]. Therefore, the tensile properties are important to the disc to maintain mechanical function. Better research and understanding of this mechanical

function would allow researchers to better model changes in mechanical function, as well as provide benchmark material property data for tissue engineered replacements [14, 73, 242, 245].

There are a range of joint loading conditions the TMJ disc must support during everyday function, including support through tension in opening and closing, tractional shear forces through articular surfaces, and also compressive forces [24, 114, 246]. The disc allows anterior-posterior translation of the jaw during opening and mediolateral translation during chewing. The disc executes a complex role in the six degrees of freedom of motion of the mandible and TMJ disc.

Type I collagen is the main extracellular matrix protein in the TMJ disc between 80-90% by dry weight. Collagen fibers run in an anterior-posterior direction throughout the intermediate region of the disc. The fibers run in a random-circumferential direction around the outside edges of the disc [27]. A variety of joint loads have been analyzed by FE models. These models indicate that loading conditions such as stress field translation running perpendicular to collagen fiber alignment could provide a unique pathological loading environment that may promote injury to the disc. Stress from the condyle running mediolaterally and perpendicular to collagen fibers could provide mechanical injury to the disc. Therefore a primary goal of this study is to understand the tensile anisotropy that may exist in the TMJ by measuring the tensile properties in the anteroposterior verses mediolateral direction [24, 73, 114, 245].

In addition to exploring anisotropy in the TMJ disc, this research study seeks investigate TMJ disc's viscoelastic response under tensile strain using the quasi-linear

viscoelastic model. This model has been well documented in other soft tissues but remains to be applied to TMJ disc tissues [56, 247, 248].

Previous tensile studies have investigated the TMJ disc under incremental stress relaxation on cyclic loading in tension. Detamore used porcine tissues with different regional orientation to determine incremental stress relaxation properties of the tissue [24]. The disc was shown to have an instantaneous linear elastic response to increments of tensile stress. The disc exhibited anisotropy between mediolateral and anterior posterior orientation [249]. Beatty et al analyzed pig discs under a 0.5, 50 and 500 mm/sec initial load with an AP modulus of 76.4 MPa at 500 mm/min and 27 MPa at 0.5 mm/min and a ML modulus of 3.2 MPa at 500 mm/min [250]. These studies vary widely on the reports of the TMJ disc tensile modulus, from 1 MPa to 500 MPa. This is in large part due to the tensile test setup and different load rates of 1 mm/sec for Detamore, 3 mm/min for Tanaka, and 500 mm/sec for Beatty [244, 249, 250]. In addition, few human tissues have been tested in tension except for Tanaka et al and Kalpakci et al [70, 71]. As a result, most FE models and tissue engineering studies rely solely on either porcine or canine tissue properties.

The goal of this study was to characterize human TMJ discs sampled from male and female subjects. The protocol developed for this study was determined through careful consideration of previous tensile studies as well as analysis of other soft tissues. The main objectives of this study were to determine the tensile modulus under consistent, relevant loading protocol, investigate viscoelastic response and anisotropic variation, and compare male and female moduli. This understanding of human mechanical

characteristics will be valuable to models that evaluate dynamic joint function as well as patient specific models of anatomy which monitor progression of TMJ disc tissue degeneration.

6.3 Materials and Methods

Sample Preparation

Human TM joints were dissected from 6 male (67.5±8.4 years) and 6 female (70.33±8.69 years) subjects in accordance with IRB guidelines. Donors were fresh frozen and not formaline fixed. After the joints were removed, they were wrapped in cellophane and PBS soaked gauze and placed in a specimen bag and frozen until use. Joints were thawed 12 hours and the TMJ disc removed. Discs were visually inspected for signs of trauma or degeneration. Only healthy TMJ discs were used in the study. The left joint were used for mediolateral tensile strips while the right TMJ disc was used for anterior posterior specimens see

Figure 31 below for strip orientation. Tissue tensile strips were prepared using a 2mm spacer and parallel razor blades. For the mediolateral strips, three specimens were taken from each disc in the mediolateral central, anterior, and posterior regions of the disc. Likewise, specimens from the anterior posterior orientation were taken in central, lateral and medial portions of the disc. Care was taken to remove specimens in equal spacing and avoid peripheral attachments on the outer edges of the disc.

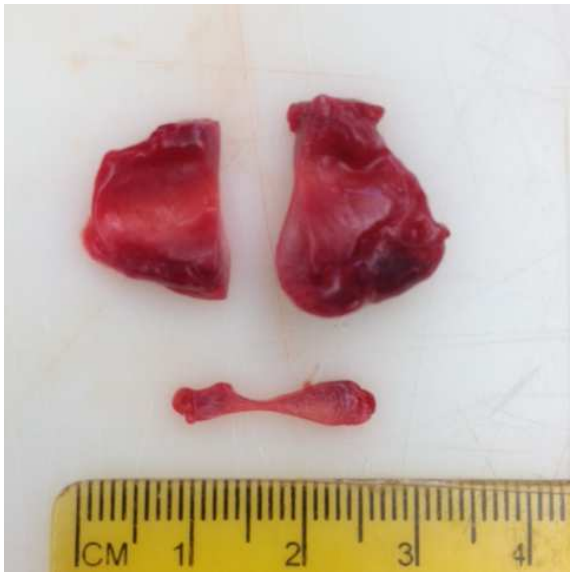

(a)

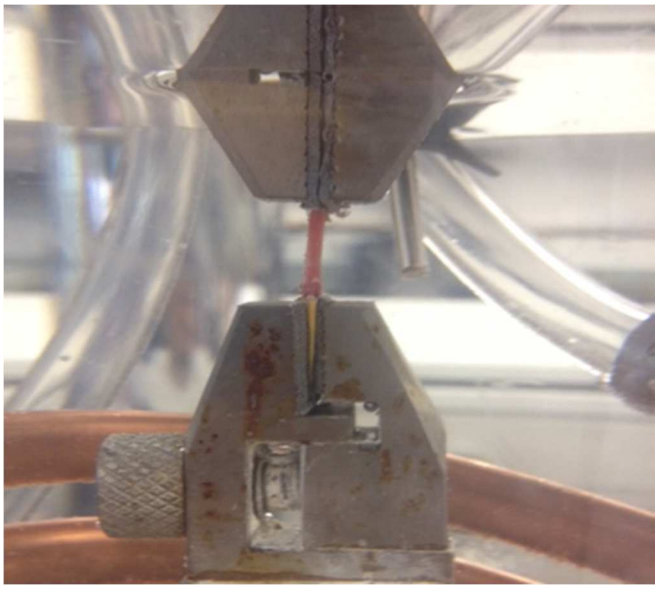

(b)

Figure 31 Specimen preparation and specimen attached to tensile grips for testing

Figure 31a shows a 2mm strip of tissue sampled anteriorposterior from a human TMJ disc. The tissue specimen was clamped between load grips and the temperature control chamber was filled with PBS in Figure 31b.

After dissection, tissue strips were immediately transferred to a microtome. Inferior and superior portions of the tissue samples were removed, to remove biconcavity and ensure even, parallel cross-sections of the tissue for testing. The tissue strips were measured for width and thickness using current sensing micrometer, with the dimensions recorded before submersion into the temperature control (37^{o} C) bath with PBS.

Biomechanical Testing

Stress relaxation tests were conducted on a Bose 3200 (Eden Prairie, MN). A custom designed acrylic environment chamber was constructed to fit the Bose using enclosed water circulation to maintain 37^{0}C of the 0.1M PBS bath. The saline bath was enclosed to prevent evaporation during testing. After each test, the bath was filled with

fresh PBS. Stress relaxation tests were programed using WinTest software. Specimens were attached to the Bose tensile clamps using cyanolacrylic. The chamber was filled with PBS and allowed to equilibrate for 10 minutes see Figure 32 below.

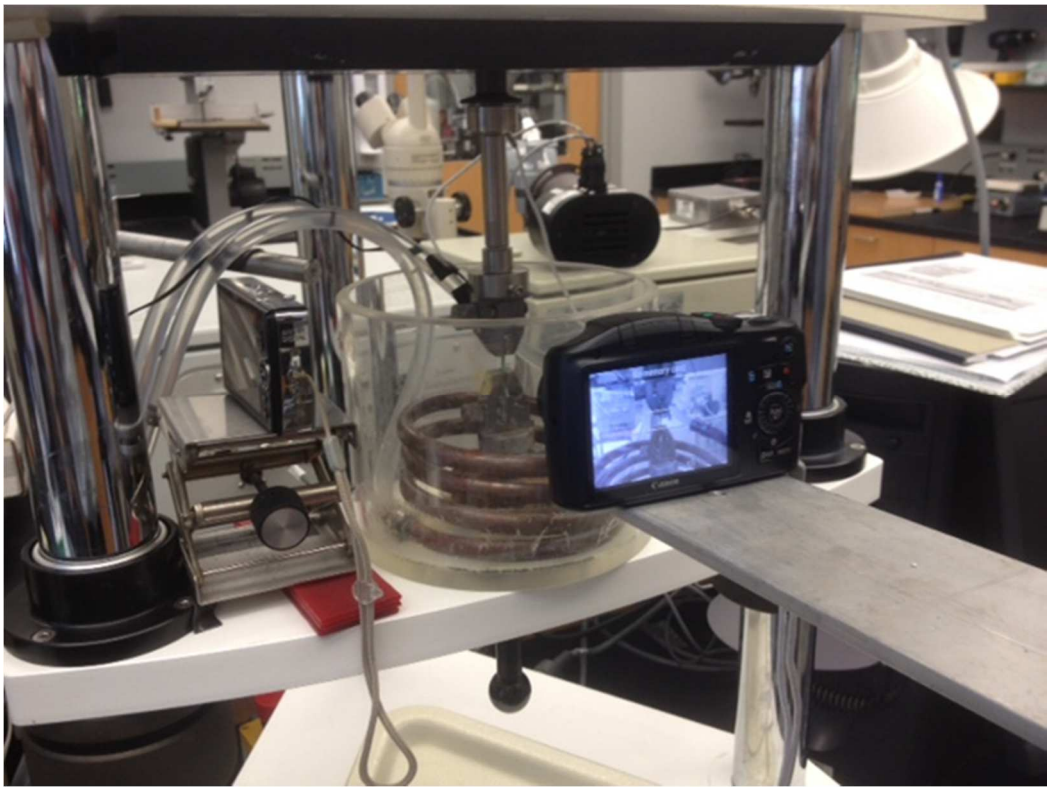

Figure 32 A temperature controlled PBS chamber and a Bose 3200 axial tester
Cameras were initially used to measure the change in cross sectional area of the specimen under load.

A 0.1 Newton (N) tare load was applied the specimen and the initial height of the specimen was recorded though the load arm height. Using the specimen height at tare load, a rate of 1% per second was calculated and used as the ramp loading speed between dwell times. The specimen was loaded at 5%, 10%, 15%, 20% and 30% stain increments with dwell times for relaxation of 15, 15, 15, 20, and 30 minutes, respectively to ensure

equilibrium was reached, see Figure 33 below The times were based on preliminary tests results that ensured the tissue had reached equilibrium. The load rate of 1% per second was chosen to maintain a uniform loading rate for each specimen regardless of length. Therefore, each specimen was loaded at a consistent rate as a ratio to length.

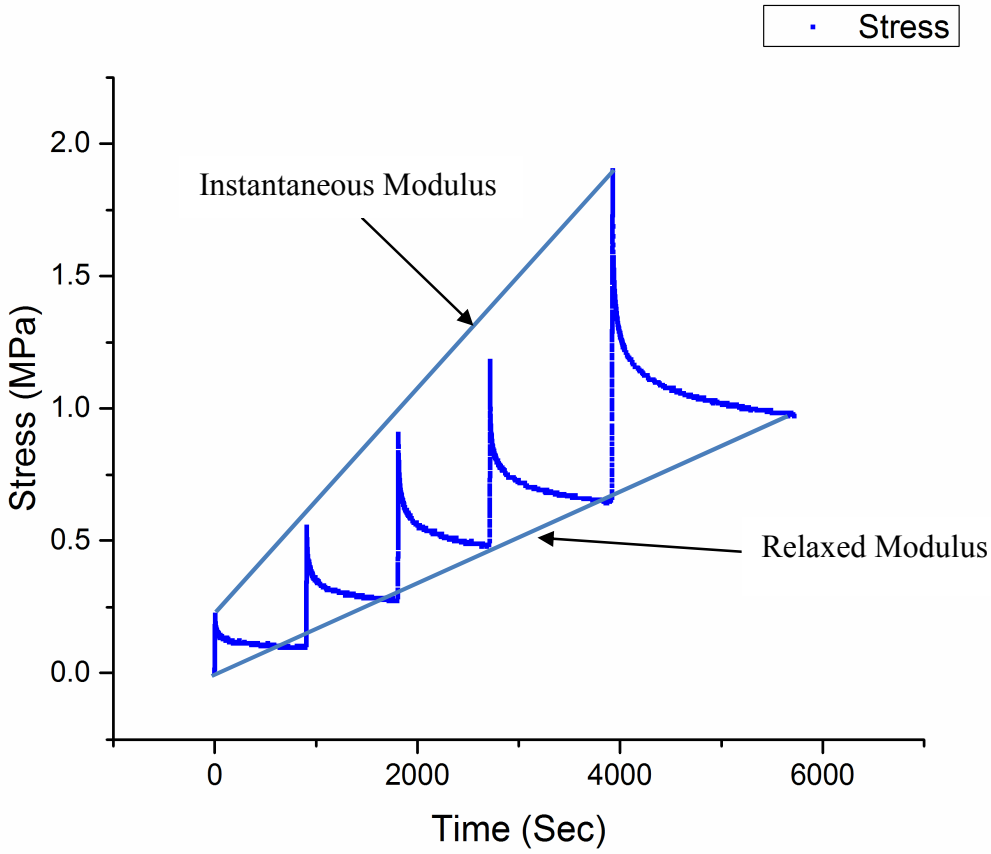

Figure 33 An example of the stress-relaxation response to incremental increases in strain.
For each strain increment, the tissue response is a peak instantaneous response followed by a decrease in stress as the tissue is held at constant strain, until the tissue reaches the relaxed/equilibrium stress. After a designated time increment, the strain is increased and the stress response follows a similar pattern of relaxation. The peak instantaneous response and relaxation stress at equilibrium were plotted to determine the

instantaneous modulus and relaxed modulus as indicated on the figure above.

Quasilinear Viscoelastic Theory

The quasilinear viscoelastic theory was based on YC Fung's theory for non-linear elasticity which accounts for the previous strain history which affects the stress in biologic materials [56]. The theory was formulated based on continuous spectrum of relaxation rather than combining many Kelvin or Maxwell models. The reduced relaxation function derived from the QVT is used to fit stress data that has been normalized with respect to the peak stress and initial time. The reduced relation function is fitted with an exponential integral and resolved using a short time constant, τ_1 and long time constant τ_2 based on a logarithmic scale, while a material constant C is used as the final fitting parameter to account for the load dissipating property of the biologic material shown in Equation 17 [56]. See Figure 34 below for τ_1, and τ_2

Quasilinear Viscoelastic Theory Curve fitting of reduced relaxed function was completed using Origin Pro 9.1 software (Cambridge, Massachusetts). All samples were normalized by stress and time so that at t=0 the initial time began at 0 and the initial peak stress began at 1.

Each relaxation curve was then fit using the reduced relaxation function yielding parameters C, τ1, τ2 for each curve Figure 35 below**.** Figure 36 below shows the relaxation curves for 5%, 10%, 15%, 20% and 30% strains which have been normalized in order to be fit with the reduced relaxation function in Equation 17:

$$G(t) = \frac{1 + C * \left[E_1\left(\frac{t}{\tau_2}\right) - E_1\left(\frac{t}{\tau_1}\right) \right]}{1 + C * \ln\left(\frac{\tau_2}{\tau_1}\right)}$$

17

$$E_1(z) = \int_z^{\infty} \frac{e^{-t}}{t} dt$$

18

where E_1 is the exponential integral function in Equation 18. An exponential approximation was used to fit peak instantaneous response for each level of incremental strain ($\sigma^{\varepsilon}(\varepsilon)$), where A and B were material constants:

$$\sigma^{\varepsilon}(\varepsilon) = A\left(e^{B\varepsilon} - 1\right)$$

19

However, when the instantaneous peak response was fit for the samples, the fit was linear.

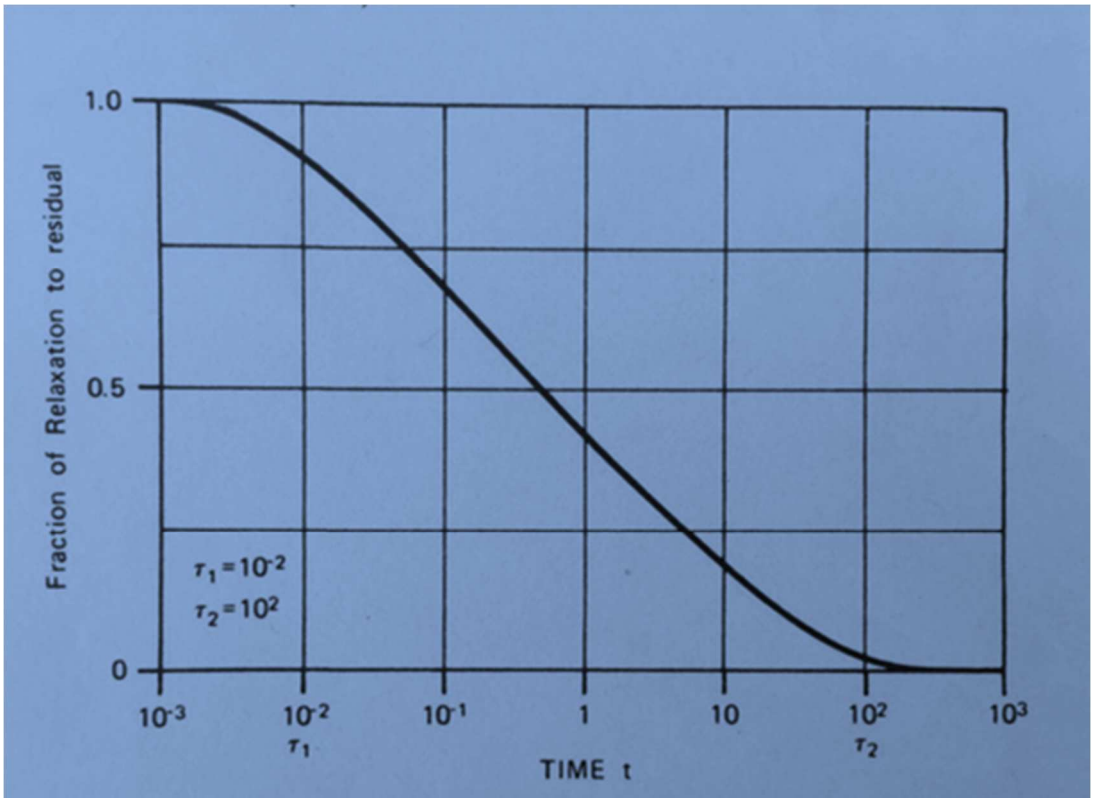

Figure 34 The reduced relaxation function G(t) of a solid with a continuous relaxation spectrum $S(\tau)=c/\tau$ for $\tau_1<\tau<\tau_2$ from Neubert 1963, reprinted Fung [56].

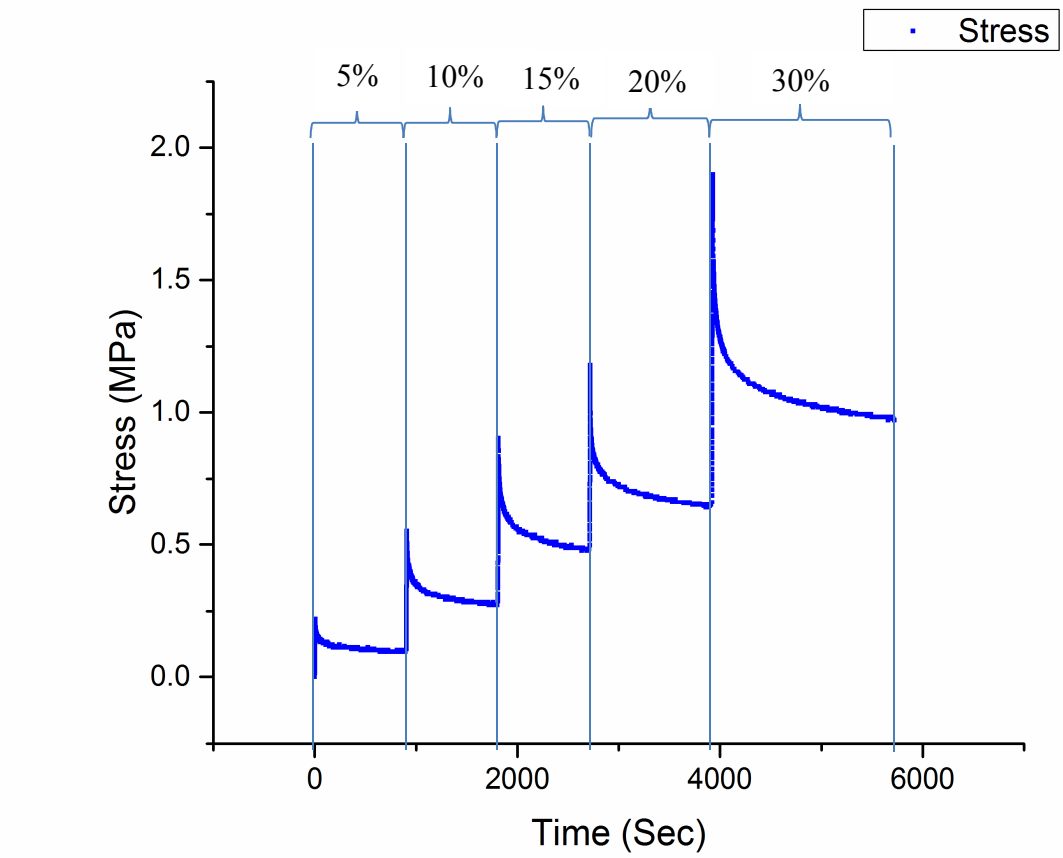

Figure 35 Example plot of stress relaxation test with each relaxation curve divided into their respective strain increments before normalizing and curve fitting with quasilinear viscoelastic theory.

In order to plot the reduced relaxation function for each strain increment, the maximum stress was normalized to σ_{max}/σ and the time was normalize to $t_o=0$, therefore G(0)=1. The reduced relaxation function (Equation 17) was used to fit the relaxation curve for each strain increment, yielding the material constant, C and time constants $\tau 1$, $\tau 2$.

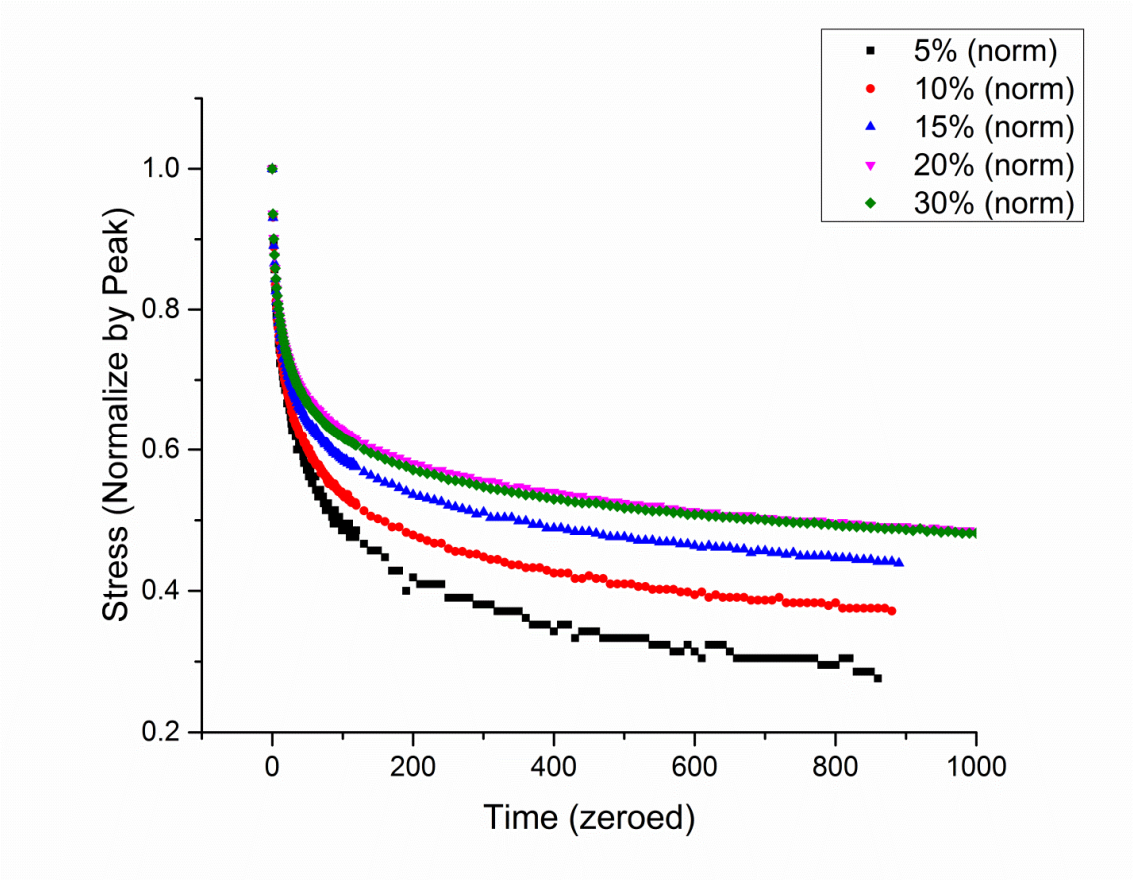

Figure 36 Quasilinear Viscoelastic Theory Curve fitting of reduced relaxed function for a single specimen.
Note the curve for each strain level was fit individually with the reduced relaxation function. Before curve fitting with the reduced relaxation function proposed by Fung, relaxation curve from each increment of strain were normalized by stress (G(t)=1) and time (t(0)=0). Then each relaxation curve was fit using the reduced relaxation function yielding parameters C, $\tau 1$, $\tau 2$ for each curve.

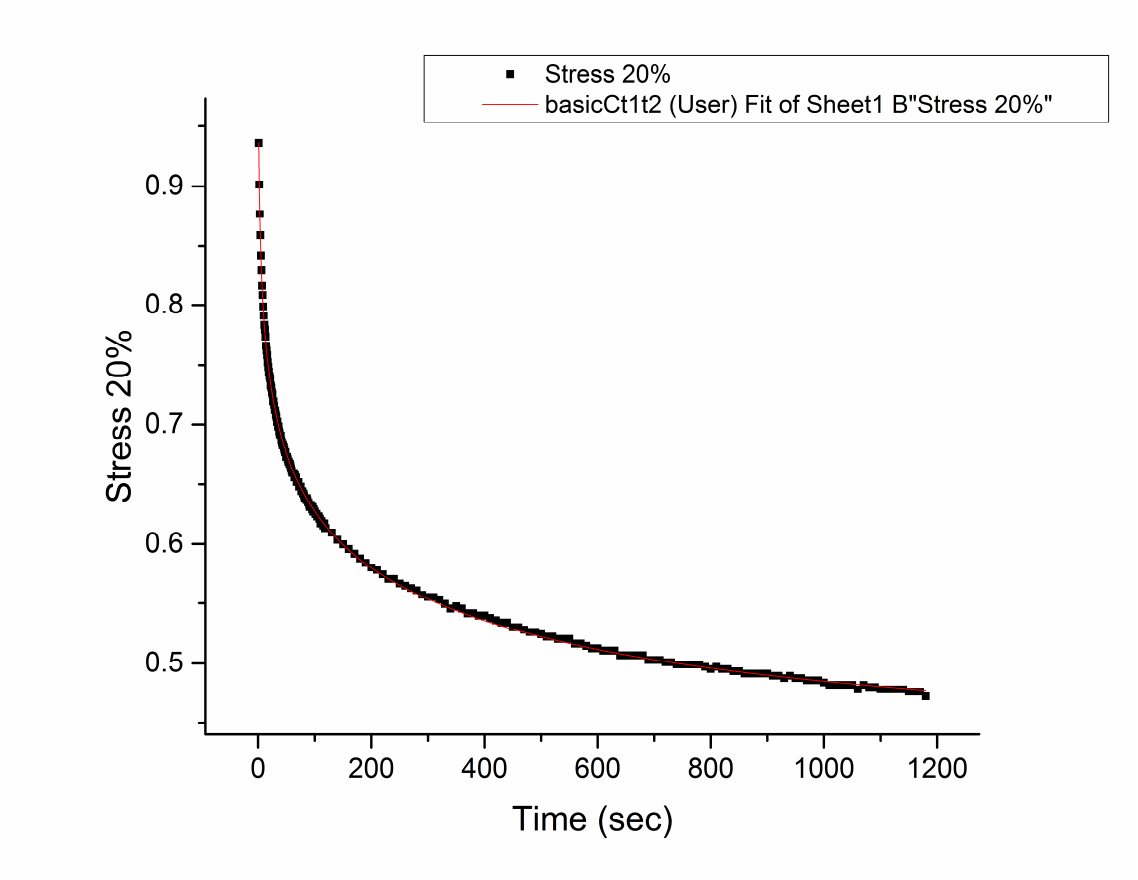

Figure 37 Example curve fit of the reduced relaxation function for 20% strain

6.4 Results

The overall instantaneous modulus was 7.59 ± 3.26 MPa and relaxed modulus was 3.27 ±1.39 MPa. Female instantaneous modulus 8.87± 3.34 MPa was greater than male instantaneous modulus 6.46 ± 2.77 MPa (p=0.003, two sample t-test). Female relaxed modulus 3.94± 1.54 MPa was greater than male relaxed modulus 2.67 ± 0.93 MPa (p=0.002, two sample t-test). See Figure 38 below for a comparison of male and female modulus. See Figure 39 below for a regional comparison of modulus and Figure 40 below for regional energy (area under load curve) by region.

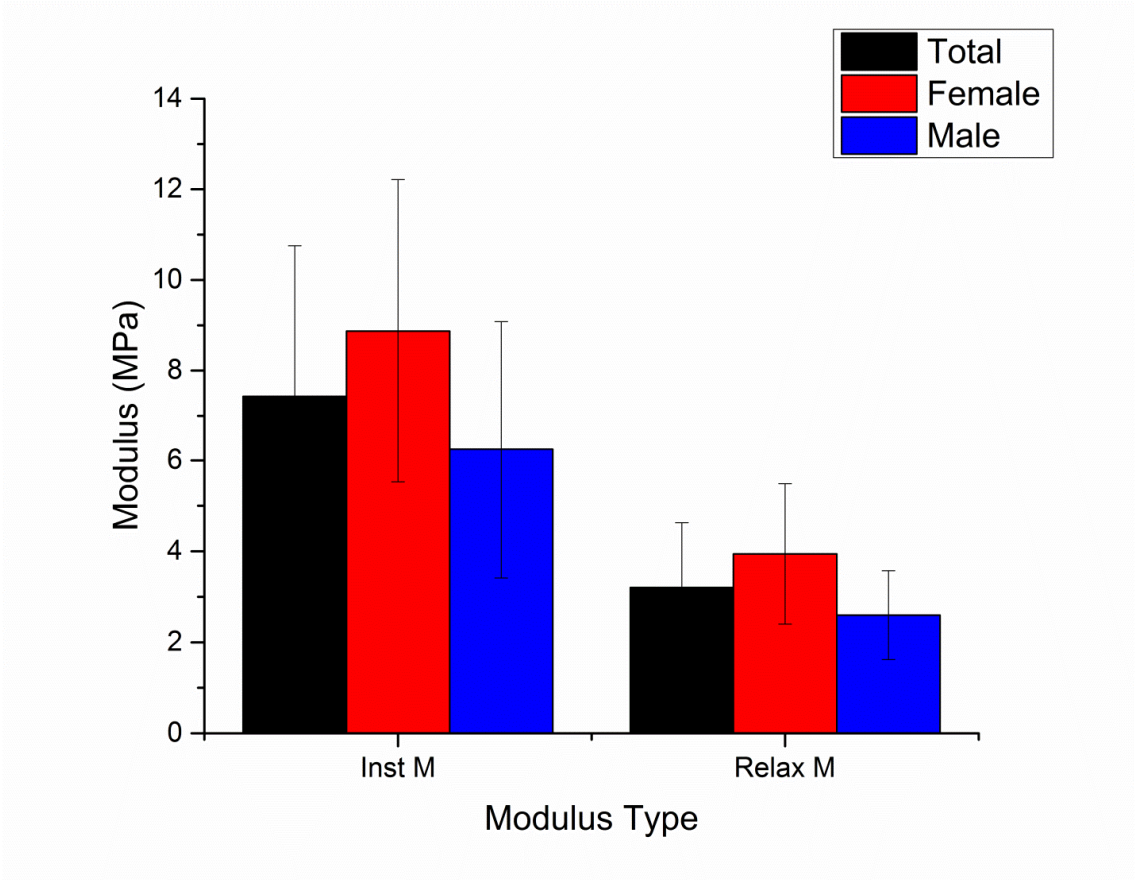

Figure 38 Bar plot of the instantaneous and relaxed modulus according to gender

Using two sample t-test, at the 005 level, the population means of both instantaneous and relaxed modulus are significantly different between male and female, $p<0.05$. Male and female groups $n=36$.

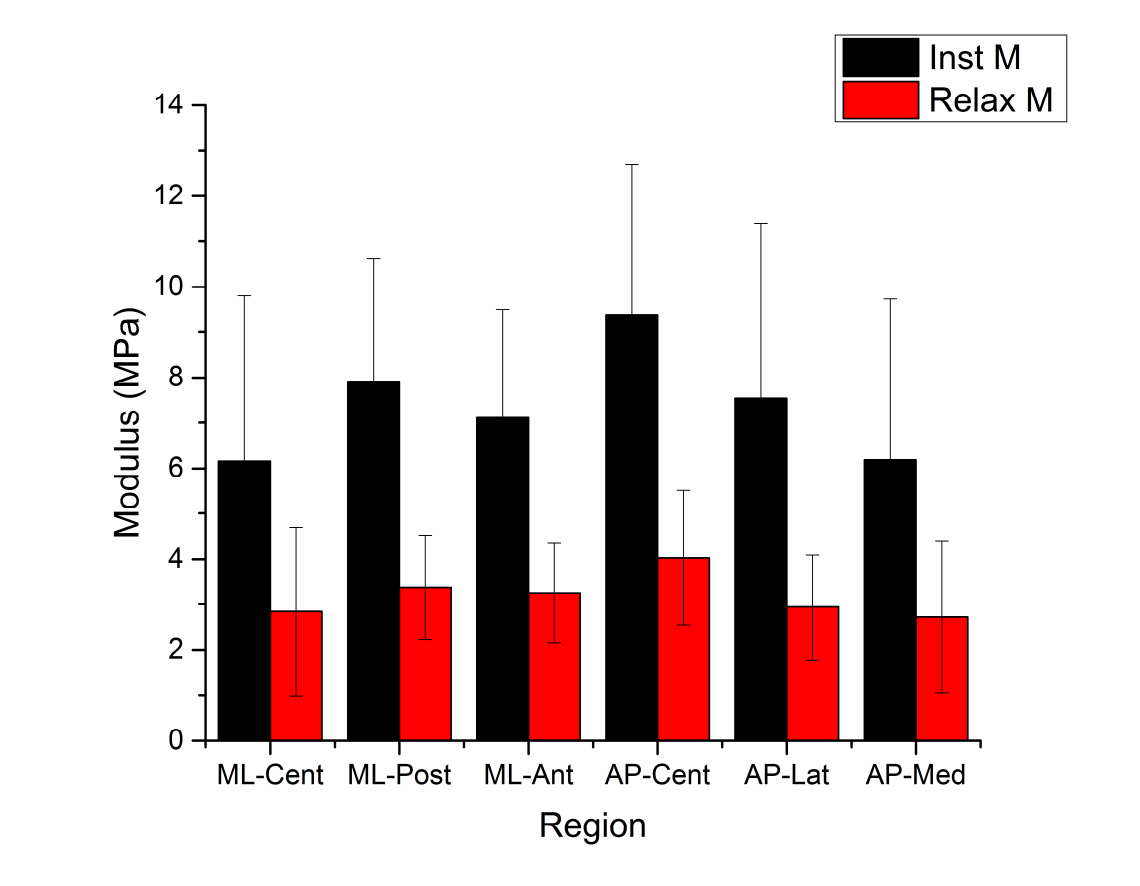

Figure 39 Regional instantaneous and relaxed modulus for combined male and female groups

No regional differences were detected. A Shapiro-Wilk test was first conducted to determine normality for the sample set ML Cent through AP-Med with n=11. Normality was confirmed, $p<0.05$. A One-way ANOVA was run with 6 groups and found that the means were not statistically significant, $p<0.05$ for both the instantaneous and relaxed data set. At the 0.05 level, the means between region (n=11) are not significantly different.

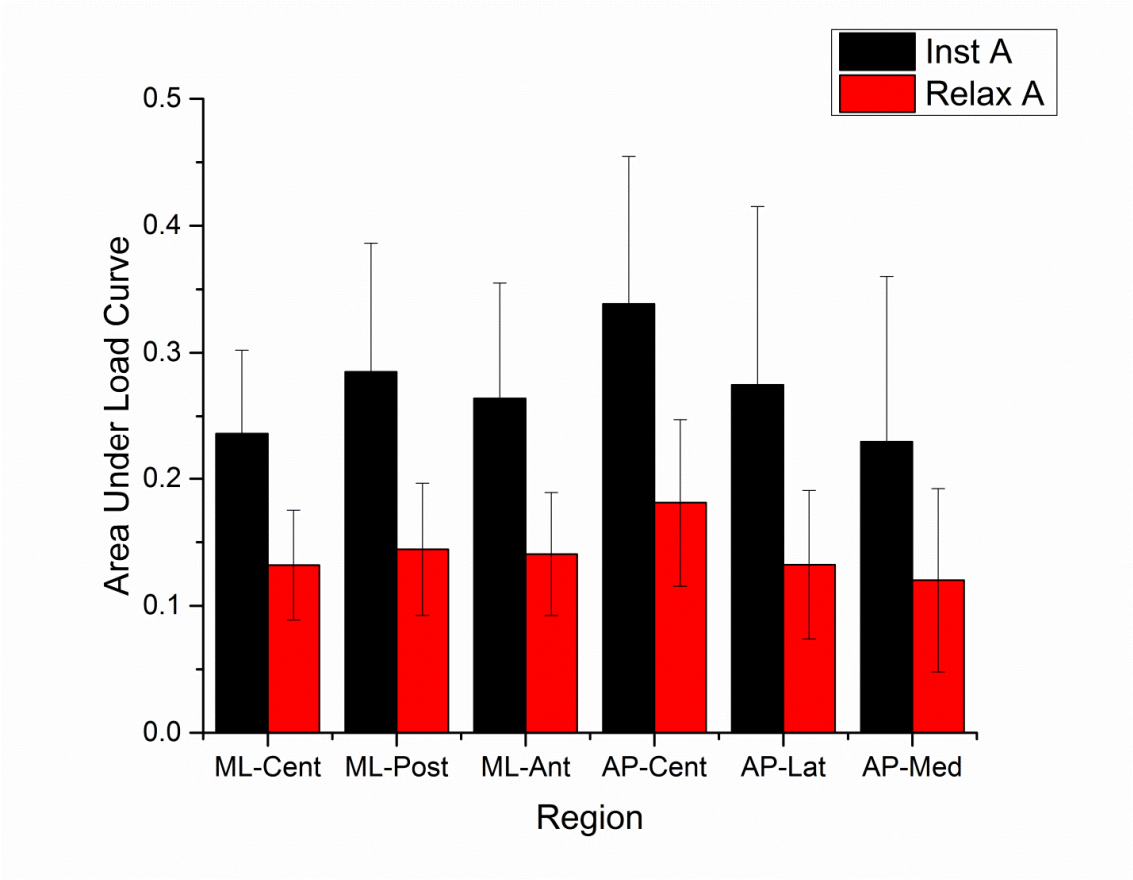

Figure 40 Results of human tensile instantaneous and relaxed energy by region

Table 5 Curve fitting parameters for each level of strain

Strain %	C	+/-	$\tau 1$	+/-	$\tau 2$	+/-
5	0.465	0.013	1.813	0.086	895.02	105.08
10	0.299	0.012	1.375	0.033	3041.31	1291.15
15	0.217	0.002	1.32	0.024	2700.91	432.88
20	0.178	0.001	1.077	0.014	2738.08	118.32
30	0.185	0.001	1.049	0.018	2533.56	88.31

Results of previous studies for comparison:

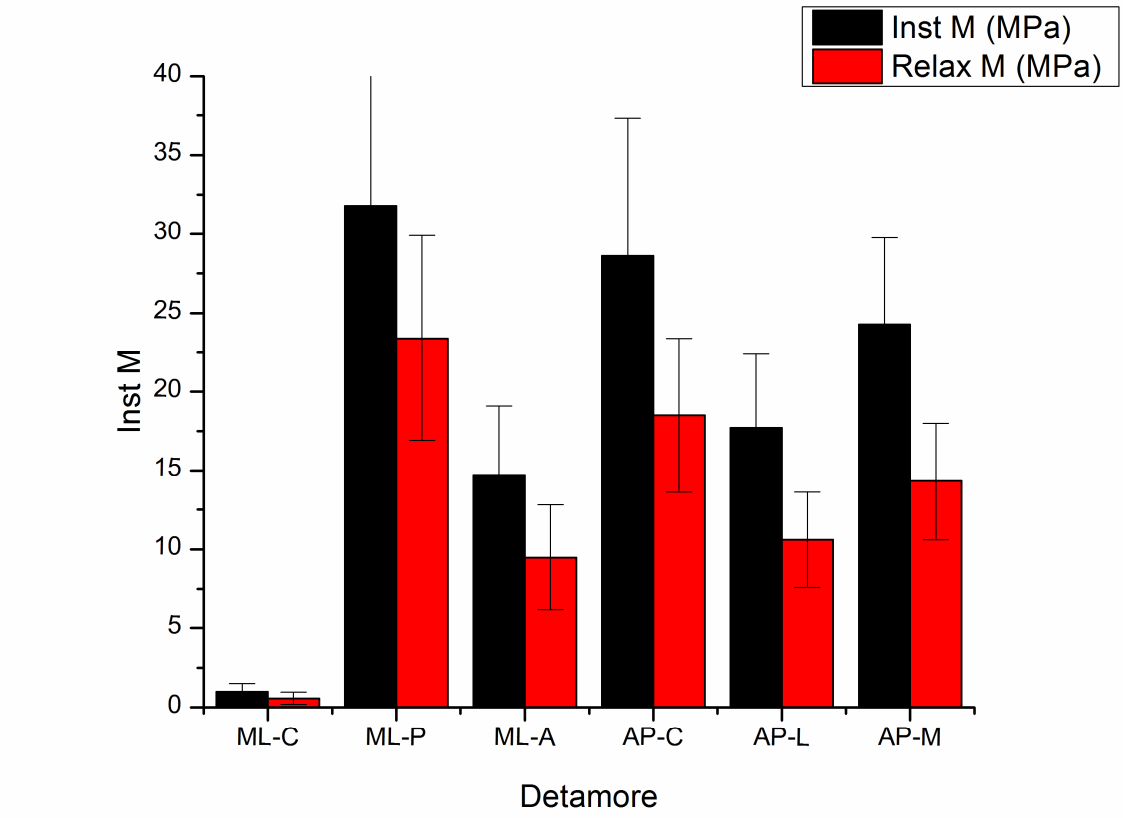

Figure 41 Detamore et. al. results from porcine testing for comparison [24] Significant anisotropy between ML-Cent region and AP regions were detected.

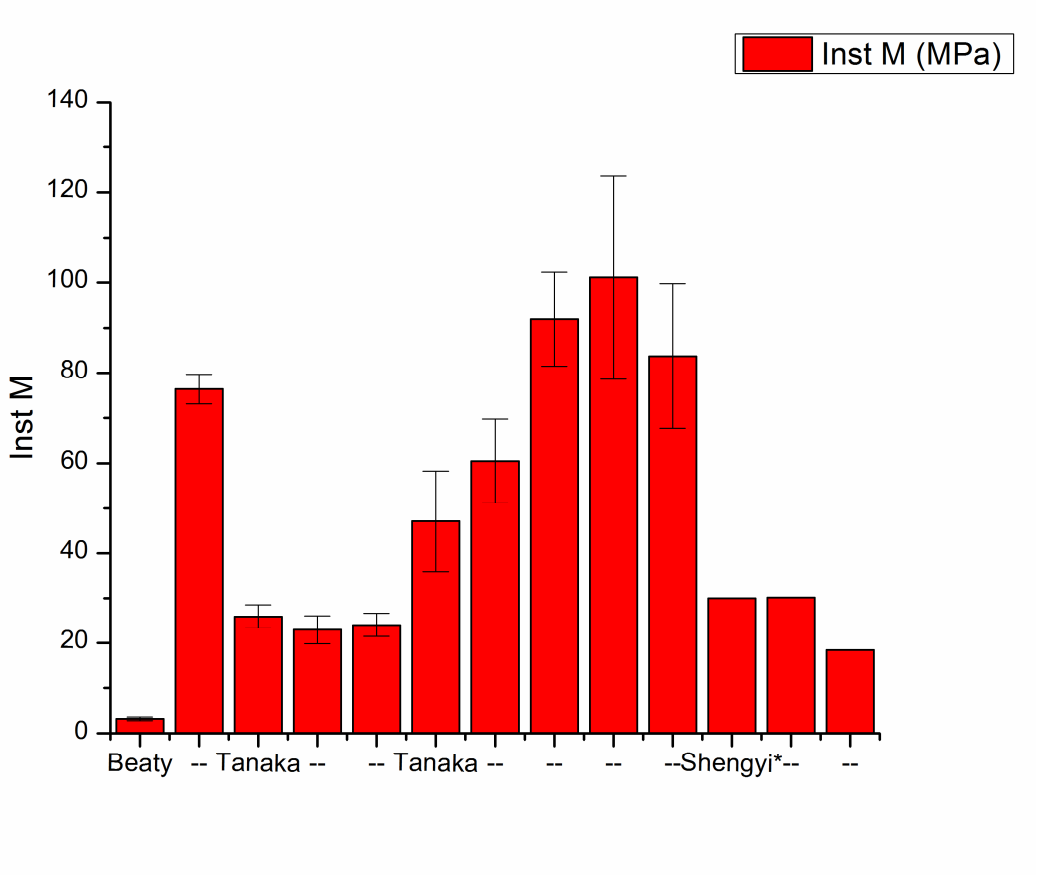

Figure 42 Compilation of results from previous tensile studies emphasizing the variation in tensile modulus [23, 70, 128, 129]

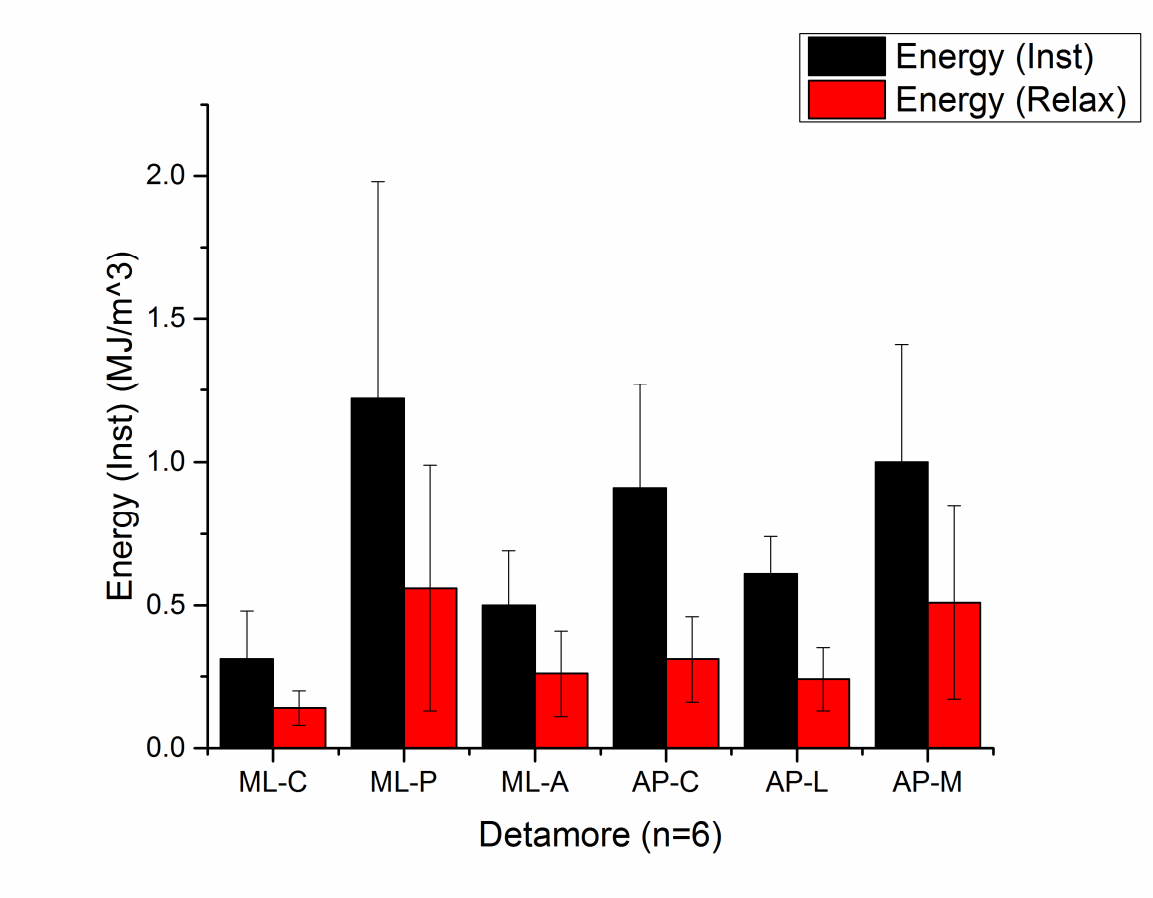

Figure 43 Results of Detamore et al. porcine tensile instantaneous and relaxed energy for comparison [24]

6.5 Discussion

The modulus values for the TMJ disc were less than other fibrous musculoskeletal tissues such as the human patellar tendon 504-660 MPa, human supraspinatus tendon 86 MPa, articular cartilage 13.6 MPa [248, 251]. The modulus was lower than previous human TMJ disc elastic modulus tested previously by Tanaka as 44.0 MPa [70]. By comparison, the instantaneous modulus of the human TMJ disc was found to be between 6-10 MPa. The value was much less than moduli found for tendon in previous studies and much closer to the value for articular cartilage. See Figures 41-43 above for comparison of previous studies. However, the instantaneous modulus found for human TMJ disc in this study was significantly different from porcine TMJ discs (14-30 MPa excluding the mediolateral intermediate oriented samples) [24].

The modulus value for female TMJ discs was higher than male TMJ discs. This was somewhat surprising given the amount of biologic variation between material properties in subjects overall. In addition, this material property value was independent of sample length or thickness size since all ramp loads were conducted at 1% per second constant strain rate. Modulus values for female were greater both in the AP and ML direction. Similarly, the relaxed modulus was consistently greater in females. More research is needed in order to understand the direct relationship the increased modulus has with the structure, function in human TMJ discs. During dissection, the female discs were consistently smaller and had a much more convex shape over a small condyle. The slope of the eminence was generally steep. The differences in anatomical morphology

should be matched with normal joint function to better understand the mechanical role of the TMJ disc.

Although sex differences in modulus were determined, no AP to ML oriented differences were found. The finding was consistent between the male and female groups. The lack of differences between AP to ML oriented samples does not agree with previous studies that found large variation between 5-25 times greater strength in the AP direction than ML direction [249, 250, 252]. In this study, there was a greater average modulus for AP oriented samples, though the value was not statistically significant. Animal tissues by comparison may exhibit more anisotropy due to the tissue being well defined in terms of matrix. Human tissues that were tested in this study averaged ~67 years of age. Due to age of subjects, older tissue may lose some anisotropy and become more uniform. The age of tissues may also explain why the values for modulus were generally lower.

The overall modulus compared to porcine tissues were much greater in pigs 14-30 MPa compared to 7.59 MPa in humans [249]. Pig tissues could have an overall larger strength based on the structure of anatomy. These were young tissues compared to older tissues in adult humans. In the pig study, the ML Center oriented samples of the TMJ disc was extremely weak in comparison to other regions. In this study the ML center oriented samples had the lowest average modulus between oriented samples, however this value was not significant based on the biologic variation. An interesting observation in this study was the value for ML center modulus in females had both the largest and smallest values for modulus within all the groups and greatest standard deviation among tissues. This phenomenon should be investigated further to understand if this region

shows signs of degeneration or changes in tissue composition and structure after injury or age. Finally, a morphological comparison between porcine tissues may help understand differences with regard to the human. The porcine animal model has been shown to be the most relevant to the human [25, 35]. In order for this model to translate well to the human, fundamental differences between the pig biconcave shape and size of the disc would have to be investigated. For instance, the morphology between human and pig TMJ discs must be compared with relation to jaw function between species.

In comparison to other human studies, Kalpakci et al found the instantaneous modulus to be significantly higher 55 MPa compared to 7.59 MPa in this study [252]. This modulus value was significantly greater than the other animal modulus values concluded in the study. In addition, the disc showed significant anisotropy with the AP Cent modulus being much larger than the ML Cent regions. The age range and load rate for human samples were not listed. Therefore, it was difficult to make a comparison between studies on that basis.

In our experience with mechanical testing in this study, we found the stress strain response to be highly dependent on load rate which is characteristic of viscoelastic materials. It is likely that such anisotropy exists between the AP and ML groups due to the many studies of SEM evidence of collagen fibers running in the AP direction. However, with regard to tensile testing, if a constant load rate was applied to each sample as in the case of Detamore and Kalpakci of ~1mm/sec then the length of sample may have an influence in the stress strain response [249, 252]. The AP length is generally 10 mm while the ML width of the TMJ dis is usually 18-25 mm, with the longest section

being in the ML center. If a uniform tensile load was applied to an AP and ML sample at a rate of 1mm/sec samples, then the rate at which the load was applied could affect the sample response, thus causing a larger modulus for the shorter sample (AP) and a small modulus for the long sample (ML). In this case, the AP sample could be loaded under twice the load rate. This may account for some of the large differences in anisotropy; however, it should be true for the ML Anterior and ML Posterior cases, which much more isotropic compared to AP. In our case, the AP and ML showed little anisotropy under a uniform 1 %/sec load rate but due to a much lower modulus and larger standard deviation, other factors with the biologic samples could have been a factor. Therefore, in the future the gage length of the samples tested along with the load rate should be listed or sample should be loaded at a uniform rate, so that results from these test can be compared acknowledging the load rate.

In this study, a linear response to strain was consistent throughout all regions (R^2~0.997). In determining both the instantaneous and relaxed modulus through linear fit, the stress response was linear for all strains, in this case strains through 30%. In other tissues, such as tendon, the nonlinear response both instantaneous and relaxed modulus became apparent with strains over 30% [56]. This was similar to other tensile studies on the TMJ disc [249, 252].

The differences between the instantaneous modulus (7.59 MPa) and relaxed modulus (3.27 MPa) were significant. This was also true for the instantaneous and relaxed areas under the stress-strain plots, since they were essentially calculated from the same values. Detamore et al. referred to the area under these plots to indicate the strain

energy absorbed by the disc [24]. The large difference ~50% between strain energies of the instantaneous and relaxed energy may indicate the disc's ability to dissipate large strain energies upon initial loading. These large strain energies may be absorbed through viscous response while the linear elastic response appears to be maintained through 30% strain. An analysis of the individual relaxation curves for each sample is needed to further understand the viscoelastic response between the initial loading and relaxed equilibrium.

In order to model individual stress relaxation response with respect to time, a reduced relaxation function proposed by Fung was used [56]. This model was proposed based on the quasilinear viscoelastic theory (QLV). The theory was chosen early on instead of Maxwell, Voigt and Kelvin models due to the nonlinear behavior of biologic tissue which often depends on strain history. The QLV theory appears to account for strain history for finite deformations and has been used to model many types of cartilaginous and other soft tissues.

For individual strain response, the time and stress was normalized to time=0, stress =1. Each stress relaxation curve began at the peak instantaneous response and ended at equilibrium for each strain increment. For each sample that was tested, five relaxation curves (according to strain %) were curve fit by the reduced relaxation function. The reduced relaxation curve fit involved a logarithmic fit with an exponential integral. The curve fit yielded three relaxation parameters: C, τ_1, τ_2. The physical meaning of the curve fitting parameters corresponded to a short time constant, τ_1 to model the initial instantaneous drop in stress and a long time constant; and τ_2, to model

the equilibrium portion of the relaxation curve. The parameter, C accounts for the energy dissipation in the tissue. The initial stress as a response to a step increase in strain was not modeled as with an exponential model but rather a linear model due to the linear response to step increases in strain (R^2~0.997). When the initial and relaxed response to step increase in strain was modeled using $\sigma=A*(e^{B\varepsilon}-1)$, the material constant B, A resulted in a linear fit instead of exponential.

The curve fitting parameters C, τ_1, τ_2 were strain dependent for all strains, 0-30%. These values were significant, indicating that the viscoelastic relaxation response to a step increase in strain in TMJ disc tissue appears to be strain dependent. At 0-10% strain, the TMJ disc tissue appears to exhibit a much larger C than other strains which could possibly indicate a greater storage modulus and energy dissipation capacity. From 10-30% this energy dissipation property appears to remain constant. One possible interpretation of this value could be that the tissue within 5-10% strain could react and distribute strain energy without a large influence on the matrix, then past 10% the tissue loses much energy dissipation capacity and the loading shift to being carried by the solid matrix, mainly collagen.

The results for the time constants also indicate significant differences based on strain. The long time constant τ_2 appears to be small (895 seconds) for the initial 5% strain, while the long time constant increases rapidly from 3000-2500 for strains 10-30%. This may indicate the tissue reaches equilibrium much sooner under strains up to 5%, but afterwards the tissue requires much more time for the stress response in the tissue to reach equilibrium. The opposite is true for the initial short time constant; where the

initial response at 5% strain takes much longer dissipate than strains 10-30%. The stress response then shifts at the 10-30% strain levels, towards a tissue that immediately drops in response to initial strain taking longer to reach equilibrium. This tissue behavior provided some of the most interesting considerations for future studies. Typically, viscoelastic response is examined for a very thin layer of articular cartilage or small sample of tendon. These tissues are usually extremely anisotropic. The TMJ disc however, has a very unique bioconcave shape with anterior and posterior bands in some cases 5-10 mm thick with an intermediate region sometimes as thin as 2 mm. This unique morphology combined with a unique viscoelastic tensile behavior should be combined with other loading mechanisms within a finite element model to understand the possible large, stress shielding mechanism that could exist in the disc. The bioconcave shape of the disc, the thinness of other articular surfaces of condyle and glenoid fossa, and the local attachments of the retrodiscal tissue and lateral pterygoid should also be considered in the model.

In addition to the cumulative viscoelastic fitting parameters, the fitting parameters were not affected by gender ($p=0.286$) or AP or ML orientation ($p=0.467$). Overall, the specific region-orientation did not affect the parameters ($p=0.141$).

In conclusion, this study found the modulus for 12 human subjects to be 7.59 MPa. Female modulus values were found to be higher than male values. The average AP direction of the tissue had a higher modulus; however, these values were not statistically significant. Overall, the tissue exhibited viscoelastic behavior that was dependent on strain percent. In the future, the effect of tensile properties of the disc

should be modeled with finite element models. In addition, consideration should be given for regional behavior of the disc as well as discal attachments that may affect disc behavior in response to loading.

7 GENERAL CONCLUSIONS AND FUTURE WORK

The purpose of this research was to conduct a biomechanical characterization of the human TMJ disc. Through experimental methods the biomechanical environment of the disc was investigated through strain dependent diffusivity and fixed charge density measured by the conductivity method and the viscoelastic tensile properties of the disc measured by incremental stress relaxation. These important properties will have a bearing on the TMJ disc biomechanical function under mastication and will give us insight on the nutrient concentration gradient across the disc as well as the electrochemical signaling environment within the disc.

Conductivity, Diffusivity, and Nutrient Transport within the Human TMJ Disc

From the electrical conductivity study, we found mechanical strain decreases the porosity of the disc and thereby decreases conductivity of the disc, which is proportional to diffusivity. This finding supports *our overall hypothesis* that mechanical strain significantly affects the transport behavior of the disc and may play an important role in altering the nutrient environment within the tissue leading to tissue degeneration. With strains of 10% and 20% the diffusivity of small ions Na^+ and Cl^- decreased by -12.3% and -23.5%, respectively. In studies conducted since, we have found the diffusivity of larger solutes such as glucose decreased by as much as 40% under a 20% strain. This would indicate a much steeper nutrient concentration gradient than indicated by the electrical conductivity study; further, the impact of mechanical loading may have an even greater impact on diffusion with much larger growth factors and cytokines. Our FRAP

studies support similar findings [58]. This provides further rationale for the need to develop an accurate 3D finite element model to investigate the effect of mechanical strain on the diffusion of different solutes within the disc and their effect on cell behavior and matrix remodeling.

The conductivity of female TMJ discs (5.84 mS/cm) were slightly greater and affected more by mechanical strain than the conductivity of male TMJ discs (5.14 mS/cm). This may indicate slight differences in the extracellular matrix of TMJ discs of males and females. We found the human TMJ disc conductivity (5.45 mS/cm) to be much greater than the conductivity we found in our porcine study (3.10 mS/cm). This should be taken into account when working with young porcine tissues to investigate treatments and tissue engineering strategies for human TMJ discs. Although the conductivity in porcine TMJ discs was much lower corresponding to a lower porosity, they were affected by mechanical strain in a similar manner. This observation is important to keep in mind when comparing or translating models. Overall conductivity of the TMJ disc (5.5 mS/cm) is ~25% lower than IVD and hyaline cartilage (7.5 mS/cm). However, when moving to oxygen and glucose diffusion, the diffusivity of TMJ disc tissue was much lower (~50%) than IVD and hyaline cartilage. It must be emphasized that our results for conductivity can only be interpreted for small solutes investigated in the experimental tests. When moving to large solutes, the effect of mechanical loading may have more effect on solute diffusivity. In addition, when the conductivity comparisons are made between other types of cartilages, the conductivity values do not

account for the fixed charge density that may further affect diffusivity especially in cartilages that have a much greater concentration of fixed charge density.

Fixed Charge Density in Human TMJ Discs

The fixed charge density is a material property of cartilage which results from highly charged proteoglycans present in cartilaginous tissues. This material property is unique to cartilage and is responsible for high osmotic swelling pressure which maintains load and also for unique streaming potentials and electrokinetic affects within cartilage. The fixed charge density (FCD) found in human TMJ discs was 0.05 mEq/g wet tissue and was comparable to previous studies that found the FCD for annulus fibrosus tissue of porcine to be 0.06 mEq/g wet tissue.

The fixed charge density must be taken in to account when modeling tissue especially since the TMJ disc is believed to incur large deformations under mechanical load which would effectively increase the fixed charge density concentration. Inside the TMJ disc the electric potentials generated by fluid pressure moving through the charged matrix may alter electrochemical signals within the disc. Further, the alignment of matrix fibers has been shown to be anisotropic through SEM analysis, due to this observation the streaming potentials based on direction of fluid flow may be anisotropic in the TMJ disc. This physicochemical signaling environment will need further investigation in the TMJ disc model.

Finally, the human specimens measured for FCD were relatively old (81 years) and had been stored previously in refrigeration. The value measured in the study provides an overall basis for FCD, arguably on the low end of what could be expected in

persons within the age of onset of TMDs (25-45). The role of FCD and streaming potential within the disc must be investigated further from the standpoint of the large deformations the TMJ disc undergoes to provide stress shielding and lubrication of the joint. The FCD should be investigated for concentrations through the inferior to superior directions, with emphasis given to the surface charges along the outer surface of the disc. A double layer effect could be present on the surface of the disc which is dependent on the TMJ disc fixed charge density and allows for extreme lubrication of the disc in addition to the hyaluronan within the synovial fluid. This effect should be studied in more detail and compared to shear-tractional studies by Nickel et al. [144].

TMJ Disc Mechanical Behavior

To determine the tensile properties of the TMJ disc, an incremental strain was placed on the tissue and the viscoelastic stress relaxation response was recorded. In determining both the instantaneous and relaxed modulus through linear fit, the stress response was linear for all strains. In other tissues such as tendon, the nonlinear response to both instantaneous and relaxed modulus became apparent with strains over 30% [56, 69]. In previous work, the TMJ disc was shown to exhibit anisotropic tensile responses between the anteroposterior and mediolateral directions [24]. In our case, the TMJ disc did not appear to exhibit anisotropy between regions and exhibited a tensile modulus lower than previous studies likely do the age of donors in this study.

When analyzing the viscoelastic stress relaxation we found significant differences to load response based on strain. We found that the tissue reaches equilibrium much sooner under strains up to 5% but afterwards the tissue requires much more time for the

stress response in the tissue to reach equilibrium with 10-30% strain. This could indicate a shift load in response under physiological loading conditions, for instance an elastic response within 5% strain followed by fluid pressurization response. The results of viscoelastic response must analyzed with respect to the highly bioconcave anatomy of the TMJ disc. It is likely the TMJ disc exhibits complex biomechanical function through its viscoelastic behavior and anatomical structure which can only be analyzed with through FE modeling.

7.1 Future Work

The body of this research has focused on the direct measurement of key biomaterial properties of the human TMJ disc. Understanding these properties has allowed us to model and understand the disc in relation to other types of cartilages. But for the experimental properties measured in this study to apply to the human patient, a 3D model of patient specific anatomy, joint loads, and material reaction must be constructed. This 3D finite element model will allow us to not only investigate how each parameter influences disc behavior under loading, but it will also allow us to investigate how the parameters influence each other during joint function, a multiphasic true material characterization. (i.e. fixed charge density effects on diffusivity). This model can also be constructed with key cell metabolic data from our explant studies that will allow us to predict the physicochemical environment of the disc in response to physiologic and pathologic loading (i.e. how does the change in disc diffusivity through sustained loading alter the available oxygen content thereby affect local cell metabolism?)

Developing a Multibody Model through Dynamic Stereometry: Patient Anatomy Combined with Jaw Kinematics

To generate a patient specific model, the TMJ disc's anatomy and motion must first be measured during function. A multibody model is generated to model and predict inner joint loads acting on the disc which will be used later in the finite element stress analysis. A multibody model alone is a useful diagnostic tool that traces condylar motion and allows researcher to analyze condyle, disc and fossa motion in real time. This tool can be used to classify patient pathology given enough patient numbers in our predictive study. One main difficulty we have encountered using the multibody model to classify patient pathology is the condylar motion path is so complex during mastication combined with many different classifications of TMD's.

We have implemented a system in our lab first pioneered by Gallo and co-workers to combine high-resolution MRI with real-time 3D motion tracking during jaw function (Fig. 2). This technique uses high-speed infrared cameras to track target frames on the mandible and maxilla in 6 degrees of freedom (DOF). The motion data is combined with three-dimensional TMJ anatomies obtained from high-resolution MRI using a computer CAD program then analyzed using a finite element program (COMSOL (Comsol, Burlington, MA) [4].

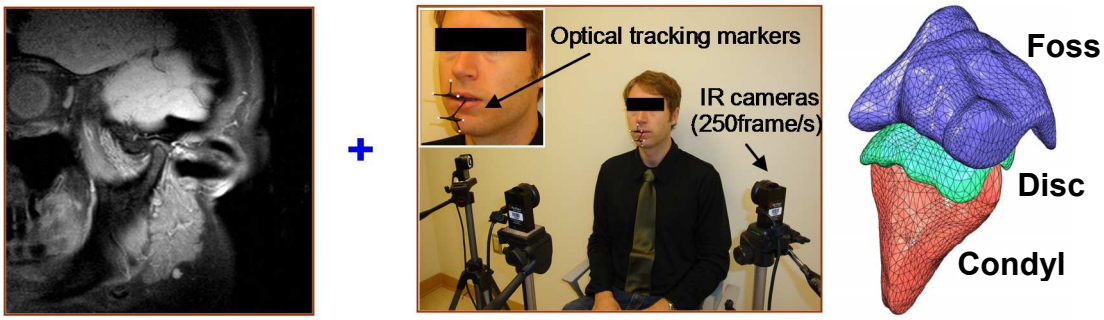

Figure 44 The dynamic stereometry system consists of (A) high resolution MRI, (B) 6 DOF jaw tracking, and (C) Algorithms to reconstruct dynamic TMJ anatomy into a finite element model.

MRI Imaging: Dicom images from MRI were segmented in Amira (Amira, Burlington, MA) to generate at 3D solid mesh of the patient TMJ, including condyle, fossa, and disc. The solid mesh was imported to SolidWorks (Waltam, MA) where trajectories were applied to run the motion analysis. The anatomy of the TMJ bony and disc structures in the different jaw positions was obtained by recording a series of 14 magnetic resonance parasagittal slices through the TMJ using a 1.5 T scanner and 12-cm Ø surface coils.

Human TMJ Mechanical Characterization: In order to define TMJ disc's multiphasic properties in the model, we will measure the compressive modulus, tensile modulus as well as the strain dependent transport properties of human cadaver TMJ discs.

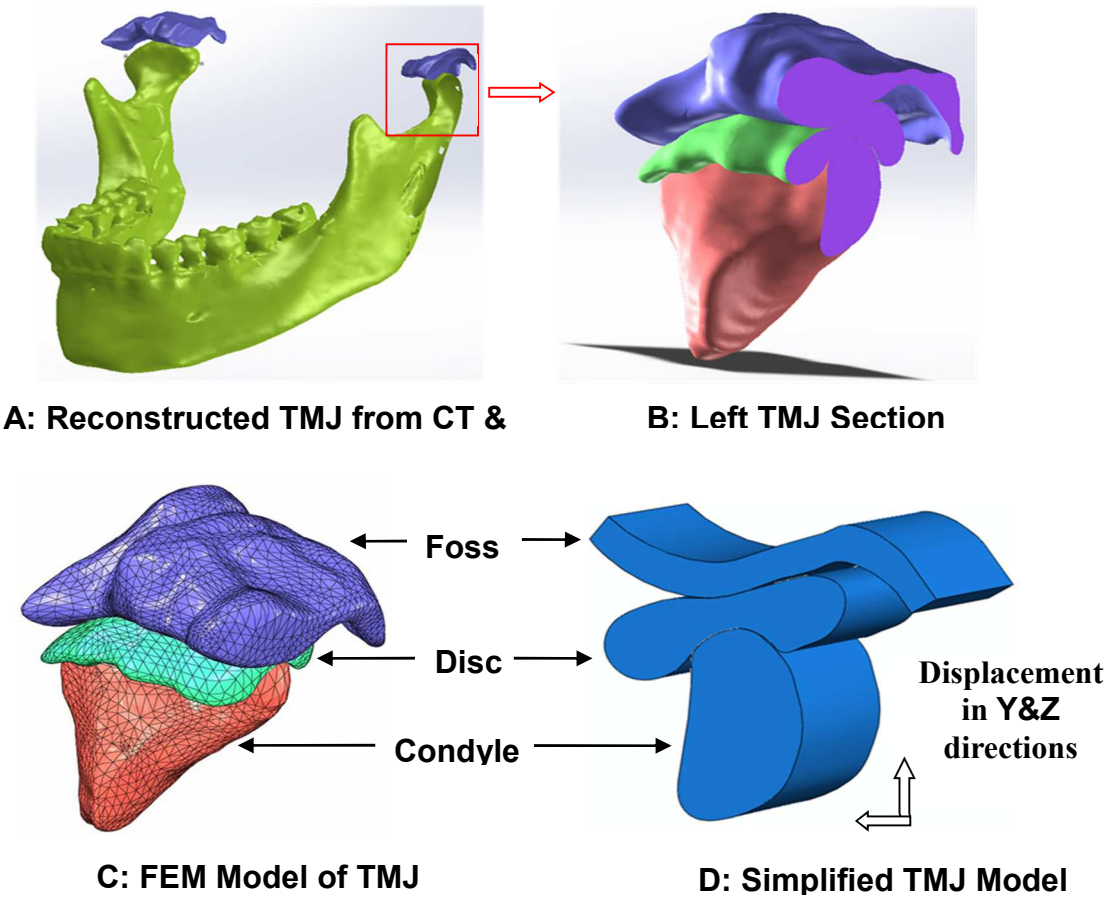

Figure 45 Showing the MRI/CT reconstruction of a TM joint MRI/CT to meshed solid Finite Element model

Patient specific anatomy was constructed from (a) MRI/CT geometries, (b) section view of solid, (c) Solid geometries were formulated into a tetrahedral mesh and (d) evaluated with patient motion data in simplified model.

7.2 Finite Element Model

Because of the lack of appropriate animal models and the difficulties of in vivo measurements, finite element modeling is the only means possible to examine the relationships between coupled physical properties of the disc. This 3D multiphasic model of the human TMJ disc will allow us to determine the effect of mechanical loading on the nutrient diffusivities within the tissue. In addition, attempts at dynamic MRI to analyze jaw function have been ineffective due to lack of resolution and absence of true masticatory motion. As a result, the dynamic stereometry of the TMJ developed by Gallo et al is the only validated technique to provide 3D dynamic TMJ anatomy during jaw function [14]. This study will incorporate dynamic stereometry to obtain patient specific geometries and jaw function to build a 3D model of the TMJ disc from the validated 2D model.

Develop and validate a 2D axial symmetric finite element model of cylindrical TMJ disc explants using material properties.

The 2D model will be based on the triphasic theory developed by Lai et al. combined with our extended multiphasic mechano-electrochemical theory [20]. Our model considers charged hydrated tissue as a mixture of distinct phases (charged solid, interstitial water, ions and neutral solutes). Material properties such as region-dependent aggregate and tensile modulus, strain-dependent fixed charge density, hydraulic permeability, and solute diffusivities in five disc regions will be inputs that define the material [46]. The weak form of the governing equations will be formulated from Galerkin residual method and solved using implicit Euler backward scheme with

software, COMSOL (Comsol, Burlington, MA) [45]. The model will calculate changes in streaming current and solute diffusivities under compressive load. The finite element model of the TMJ explants will be validated in a well-controlled unconfined stress relaxation compression test on cylindrical samples from five regions of both human and porcine discs (n=10). The disc will be subjected to a stress relaxation test (TA Q800 Dynamic Mechanical Analyzer) and the responses of axial load and streaming current recorded (Model 2400, Keithley Instruments Inc., Cleveland, OH.)

A 2D dynamic multiphasic finite element model of TMJ disc explants will be obtained for the human model and the porcine model. The responses of axial load and streaming current (I) under the relaxation tests will be recorded in real-time. The precision of the finite element model will be evaluated by comparing the outputs of model prediction to recorded axial load and streaming current measured at the center of the specimen.

Integrate the dynamic stereometry and the multiphasic finite element model to establish the 3D patient specific model.

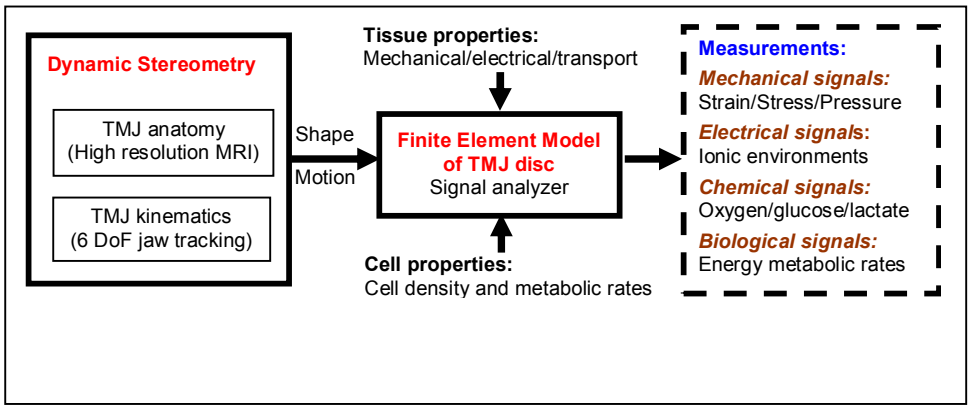

Figure 46 Schematic of integrating the dynamic measuring system

The validated 2D finite element model can be mathematically extended to a 3D model of the TMJ disc without significant difficulties. This material model will be developed into a patient specific model through the MRI (Siemens Trio 3T) acquired TMJ disc anatomy. Dicom images from the MRI will be segmented in Amira (Amira, Burlington, MA) to generate at 3D solid mesh of the patient TMJ, including condyle, fossa, and disc [48]. The nutrient supply at the margin of the disc from the synovial fluid and capillary will be considered by the concentration boundary conditions. The segmented mesh will be exported for analysis in Hyperworks (Hyperworks, Troy, MI). In Hyperworks, trajectories recorded using 6 DOF jaw tracking will be applied to the patient anatomy to run the motion analysis. We will transfer stress strain profiles from Hyperworks to (Comsol, Burlington, MA) to analyze the mechanical, electrical, chemical, and biological signals.

Results and Interpretation: The patient specific model will be analyzed based on individual kinematics to determine stress field translation [49], nutrient concentrations, and metabolic rates within the disc. Patient specific models will be analyzed individually and across patient populations to develop bio-indicators (e.g., nutrient levels and energy metabolic rates) and evaluate risk among patient groups. We anticipate that the mechanical loading will dramatically impede the nutrient transport, resulting in extremely low oxygen/glucose concentration profiles within the TMJ disc which will significantly affect cell matrix synthesis and even cell death. The effect is mainly due to the strain-dependent oxygen/glucose diffusivities and hydraulic permeability.

Potential Difficulties and Alternative Strategies: Because the nutrient concentrations and metabolic rate are interrelated, these measurements are expected to be correlated among themselves within disc region, among disc regions within a disc, and across the loading settings. Thus, it may be possible to gain efficiency by jointly modeling these outcomes rather than evaluating them separately, although at a cost of greater model complexity. If statistically significant bio-indicators do not emerge from analyses of each outcome, we will investigate joint models that incorporate both known relationships and flexibly permit both positive and negative correlations among the outcomes.

Innovation: The innovation of this study lies in the project's unique approach to use a patient specific model to build a pathway between biomechanics and pathobiology while bringing the clinical field a crucial, non-invasive method to detect early indicators of TMJ disorders.

Human Finite Element Model from Patient Specific Model

Centric Occlusion

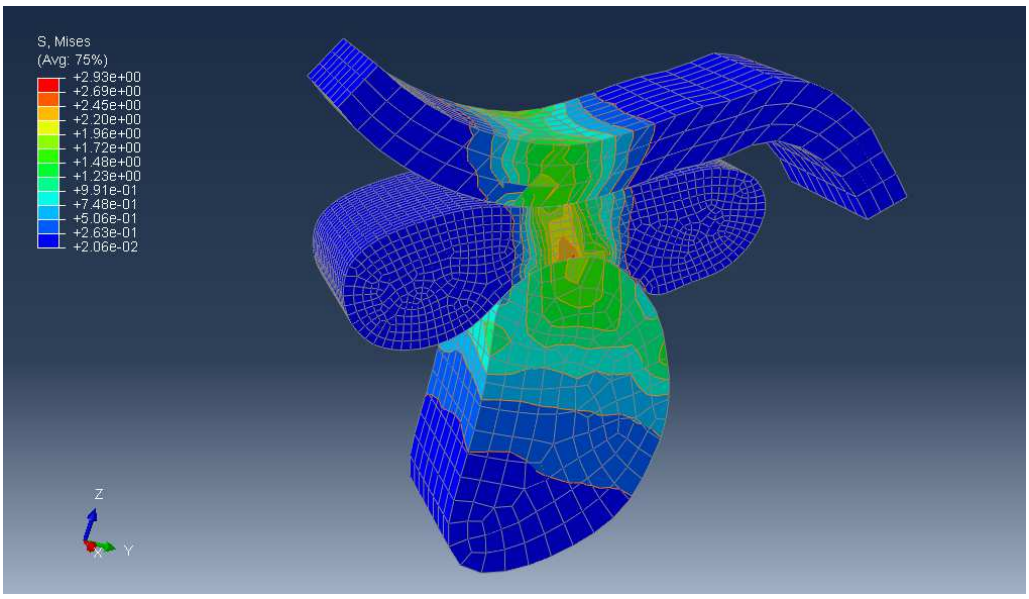

Protrusion

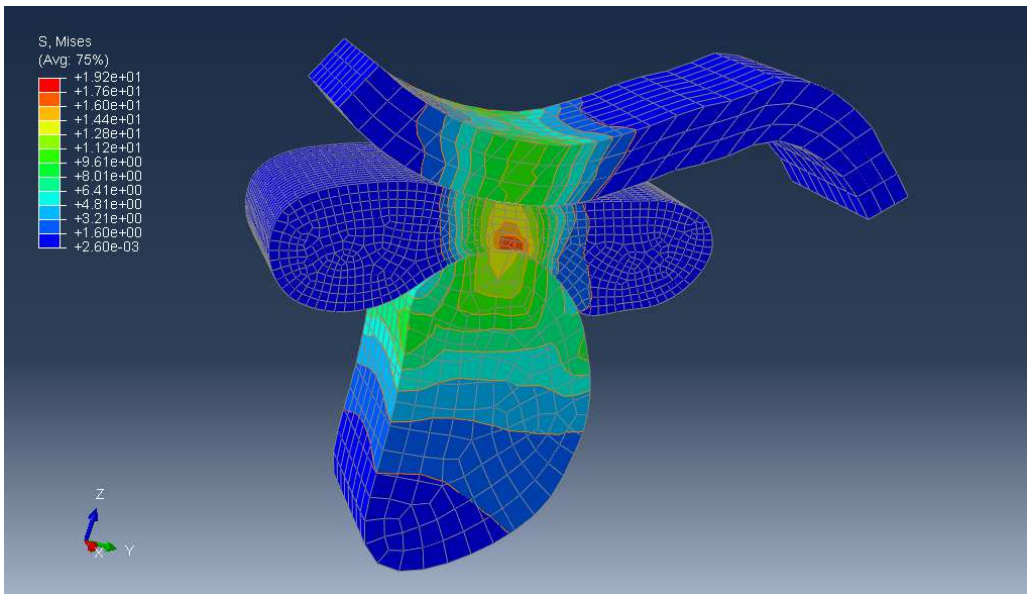

Figure 47 The resulting FE model conducted in Abaqus shows the stress translation profile within the disc based on normal jaw opening and closing.

APPENDIX

8 APPENDIX

A biomechanical investigation of thoracic hyperkyphoscoliosis in EOS treated with rib fixation

8.1 Abstract

Study Design: Biomechanical comparison in an immature porcine model of different anchorage techniques, pedicle screw fixation and a newly developed rib hook construct.

Objective: The goal of this research study was to examine kyphotic deformity effects on upper thoracic fixation, specifically pedicle screws and laminar hooks placed on the ribs.

Summary of Background Data: After a successful clinical outcome in treating over 50 patients with severe kyphosis, a biomechanical validation of a 4 rib fixation in the upper thoracic region is investigated.

Methods: Twelve full-immature pig spines (8 weeks) were instrumented with growing rods bilaterally. In two test groups, 6 spines were instrumented with pedicle screws and 6 spines were instrumented with lamina hooks to the ribs in proximal fixation. All spines were potted distally. The spines were loaded with a pure bending load at the potted proximal connection (MTS, Eden Prairie, MN).

Results: For the pedicle screw group, fixation failure was recorded on all six tested spines. Failure was pedicle screw pull out. The average deflection angle at the failure point was 35.8±1.3 degrees with average maximum bending force of 118.6±25.7N. For the rib construct group, no fixation failure was observed on all six tested spines through

average maximum deflection angle of 50.3±9.1degrees, while the average maximum force was recorded 119.7±13.9N without failure.

Conclusions: The rib construct provides superior proximal fixation for resistance to kyphotic bending forces.

8.2 Introduction

In Early Onset Scoliosis, significant surgical gains have been made to manage severe scoliosis without spinal fusion [253]. This allows continued growth of the spine through development, providing curve correction while minimizing risk to pulmonary function [254]. Each case is different developmentally and provides the surgeon with a unique challenge to assess future progression based on current skeletal development and syndromic etiology. A surgical plan is developed based on age, potential growth, and specific etiology [255, 256]. When planning for surgical intervention, the dual growing rod system has been shown as the accepted method compared to the single rod fixation, hybrid constructs, Harrington rods and Luque trolley [257-261].

For severe cases, with severe Cobb angle and kyphosis greater than 45 degrees (hyperkyphosis), dual growing rods are commonly used. Distal fixation is anchored by sacral S-hooks or pedicle screws in the lower lumbar. For upper thoracic fixation, pedicle screws or lamina hooks are used. Studies haved indicated that dual growing rods are the safest technique among the single growing rod and VEPTR, are the preferred method in the presence of kyphosis [258]. Several research groups have documented prospective as well as follow up studies identifying complication rates and method of

implant failure in patients [257, 262-265]. The studies indicated a complication rate between 48-52%. A common direct implant related complication was at the proximal fixation, either through pedicle screw pullout or lamina hook failure. Although Sankar et. al did not find a correlation with preoperative levels of kyphosis and complication rate [265], a recent study by Watanabe has indicated that kyphosis level increases for every 20 degrees was an independent risk factor for failure of the proximal fixation [266]. Increasingly, in both studies and conference proceedings, significant kyphosis has been a concern for effective dual growing rod treatment, especially in upper thoracic fixation [267].

The difficulty with controlling kyphosis with growing rods comes with the inherent pullout forces generated in the upper thoracic curve. The problem is compounded by deformed vertebra and often osteoporosis in this region. Adult cadaver studies have shown that reduction in bone mineral density due to osteoporosis significantly reduces pedicle screw pull out strength [268-270]. The studies show the significant risk with pedicle screws in osteoporotic spine. Further, in the review of early onset scoliosis complications, lamina hooks with lamina anchorage in this region are also reported with the same incidence of failure, if not higher [266]. From a biomechanical perspective, an inherent risk is involved in the placement of rigid titanium rods, securely anchored in the sacrum or lower lumbar, to a proximal foundation with questionable bone density and size with distraction forces directly opposing the anchor in the presence of kyphosis.

The clinical basis of this study came as a result of experiencing this problem in two cases with kyphosis angles of greater than 50 degrees. In each case, neither pedicle screw fixation or the VEPTR was recommended. Since the patients had a kyphosis angle greater than 40 degrees, the VEPTR was excluded. Since the patients were considered osteoporotic by the WHO criteria, pedicle screw fixation was excluded. The initial case was a revised surgery where pedicle anchorage in place had already failed. In order to move fixation away from the pedicle, the surgeon developed a 4 rib construct which anchored lamina hooks to the ribs [271]. In both cases, the patients had satisfactory outcome with no complications with 3 year follow up [271]. The procedure has been proven effective in over 50 cases involving severe kyphosis over 50 degrees, including 9 cases of kyphosis over 100 degrees. With an average of 2 year follow up, the construct has provided significant improvement in both Cobb (24 degrees) and thoracic kyphosis (34 degree improvement pre vs post op). In all cases, only two indications of proximal dislodgement or failure have been indicated. Only one construct was removed due to infection.

Rather than recommend the 4 rib construct for wide spread use based on clinical observation, this research group developed a controlled biomechanical model by which to test the upper thoracic fixation strength of the 4 rib construct with the currently used pedicle screw fixation. In the biomechanical model, immature pigs spines were used (~21.3 kg) to simulate the spine of a 31.75 kg pediatric patient. To simulate kyphosis acting against the proximal fixation, a pure bending test was conducted across the full length of immature porcine spines. Two groups were used for the study with anchorage

to the proximal fixation, a control group with pedicle screw fixation and an experimental group consisting of the 4 rib construct. Although, many pullout studies have investigated pedicle screws and lamina hooks on individual vertebra in animal and cadaver models [272] [273], this group sought to examine full bending of the construct to investigate the mode of fixation failure between the novel 4 rib construct and the control pedicle screw group.

8.3 Materials and Methods

Twelve pig spines (6 for the pedicle group, 6 rib for the construct group) were obtained from the Strom Thurmond research center (Medical University of South Carolina, Charleston, SC). Spines were harvested from Yorkshire domestic male pigs (8 weeks, weight 21.3 kg (+/- 1.3 kg) by the surgeon from T1 to L5 with thoraces intact in the animal OR under IACUUK guidelines. The size and weight of both spine, rib cage and pedicles were equivalent to the skeletal size of a 31.75 kg patient as determine by the surgeon as representative of the patient population. Titanium growing rods (5.5 mm) were instrumented bilaterally in both groups. No instrumentation was included distally, since the distal foundation was potted for biomechanical testing. In the proximal fixation, for the pedicle screw group, pedicle screws were placed in T3 and T4 bilaterally in accordance with previous methods, see Figure 48a below and Figure 49a below [258]. When setting the pedicle screw group in the animal OR, a fluoroscope was used for placement, see Figure 49 below. In the 4 rib construct group, lamina hooks were placed on ribs 3-6 by the same surgeon relating the porcine anatomy to the pediatric patient. Lamina hooks (wide blade for 5.5mm rod, Medtronic Memphis, Tennessee) were used on

the ribs in block formation, with 2 down-going hooks on ribs 2 and 3 and 2 up-going hooks on ribs 4 and 5, affixed to bilateral growing rods, see Figure 48b below and Figure 49b below. During placement of the hooks, hooks 2 and 4 were gently compressed, then hooks 3 and 5 are compressed with a parallel compressor (Medtronic, Memphis, Tennessee). All titanium rods, pedicle screws and lamina hooks, and surgical tools were used as in the conditions of normal pediatric surgery (Medtronic, Memphis, Tennessee).

(a)

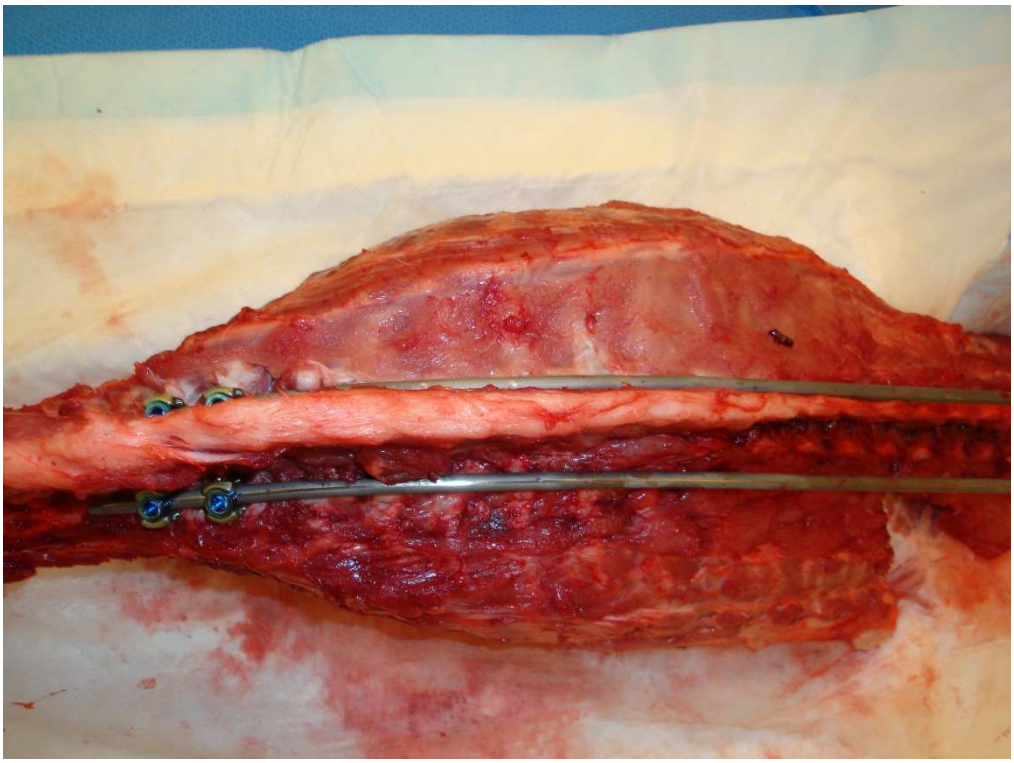

(b)

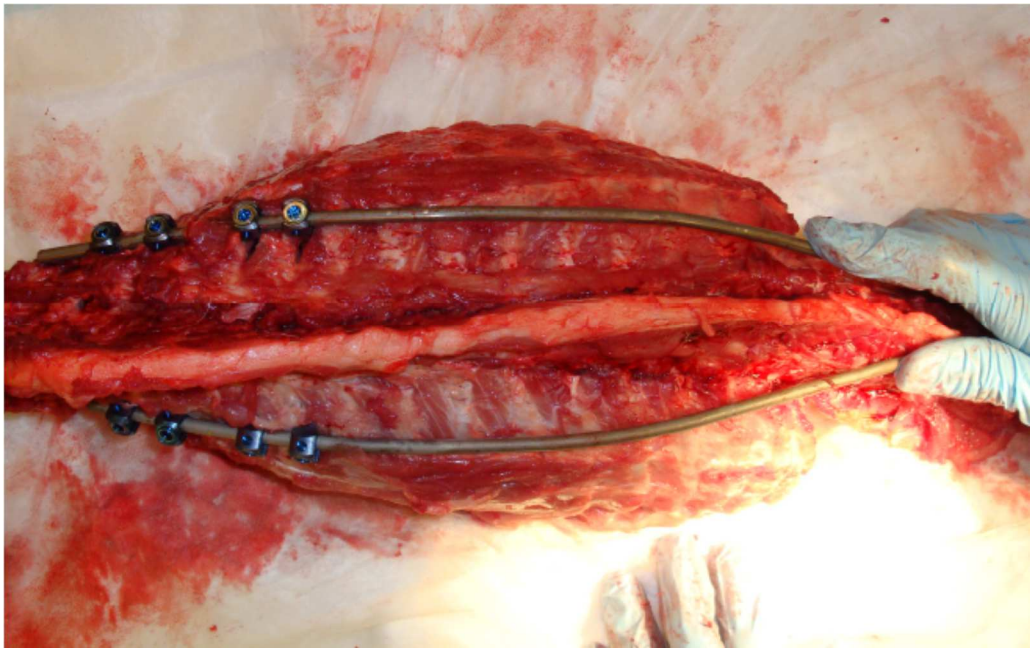

Figure 48 a) Pedicle screw fixation on T3 and T4. b) 4-Rib Construct fixation on ribs 3-6.

(a)

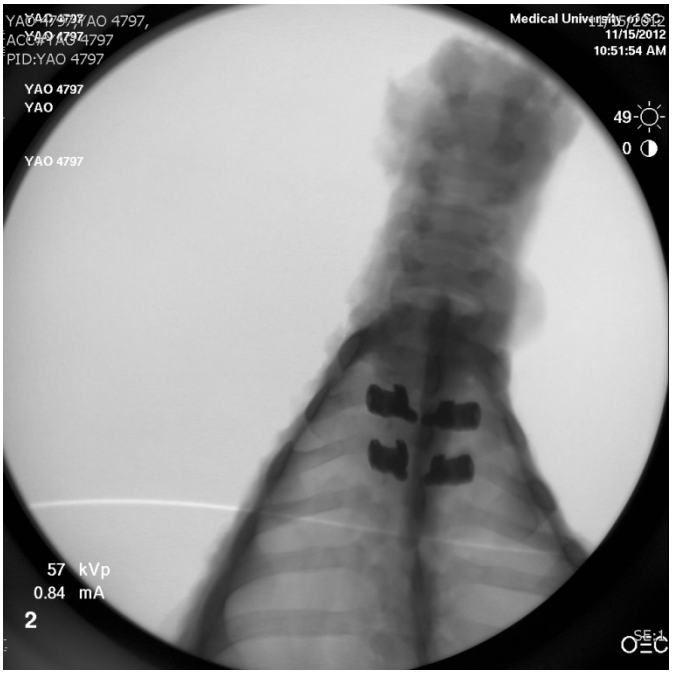

(b)

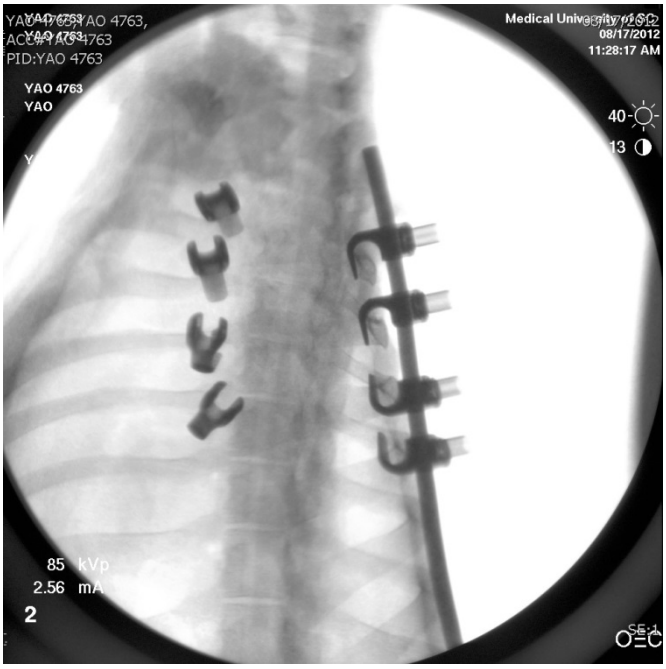

Figure 49 showing placement of pedicle screw and hook constructs by fluoroscopy in the animal OR

a) Pedicle screw placement on T3 and T4, b) Rib construct placement on ribs 3-6.

After the pig spines were instrumented and imaged, they were refrigerated (4 degrees C) until mechanical testing. Studies have shown musculoskeletal that samples retain biomechanical strength for up to 5 freeze thaw cycles [148]. The samples were potted (Bondo-Marhyde, Atlanta, GA) proximally and distally in custom designed potting fixtures for mounting, see Figure 50 below. In the distal pot, growing rods extended past the lower lumbar and were used to align the base of the spine within the pot. Similarly, the proximal end of the specimen was potted to T1 with small acrylic rods (1mm diameter) extending past T1 for alignment. Thus, all spines were consistently aligned within both proximal and distal pots along the horizontal and vertical axis before testing.

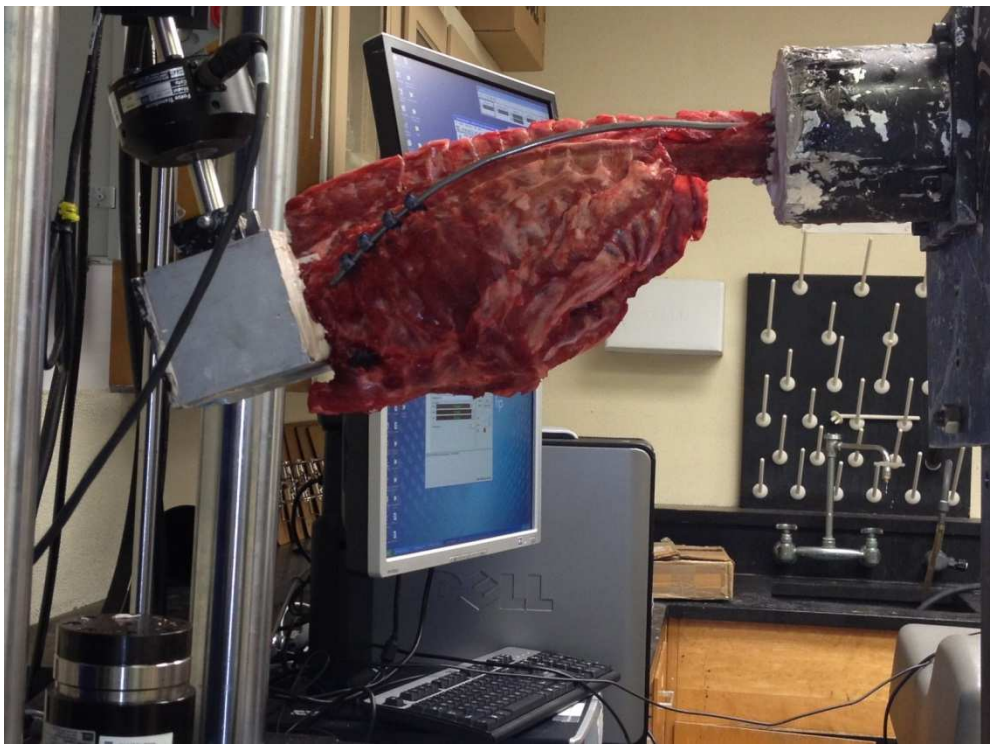

Figure 50 Test configuration for full spine bending
Inline load cell with actuator measured bending force at potted proximal connection at T3

The distal potted end of the spine was anchored to a custom built mount which securely anchored the base of the spine perpendicular to the MTS instrument (MTS, Minneapolis, Minnesota), see Figure 50 above. A pure bending force, which simulated kyphosis, was applied to the spine by the MTS at the proximal potted fixation (see Figure 50 above) [274]. The force was applied by using the MTS load arm which was able to generate bending from 0 to 90 degrees for each specimen. The bending force was measured by a load cell in line with the actuator. A pin-pin connection was used to attach the actuator to the load arm of the MTS along with a pin-pin connection to the proximal pot, in order to apply a pure bending force without generating a moment at the proximal pot.

All spines were loaded from 0 to 90 degrees deflection angle, with the resulting load measured. MTS load data were synched with video data. ImageJ was used to determine deflection angle and displacement. Maximum bending force was determined as a 20% decrease in load as a result of fixation failure or maximum force at the end of the experiment when no failure had occurred.

8.4 Results

For the pedicle screw group, fixation failure was recorded on all six tested spines, see Figure 51 below. Failure was pedicle screw pull out. The average deflection angle at the failure point was 35.8±1.3 degrees. Angular deflection was reported as normalized, with each specimen beginning at zero degrees. The average bending force at the failure point was 118.6±25.7N.

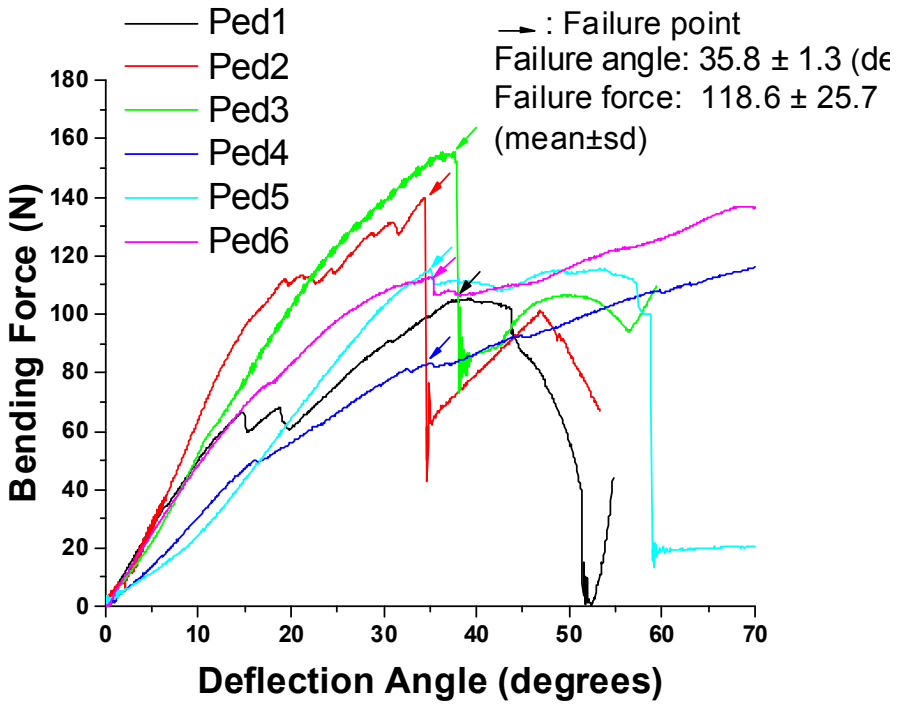

- **Figure 51 Pedicle Screw Results: Fixation failure was recorded on all six spines tested. Failure was pedicle screw pull out.**

For the rib construct group, no fixation failure was observed on all six tested spines, see Figure 52 below. Each bending test reached the maximum spine deflection allowed by the testing system. The average maximum deflection angle was 50.3±9.1degrees (normalized). The average maximum bending force was 119.7±13.9N without failure. Stiffness was calculated as the slope of the force vs angular displacement curve. The average stiffness of the pedicle screw group was 3.634, significantly higher than the 4 rib construct group average of 2.037.

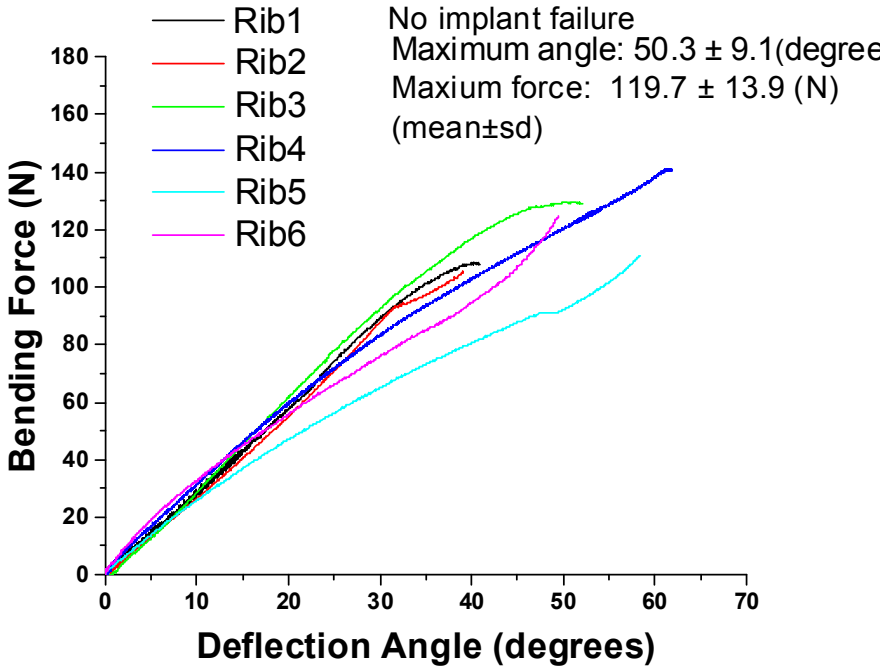

- **Figure 52 Rib Construct Results: No fixation failure was observed on all six spines tested. Each bending test reached the maximum spine deflection allowed by the testing system**

Figure 53 below shows an example failure curve a pedicle screw sample compared to the 4 rib construct.

Figure 54 below shows a comparison of the pedicle screw and 4 rib construct results.

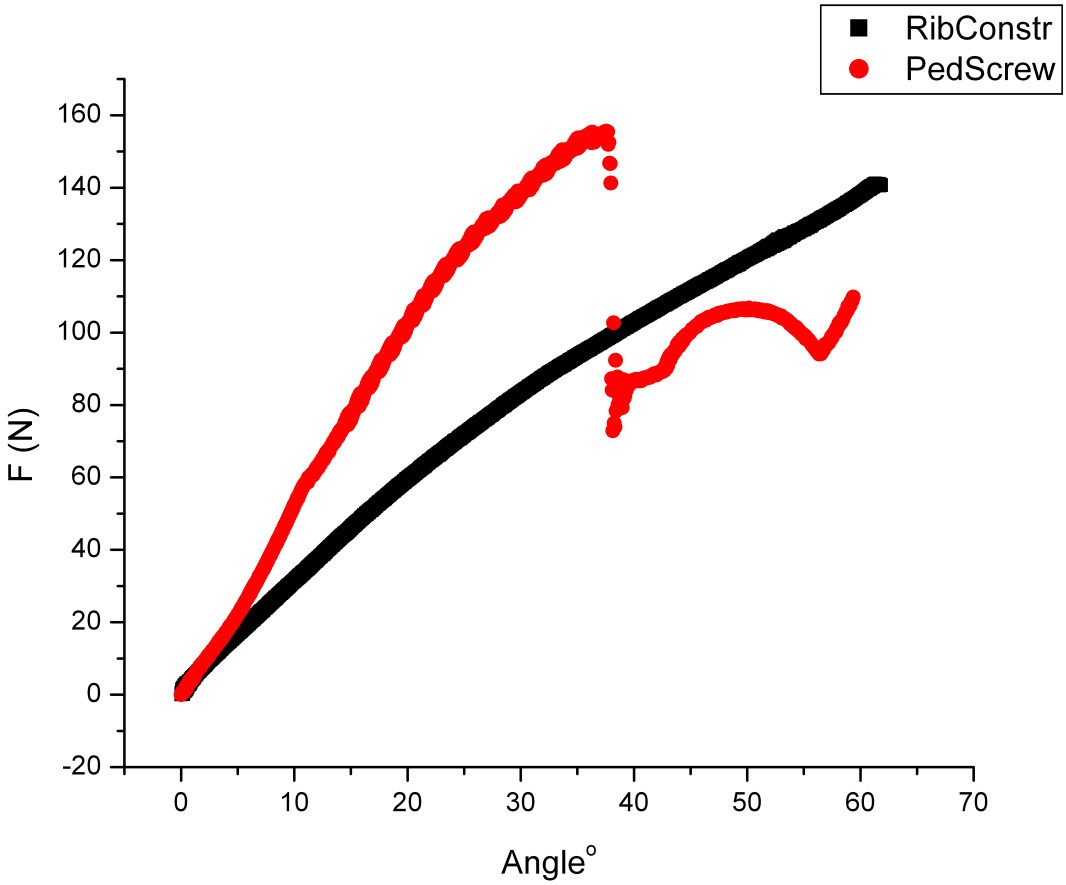

Figure 53 Example failure curves of pedicle screw (red) and 4 rib construct (black).
Pedicle screw constructs consistently failed at 35.8 +/- 1.3 degrees while 4 rib construct did not reach failure through the same angle of deflection.

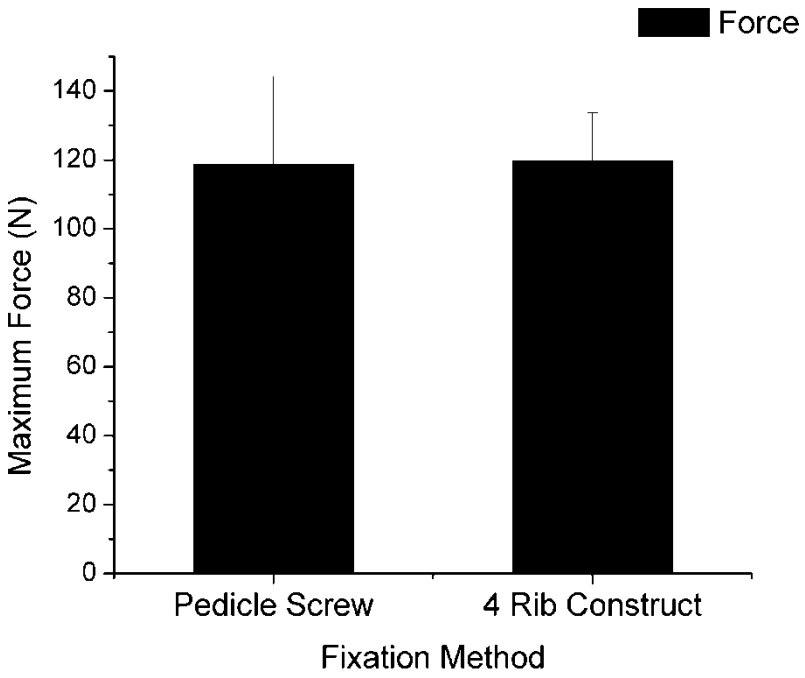
Force
Maximum Force (N)
140
120
100
80
60
40
20
0
Pedicle Screw
4 Rib Construct
Fixation Method

(a)

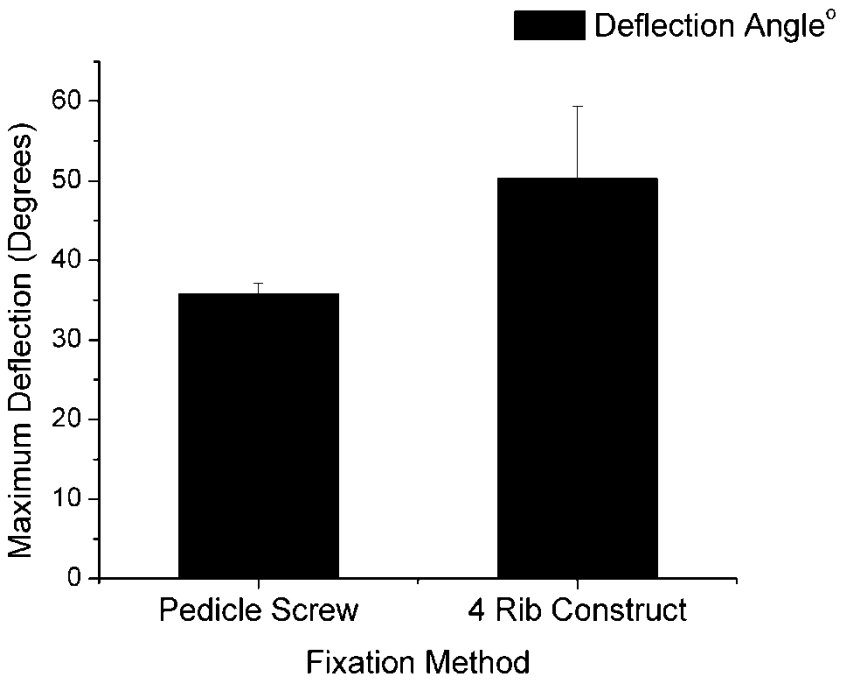

(b)

Figure 54 showing maximum force and maximum deflection for the pedicle screw and 4 rib construct group
Average maximum force (N) and deflection (degrees) for the pedicle screw (n=6) and 4 rib construct groups (n=6) tested. a) Maximum force with n=6 for each group, b) Maximum deflection with n=6 for each group.

Table 6 Maximum force and deflection

	Maximum Force (Newtons)	**Maximum Deflection (degrees)**
Pedicle Screw	118.6±25.7	35.8±1.3
4 Rib Construct	119.7±13.9*	50.3±9.1*

*Denotes maximum force/deflection at end of testing without failure

8.5 Discussion

The objective of this study was to compare upper thoracic fixation methods in early onset scoliosis in the presence of severe kyphosis. For this study, a novel 4 rib construct was compared to a control group with standard pedicle screw instrumentation. A well-controlled spine bending mechanical model was developed using bilateral titanium growth rods instrumented to intact immature porcine spines.

The spine was loaded through 90 degrees angular deflection to simulate severe kyphosis before load frame stroke length of the MTS was reached. Both the pedicle screw group and 4 rib construct group were loaded through the same deflection angle. However, each pedicle screw specimen failed within this range whereas no specimen in the 4 rib construct group failed. The average deflection angle at failure for the pedicle screw group was 35.8±1.3 degrees. The 4 rib construct group was able to deflect through a mean of 50.3±9.1 degrees before the test was stopped, without reaching failure. These results indicate that the 4 rib construct can withstand much higher levels of angular deflection, and as a result, indicate that the 4 rib construct provides fixation through greater kyphosis angles than pedicle screws. The reason the results are stated in angular displacement instead of linear displacement is to keep to a physiologically relevant measure of displacement, with the angular displacement being equivalent to kyphosis angles.

When comparing maximum bending force reached by the implant recorded during angular deflection, the pedicle screw group obtained 118.6±25.7 N and the 4 rib construct group obtained 119.7±13.9 N. However, in the pedicle screw group, the maximum force

was recorded at failure and represents the maximum level of force and corresponding angle (35.8±1.3 degrees) the construct can withstand (see Figure 51 above for failure curve). In the 4 rib construct group, the average force of 119.7±13.9N was the maximum force recorded at the end of the test and therefore was a representation of the maximum force experience by the implant without failure at the end of the MTS load limitations at an average angle of ~50.3±9.1 degrees (see Figure 52above for failure curve). These results indicate both constructs experience similar maximum loads through the application of bending/kyphotic force but the associative force-displacement response is different between groups. In order to explain why the pedicle screw group failed and the 4 rib construct did not, the force vs angular displacement curves must be analyzed to understand the loading response in regard to the stiffness of implant.

From observation of the experiments and analysis of the data, the pedicle screw group resisted bending at the start of the test, incurring a large initial force from the onset of bending. This was due to the rods being rigidly attached to vertebral bodies 3 and 4, which resulted in close alignment with little contour. Once 30 degrees bending had occurred in the spine, a peak in loading occurred with the implant failing through pedicle screw pull out. Stiffness was considered for the entire construct as a ratio of force to angular displacement. The overall stiffness was measured from the slope of the load vs angular displacement curve was 3.634 which was significantly larger than the 4 rib construct stiffness of 2.037. The lower stiffness value resulting from the 4 rib construct group was likely due the contour of the rod during rib placement, flexure allowed by the lamina hooks, and also slight flexure of the ribs. This resulted in a construct that allowed

much more flexure without the load-up in bending force that produced failure of the implant. First, the rods were contoured over the ribs, which resulted in an initial kyphotic contour. Rods were attached to lamina hooks placed at the tubercle, with abduction of the rods and a kyphotic contour along the ribs. The combination of the 4 rib construct's a "wide stance" in contour with the ribs and slight flexure of the ribs allowed more flexure in the construct. From observation of the tests, the 4 rib construct specimens flexed evenly through bending. The resulting force response was a gradual increase in load, even though deflection angles were increasing. This produced a force vs angular displacement groups without a sharp spike in load response unlike the pedicle screw group, which demonstrated a sharp rise in force response, with catastrophic failure of the screw implant.

In addition to a lower stiffness, the connection of the 4 rib construct proved superior. The opposite facing lamina hooks resisted the large distraction forces from kyphotic bending much better than the pedicle screw group. The inferior facing lamina hook on rib 3 was crucial at the beginning of the block fixation, which represent the anatomical location of rib 2 for the most superior rib in human fixation. Interestingly, biomechanical studies have shown the pedicle screw pullout strength was much larger than pullout strength of the lamina hooks on the lamina, usually from failure of the lamina. We found in this study that lamina hooks placed at the tubercle resulted in higher fixation strength than the pedicle screw. One of the weaknesses of this study, however, was the exclusion of a lamina hook group with fixation to the lamina. The pedicle screw group was compared as the currently accepted standard between the growing rods and the

VEPTR. All ribs were examined for dislocation and signs of rib failure at the end of the study, but none were observed from failure analysis of force data. This would indicate a much larger range of implant loading and 4 rib fixation strength.

The full spine bending test in this study was a load by deflection until failure or maximum deflection was reached. The limitations were based on using an MTS with limited travel on which we used the load are to load samples. In the future, a testing configuration of cyclic loading would be more physiologic under these conditions, as most active patients see repetitive loading and likely not extreme deflection. Contour of the rods were based on surgical preference and not uniform over all the sample groups. We observed that titanium rods can flex through 90 degrees without implant failure. We also observed that the ribs can stay intact through extreme loading, much larger than physiologic conditions. But overall this study presents more questions in pediatric spine surgery that must be addressed. Specifically, it raises the question of when do the tradeoffs of stiffness and rod rigidity cease when compared to flexation in an active patient. From observing this study, clearly there is a payoff to having flexation in the construct in order not have to failure at the fixation site. A pediatric spine is active and yet still developing. Therefore, a crucial design parameter to determine in future studies is the amount of flexure necessary to the implant rigidity for support in both kyphosis and scoliosis curves yet withstand transverse pullout forces. It will be important to answer how stiff the implant needs to be relative to the bone density and flexural strength of the pediatric spine will help in the management of these severe cases.

In the future, research must be expanded to determine if fixation to the ribs could be a viable alternative to vertebral body fixation altogether. First, the prediction of bone strength at the fixation site will greatly enhance the outcome of surgery and allow for critical assessment of anchorage success in planning. In order to accurately pair the bone quality fixation predictions with biomechanical anchorage strength, an animal model that creates scoliosis through tethering must be developed. The animal model will not only provide a better biomechanical basis for our construct testing, but will allow a better understanding of construct performance while *in vivo*. The analysis includes not only the strength of construct from the animal spine, but also the amount of fusion and well as developmental changes the construct may either promote or inhibit. Once the constructs can be compared in a living animal model, research can progress into better fusionless constructs that will aid the development of the pediatric spine.

9 REFERENCES

1. Benjamin, M. and J.R. Ralphs, *Biology of fibrocartilage cells.* Int Rev Cytol, 2004. **233**: p. 1-45.
2. Okeson, J.P., *Management of temporomandibular disorders and occlusion*. 4th ed1998, St. Louis: Mosby. x, 638 p.
3. Almarza, A.J. and K.A. Athanasiou, *Design characteristics for the tissue engineering of cartilaginous tissues.* Ann Biomed Eng, 2004. **32**(1): p. 2-17.
4. de Bont, L.G. and B. Stegenga, *Pathology of temporomandibular joint internal derangement and osteoarthrosis.* Int J Oral Maxillofac Surg, 1993. **22**(2): p. 71-4.
5. Farrar, W.B. and W.L. McCarty, *INFERIOR JOINT SPACE ARTHROGRAPHY AND CHARACTERISTICS OF CONDYLAR PATHS IN INTERNAL DERANGEMENTS OF THE TMJ.* Journal of Prosthetic Dentistry, 1979. **41**(5): p. 548-555.
6. Gallo, L.M., et al., *Description of mandibular finite helical axis pathways in asymptomatic subjects.* J Dent Res, 1997. **76**(2): p. 704-13.
7. Solberg, W.K., M.W. Woo, and J.B. Houston, *Prevalence of mandibular dysfunction in young adults.* J Am Dent Assoc, 1979. **98**(1): p. 25-34.
8. Warren, M.P. and J.L. Fried, *Temporomandibular disorders and hormones in women.* Cells Tissues Organs, 2001. **169**(3): p. 187-92.
9. Fillingim, R.B., et al., *Potential psychosocial risk factors for chronic TMD: descriptive data and empirically identified domains from the OPPERA case-control study.* J Pain, 2011. **12**(11 Suppl): p. T46-60.
10. Fillingim, R.B., et al., *Summary of findings from the OPPERA baseline case-control study: implications and future directions.* J Pain, 2011. **12**(11 Suppl): p. T102-7.
11. Maixner, W., et al., *Orofacial Pain Prospective Evaluation and Risk Assessment study--the OPPERA study.* J Pain, 2011. **12**(11 Suppl): p. T4-11 e1-2.
12. Slade, G.D., et al., *Study methods, recruitment, sociodemographic findings, and demographic representativeness in the OPPERA study.* J Pain, 2011. **12**(11 Suppl): p. T12-26.
13. Smith, S.B., et al., *Potential genetic risk factors for chronic TMD: genetic associations from the OPPERA case control study.* J Pain, 2011. **12**(11 Suppl): p. T92-101.
14. Detamore, M.S. and K.A. Athanasiou, *Motivation, characterization, and strategy for tissue engineering the temporomandibular joint disc.* Tissue Engineering, 2003. **9**(6): p. 1065-1087.
15. Farrar, W.B. and W.L. McCarty, Jr., *The TMJ dilemma.* J Ala Dent Assoc, 1979. **63**(1): p. 19-26.
16. McCarty, W.L. and W.B. Farrar, *SURGERY FOR INTERNAL DERANGEMENTS OF THE TEMPOROMANDIBULAR-JOINT.* Journal of Prosthetic Dentistry, 1979. **42**(2): p. 191-196.
17. Landesberg, R., E. Takeuchi, and J.E. Puzas, *Cellular, biochemical and molecular characterization of the bovine temporomandibular joint disc.* Arch Oral Biol, 1996. **41**(8-9): p. 761-7.
18. Haskin, C.L., S.B. Milam, and I.L. Cameron, *Pathogenesis of degenerative joint disease in the human temporomandibular joint.* Crit Rev Oral Biol Med, 1995. **6**(3): p. 248-77.

19. Milam, S.B., et al., *Characterization of the extracellular matrix of the primate temporomandibular joint.* J Oral Maxillofac Surg, 1991. **49**(4): p. 381-91.
20. Milam, S.B. and J.P. Schmitz, *Molecular biology of temporomandibular joint disorders: proposed mechanisms of disease.* J Oral Maxillofac Surg, 1995. **53**(12): p. 1448-54.
21. Milam, S.B., G. Zardeneta, and J.P. Schmitz, *Oxidative stress and degenerative temporomandibular joint disease: a proposed hypothesis.* J Oral Maxillofac Surg, 1998. **56**(2): p. 214-23.
22. O'Dell, N.L., et al., *Morphological and biochemical evidence for elastic fibres in the Syrian hamster temporomandibular joint disc.* Arch Oral Biol, 1990. **35**(10): p. 807-11.
23. Shengyi, T. and Y. Xu, *Biomechanical properties and collagen fiber orientation of TMJ discs in dogs: Part 1. Gross anatomy and collagen fiber orientation of the discs.* J Craniomandib Disord, 1991. **5**(1): p. 28-34.
24. Detamore, M.S. and K.A. Athanasiou, *Tensile properties of the porcine temporomandibular joint disc.* J Biomech Eng, 2003. **125**(4): p. 558-65.
25. Detamore, M.S. and K.A. Athanasiou, *Structure and function of the temporomandibular joint disc: implications for tissue engineering.* J Oral Maxillofac Surg, 2003. **61**(4): p. 494-506.
26. Detamore, M.S., et al., *Cell type and distribution in the porcine temporomandibular joint disc.* J Oral Maxillofac Surg, 2006. **64**(2): p. 243-8.
27. Detamore, M.S., et al., *Quantitative analysis and comparative regional investigation of the extracellular matrix of the porcine temporomandibular joint disc.* Matrix Biol, 2005. **24**(1): p. 45-57.
28. Singh, M. and M.S. Detamore, *Biomechanical properties of the mandibular condylar cartilage and their relevance to the TMJ disc.* J Biomech, 2009. **42**(4): p. 405-17.
29. Tanaka, E., et al., *Lubrication of the temporomandibular joint.* Ann Biomed Eng, 2008. **36**(1): p. 14-29.
30. Tanaka, E., et al., *Strain-rate effect on the biomechanical response of bovine temporomandibular joint disk under compression.* J Biomed Mater Res A, 2003. **67**(3): p. 761-5.
31. Tanaka, E., et al., *Dynamic shear properties of the temporomandibular joint disc.* J Dent Res, 2003. **82**(3): p. 228-31.
32. Beek, M., et al., *Dynamic properties of the human temporomandibular joint disc.* J Dent Res, 2001. **80**(3): p. 876-80.
33. Beek, M., et al., *Three-dimensional finite element analysis of the cartilaginous structures in the human temporomandibular joint.* J Dent Res, 2001. **80**(10): p. 1913-8.
34. Spirt, A.A., A.F. Mak, and R.P. Wassell, *Nonlinear viscoelastic properties of articular cartilage in shear.* J Orthop Res, 1989. **7**(1): p. 43-9.
35. Herring, S.W., et al., *Temporomandibular joint in miniature pigs: anatomy, cell replication, and relation to loading.* Anat Rec, 2002. **266**(3): p. 152-66.
36. Ingawale, S. and T. Goswami, *Temporomandibular joint: disorders, treatments, and biomechanics.* Ann Biomed Eng, 2009. **37**(5): p. 976-96.
37. Tanaka, E. and T. van Eijden, *Biomechanical behavior of the temporomandibular joint disc.* Crit Rev Oral Biol Med, 2003. **14**(2): p. 138-50.
38. Koolstra, J.H. and T.M. van Eijden, *Combined finite-element and rigid-body analysis of human jaw joint dynamics.* J Biomech, 2005. **38**(12): p. 2431-9.

39. Nagahara, K., et al., *Displacement and stress distribution in the temporomandibular joint during clenching.* Angle Orthod, 1999. **69**(4): p. 372-9.
40. Pileicikiene, G., et al., *A three-dimensional model of the human masticatory system, including the mandible, the dentition and the temporomandibular joints.* Stomatologija, 2007. **9**(1): p. 27-32.
41. Spilker, R.L., J.C. Nickel, and L.R. Iwasaki, *A biphasic finite element model of in vitro plowing tests of the temporomandibular joint disc.* Ann Biomed Eng, 2009. **37**(6): p. 1152-64.
42. Tanaka, E., et al., *Three-dimensional finite element analysis of human temporomandibular joint with and without disc displacement during jaw opening.* Med Eng Phys, 2004. **26**(6): p. 503-11.
43. Tanaka, E., et al., *Stress distribution in the temporomandibular joint affected by anterior disc displacement: a three-dimensional analytic approach with the finite-element method.* J Oral Rehabil, 2000. **27**(9): p. 754-9.
44. Tanaka, E., et al., *Stress analysis in the TMJ during jaw opening by use of a three-dimensional finite element model based on magnetic resonance images.* Int J Oral Maxillofac Surg, 2001. **30**(5): p. 421-30.
45. Wilkes, C.H., *Arthrography of the temporomandibular joint in patients with the TMJ pain-dysfunction syndrome.* Minn Med, 1978. **61**(11): p. 645-52.
46. Wilkes, C.H., *Internal derangements of the temporomandibular joint. Pathological variations.* Arch Otolaryngol Head Neck Surg, 1989. **115**(4): p. 469-77.
47. Zarb, G.A. and G.E. Carlsson, *Temporomandibular disorders: osteoarthritis.* J Orofac Pain, 1999. **13**(4): p. 295-306.
48. Perez del Palomar, A. and M. Doblare, *An accurate simulation model of anteriorly displaced TMJ discs with and without reduction.* Med Eng Phys, 2007. **29**(2): p. 216-26.
49. Allen, K.D. and K.A. Athanasiou, *Tissue Engineering of the TMJ disc: a review.* Tissue Eng, 2006. **12**(5): p. 1183-96.
50. Detamore, M.S. and K.A. Athanasiou, *Motivation, characterization, and strategy for tissue engineering the temporomandibular joint disc.* Tissue Eng, 2003. **9**(6): p. 1065-87.
51. Detamore, M.S., K.A. Athanasiou, and J. Mao, *A call to action for bioengineers and dental professionals: directives for the future of TMJ bioengineering.* Ann Biomed Eng, 2007. **35**(8): p. 1301-11.
52. Abramowicz, S., et al., *Temporomandibular joint reconstruction after failed teflon-proplast implant: case report and literature review.* Int J Oral Maxillofac Surg, 2008. **37**(8): p. 763-7.
53. Mow, V.C., M.H. Holmes, and W.M. Lai, *Fluid transport and mechanical properties of articular cartilage: a review.* J Biomech, 1984. **17**(5): p. 377-94.
54. Shirakura, M., et al., *Activation of the hypoxia-inducible factor-1 in overloaded temporomandibular joint, and induction of osteoclastogenesis.* Biochem Biophys Res Commun, 2010. **393**(4): p. 800-5.
55. de Bont, L.G., L.C. Dijkgraaf, and B. Stegenga, *Epidemiology and natural progression of articular temporomandibular disorders.* Oral Surg Oral Med Oral Pathol Oral Radiol Endod, 1997. **83**(1): p. 72-6.
56. Fung, Y., *Biomechanical properties of living tissue*1981, NY: Springer-Verlag. pp. 196-260.

57. Almarza, A.J., et al., *Biochemical analysis of the porcine temporomandibular joint disc.* Br J Oral Maxillofac Surg, 2006. **44**(2): p. 124-8.
58. Shi, C., et al., *Anisotropic solute diffusion tensor in porcine TMJ discs measured by FRAP with spatial Fourier analysis.* Ann Biomed Eng, 2010. **38**(11): p. 3398-408.
59. Gu, W.Y., W.M. Lai, and V.C. Mow, *TRANSPORT OF FLUID AND IONS THROUGH A POROUS-PERMEABLE CHARGED-HYDRATED TISSUE, AND STREAMING POTENTIAL DATA ON NORMAL BOVINE ARTICULAR-CARTILAGE.* Journal of Biomechanics, 1993. **26**(6): p. 709-723.
60. Gu, W.Y., W.M. Lai, and V.C. Mow, *A mixture theory for charged-hydrated soft tissues containing multi-electrolytes: passive transport and swelling behaviors.* J Biomech Eng, 1998. **120**(2): p. 169-80.
61. Kuo, J., et al., *Effect of Mechanical Loading on Electrical Conductivity in Porcine TMJ Discs.* Journal of Dental Research, 2011. **90**(10): p. 1216-1220.
62. Wright, G.J., et al., *Effect of Mechanical Strain on Solute Diffusion in Human TMJ Discs: An Electrical Conductivity Study.* Annals of Biomedical Engineering, 2013. **41**(11): p. 2349-2357.
63. Jackson, G.W. and D.F. James, *THE PERMEABILITY OF FIBROUS POROUS-MEDIA.* Canadian Journal of Chemical Engineering, 1986. **64**(3): p. 364-374.
64. Kuo, J., et al., *Regional cell density distribution and oxygen consumption rates in porcine TMJ discs: an explant study.* Osteoarthritis and Cartilage, 2011. **19**(7): p. 911-918.
65. Milam, S.B., *Pathogenesis of degenerative temporomandibular joint arthritides.* Odontology, 2005. **93**(1): p. 7-15.
66. Maroudas, A., *Physicochemical properties of cartilage in the light of ion exchange theory.* Biophys J, 1968. **8**(5): p. 575-95.
67. Maroudas, A., H. Muir, and J. Wingham, *The correlation of fixed negative charge with glycosaminoglycan content of human articular cartilage.* Biochim Biophys Acta, 1969. **177**(3): p. 492-500.
68. Mow, V.C., et al., *Effects of fixed charges on the stress-relaxation behavior of hydrated soft tissues in a confined compression problem.* International Journal of Solids and Structures, 1998. **35**(34-35): p. 4945-4962.
69. Mow, V.C. and W.C. Hayes, *BASIC ORTHOPEDIC BIOMECHANICS*. Mow, V. C. And W. C. Hayes. Basic Orthopaedic Biomechanics. X+453p. Raven Press: New York, New York, USA. Illus1991. X+453P.
70. Tanaka, E., et al., *Viscoelastic properties of the human temporomandibular joint disc in patients with internal derangement.* J Oral Maxillofac Surg, 2000. **58**(9): p. 997-1002.
71. Kalpakci, K.N., et al., *An interspecies comparison of the temporomandibular joint disc.* J Dent Res, 2011. **90**(2): p. 193-8.
72. Sun, Z., Z.J. Liu, and S.W. Herring, *Movement of temporomandibular joint tissues during mastication and passive manipulation in miniature pigs.* Arch Oral Biol, 2002. **47**(4): p. 293-305.
73. Gallo, L.M., et al., *Mechanical work during stress-field translation in the human TMJ.* J Dent Res, 2006. **85**(11): p. 1006-10.
74. Gallo, L.M., et al., *Stress-field translation in the healthy human temporomandibular joint.* J Dent Res, 2000. **79**(10): p. 1740-6.

75. Mills, D.K., D.J. Fiandaca, and R.P. Scapino, *Morphologic, microscopic, and immunohistochemical investigations into the function of the primate TMJ disc.* J Orofac Pain, 1994. **8**(2): p. 136-54.
76. Archer, C.W. and P. Francis-West, *The chondrocyte.* Int J Biochem Cell Biol, 2003. **35**(4): p. 401-4.
77. Poole, C.A., M.H. Flint, and B.W. Beaumont, *Chondrons in cartilage: ultrastructural analysis of the pericellular microenvironment in adult human articular cartilages.* J Orthop Res, 1987. **5**(4): p. 509-22.
78. Okuda, Y., J.P. Gorski, and P.C. Amadio, *Effect of postnatal age on the ultrastructure of six anatomical areas of canine flexor digitorum profundus tendon.* J Orthop Res, 1987. **5**(2): p. 231-41.
79. Rufai, A., M. Benjamin, and J.R. Ralphs, *The development of fibrocartilage in the rat intervertebral disc.* Anat Embryol (Berl), 1995. **192**(1): p. 53-62.
80. Nakano, T. and P.G. Scott, *Changes in the chemical composition of the bovine temporomandibular joint disc with age.* Arch Oral Biol, 1996. **41**(8-9): p. 845-53.
81. Kapila, S., C. Lee, and D.W. Richards, *Characterization and identification of proteinases and proteinase inhibitors synthesized by temporomandibular joint disc cells.* J Dent Res, 1995. **74**(6): p. 1328-36.
82. Shi, C., et al., *Relationship between anisotropic diffusion properties and tissue morphology in porcine TMJ disc.* Osteoarthritis and Cartilage, 2013. **21**(4): p. 625-633.
83. Minarelli, A.M. and E.A. Liberti, *A microscopic survey of the human temporomandibular joint disc.* J Oral Rehabil, 1997. **24**(11): p. 835-40.
84. Cheung, H.S., *Distribution of type I, II, III and V in the pepsin solubilized collagens in bovine menisci.* Connect Tissue Res, 1987. **16**(4): p. 343-56.
85. Ghadially, F.N., et al., *Ultrastructure of rabbit semilunar cartilages.* J Anat, 1978. **125**(Pt 3): p. 499-517.
86. Girdler, N.M., *In vitro synthesis and characterization of a cartilaginous meniscus grown from isolated temporomandibular chondroprogenitor cells.* Scand J Rheumatol, 1998. **27**(6): p. 446-53.
87. Hasler, E.M., et al., *Articular cartilage biomechanics: theoretical models, material properties, and biosynthetic response.* Crit Rev Biomed Eng, 1999. **27**(6): p. 415-88.
88. Gage, J.P., R.M. Shaw, and F.B. Moloney, *Collagen type in dysfunctional temporomandibular joint disks.* J Prosthet Dent, 1995. **74**(5): p. 517-20.
89. Scapino, R.P., et al., *The behaviour of collagen fibres in stress relaxation and stress distribution in the jaw-joint disc of rabbits.* Arch Oral Biol, 1996. **41**(11): p. 1039-52.
90. Berkovitz, B.K., *Crimping of collagen in the intra-articular disc of the temporomandibular joint: a comparative study.* J Oral Rehabil, 2000. **27**(7): p. 608-13.
91. Keith, D.A., *Elastin in the bovine mandibular joint.* Arch Oral Biol, 1979. **24**(3): p. 211-5.
92. Gross, A., A. Bumann, and B. Hoffmeister, *Elastic fibers in the human temporo-mandibular joint disc.* Int J Oral Maxillofac Surg, 1999. **28**(6): p. 464-8.
93. Esko JD, K.K., Lindahl U, *Proteoglycans and Sulfated Glycosaminoglycans*, in *Essentials of Glycobiology*2009, Cold Spring Harbor Laboratory Press: NCBI.
94. Chammas, P., W.J. Federspiel, and S.R. Eisenberg, *A MICROCONTINUUM MODEL OF ELECTROKINETIC COUPLING IN THE EXTRACELLULAR-MATRIX - PERTURBATION*

FORMULATION AND SOLUTION. Journal of Colloid and Interface Science, 1994. **168**(2): p. 526-538.
95. Eisenberg, S.R. and A.J. Grodzinsky, *ELECTROKINETIC MICROMODEL OF EXTRACELLULAR-MATRIX AND OTHER POLY-ELECTROLYTE NETWORKS.* Physicochemical Hydrodynamics, 1988. **10**(4): p. 517-539.
96. Frank, E.H. and A.J. Grodzinsky, *CARTILAGE ELECTROMECHANICS .2. A CONTINUUM MODEL OF CARTILAGE ELECTROKINETICS AND CORRELATION WITH EXPERIMENTS.* Journal of Biomechanics, 1987. **20**(6): p. 629-639.
97. Frank, E.H. and A.J. Grodzinsky, *CARTILAGE ELECTROMECHANICS .1. ELECTROKINETIC TRANSDUCTION AND THE EFFECTS OF ELECTROLYTE PH AND IONIC-STRENGTH.* Journal of Biomechanics, 1987. **20**(6): p. 615-&.
98. Frank, E.H., et al., *STREAMING POTENTIALS - A SENSITIVE INDEX OF ENZYMATIC DEGRADATION IN ARTICULAR-CARTILAGE.* Journal of Orthopaedic Research, 1987. **5**(4): p. 497-508.
99. Grodzinsky, A.J., *ELECTROMECHANICAL AND PHYSICOCHEMICAL PROPERTIES OF CONNECTIVE-TISSUE.* Crc Critical Reviews in Biomedical Engineering, 1983. **9**(2): p. 133-199.
100. Lai, W.M., et al., *On the electric potentials inside a charged soft hydrated biological tissue: Streaming potential versus diffusion potential.* Journal of Biomechanical Engineering-Transactions of the Asme, 2000. **122**(4): p. 336-346.
101. Maroudas, A., *PHYSICOCHEMICAL PROPERTIES OF CARTILAGE IN LIGHT OF ION EXCHANGE THEORY.* Biophysical Journal, 1968. **8**(5): p. 575-&.
102. Nakano, T. and P.G. Scott, *A quantitative chemical study of glycosaminoglycans in the articular disc of the bovine temporomandibular joint.* Arch Oral Biol, 1989. **34**(9): p. 749-57.
103. Axelsson, S., A. Holmlund, and A. Hjerpe, *Glycosaminoglycans in normal and osteoarthrotic human temporomandibular joint disks.* Acta Odontol Scand, 1992. **50**(2): p. 113-9.
104. Lumpkins, S.B. and P.S. McFetridge, *Regional variations in the viscoelastic compressive properties of the temporomandibular joint disc and implications toward tissue engineering.* J Biomed Mater Res A, 2008.
105. Campbell, J.H., et al., *Estrogen receptor analysis of human temporomandibular disc.* J Oral Maxillofac Surg, 1993. **51**(10): p. 1101-5.
106. Wu, Y.W., et al., *17-Beta-estradiol enhanced allodynia of inflammatory temporomandibular joint through upregulation of hippocampal TRPV1 in ovariectomized rats.* J Neurosci, 2010. **30**(26): p. 8710-9.
107. Abubaker, A.O., P.C. Hebda, and J.N. Gunsolley, *Effects of sex hormones on protein and collagen content of the temporomandibular joint disc of the rat.* J Oral Maxillofac Surg, 1996. **54**(6): p. 721-7; discussion 727-8.
108. Burger, E.H., J. Klein-Nulend, and J.P. Veldhuijzen, *Mechanical stress and osteogenesis in vitro.* J Bone Miner Res, 1992. **7 Suppl 2**: p. S397-401.
109. Nitzan, D.W., *The process of lubrication impairment and its involvement in temporomandibular joint disc displacement: a theoretical concept.* J Oral Maxillofac Surg, 2001. **59**(1): p. 36-45.

110. Nitzan, D.W., *Intraarticular pressure in the functioning human temporomandibular joint and its alteration by uniform elevation of the occlusal plane.* J Oral Maxillofac Surg, 1994. **52**(7): p. 671-9; discussion 679-80.
111. Zardeneta, G., S.B. Milam, and J.P. Schmitz, *Iron-dependent generation of free radicals: plausible mechanisms in the progressive deterioration of the temporomandibular joint.* J Oral Maxillofac Surg, 2000. **58**(3): p. 302-8; discussion 309.
112. Cairns, B.E., *Pathophysiology of TMD pain--basic mechanisms and their implications for pharmacotherapy.* J Oral Rehabil, 2010. **37**(6): p. 391-410.
113. Ohshima, H. and J.P. Urban, *The effect of lactate and pH on proteoglycan and protein synthesis rates in the intervertebral disc.* Spine, 1992. **17**(9): p. 1079-82.
114. Tanaka, E. and T. van Eijden, *Biomechanical behavior of the temporomandibular joint disc.* Critical Reviews in Oral Biology & Medicine, 2003. **14**(2): p. 138-150.
115. Tanaka, E., et al., *Modeling of the effect of friction in the temporomandibular joint on displacement of its disc during prolonged clenching.* J Oral Maxillofac Surg, 2008. **66**(3): p. 462-8.
116. Ethunandan, M. and A.W. Wilson, *Temporomandibular joint arthrocentesis -more questions than answers?* J Oral Maxillofac Surg, 2006. **64**(6): p. 952-5.
117. Chung, S.C., Y.K. Kim, and H.S. Kim, *Prevalence and patterns of nocturnal bruxofacets on stabilization splints in temporomandibular disorder patients.* Cranio, 2000. **18**(2): p. 92-7.
118. Glass, E.G., A.G. Glaros, and F.D. McGlynn, *Myofascial pain dysfunction: treatments used by ADA members.* Cranio, 1993. **11**(1): p. 25-9.
119. Nitzan, D.W., M.F. Dolwick, and G.A. Martinez, *Temporomandibular joint arthrocentesis: a simplified treatment for severe, limited mouth opening.* J Oral Maxillofac Surg, 1991. **49**(11): p. 1163-7; discussion 1168-70.
120. Al-Belasy, F.A. and M.F. Dolwick, *Arthrocentesis for the treatment of temporomandibular joint closed lock: a review article.* Int J Oral Maxillofac Surg, 2007. **36**(9): p. 773-82.
121. Guo, C., Z. Shi, and P. Revington, *Arthrocentesis and lavage for treating temporomandibular joint disorders.* Cochrane Database Syst Rev, 2009(4): p. CD004973.
122. Wolford, L.M., M.C. Pitta, and P. Mehra, *Mitek anchors for treatment of chronic mandibular dislocation.* Oral Surg Oral Med Oral Pathol Oral Radiol Endod, 2001. **92**(5): p. 495-8.
123. Wolford, L.M., *Temporomandibular joint devices: treatment factors and outcomes.* Oral Surg Oral Med Oral Pathol Oral Radiol Endod, 1997. **83**(1): p. 143-9.
124. Fields, R.T., Jr. and L.M. Wolford, *The osseointegration of Mitek mini anchors in the mandibular condyle.* J Oral Maxillofac Surg, 2001. **59**(12): p. 1402-6; discussion 1407.
125. Kearns, G.J., D.H. Perrott, and L.B. Kaban, *A protocol for the management of failed alloplastic temporomandibular joint disc implants.* J Oral Maxillofac Surg, 1995. **53**(11): p. 1240-7; discussion 1248-9.
126. Teng, S., et al., *Biomechanical properties and collagen fiber orientation of temporomandibular joint discs in dogs: 2. Tensile mechanical properties of the discs.* J Craniomandib Disord, 1991. **5**(2): p. 107-14.
127. Lai, W.F., J. Bowley, and J.G. Burch, *Evaluation of shear stress of the human temporomandibular joint disc.* J Orofac Pain, 1998. **12**(2): p. 153-9.

128. Tanne, K., E. Tanaka, and M. Sakuda, *The elastic modulus of the temporomandibular joint disc from adult dogs.* J Dent Res, 1991. **70**(12): p. 1545-8.
129. Beatty, M.W., et al., *Strain rate dependent orthotropic properties of pristine and impulsively loaded porcine temporomandibular joint disk.* J Biomed Mater Res, 2001. **57**(1): p. 25-34.
130. Tanaka, E., et al., *Dynamic properties of bovine temporomandibular joint disks change with age.* J Dent Res, 2002. **81**(9): p. 618-22.
131. Chin, L.P., F.D. Aker, and K. Zarrinnia, *The viscoelastic properties of the human temporomandibular joint disc.* J Oral Maxillofac Surg, 1996. **54**(3): p. 315-8; discussion 318-9.
132. Allen, K.D. and K.A. Athanasiou, *Viscoelastic characterization of the porcine temporomandibular joint disc under unconfined compression.* J Biomech, 2006. **39**(2): p. 312-22.
133. Lumpkins, S.B. and P.S. McFetridge, *Regional variations in the viscoelastic compressive properties of the temporomandibular joint disc and implications toward tissue engineering.* J Biomed Mater Res A, 2009. **90**(3): p. 784-91.
134. Tanaka, E., et al., *Dynamic compressive properties of porcine temporomandibular joint disc.* Eur J Oral Sci, 2003. **111**(5): p. 434-9.
135. Zhu, W., et al., *Viscoelastic shear properties of articular cartilage and the effects of glycosidase treatments.* J Orthop Res, 1993. **11**(6): p. 771-81.
136. Zhu, W., K.Y. Chern, and V.C. Mow, *Anisotropic viscoelastic shear properties of bovine meniscus.* Clin Orthop Relat Res, 1994(306): p. 34-45.
137. Tanaka, E., et al., *Shear properties of the temporomandibular joint disc in relation to compressive and shear strain.* J Dent Res, 2004. **83**(6): p. 476-9.
138. Tanaka, E., et al., *Biomechanical response of condylar cartilage-on-bone to dynamic shear.* J Biomed Mater Res A, 2008. **85**(1): p. 127-32.
139. Nitzan, D.W., *'Friction and adhesive forces'--possible underlying causes for temporomandibular joint internal derangement.* Cells Tissues Organs, 2003. **174**(1-2): p. 6-16.
140. Nickel, J.C., et al., *The effect of disc thickness and trauma on disc surface friction in the porcine temporomandibular joint.* Arch Oral Biol, 2001. **46**(2): p. 155-62.
141. Werner, J.A., B. Tillmann, and A. Schleicher, *Functional anatomy of the temporomandibular joint. A morphologic study on human autopsy material.* Anat Embryol (Berl), 1991. **183**(1): p. 89-95.
142. Donzelli, P.S., et al., *Biphasic finite element simulation of the TMJ disc from in vivo kinematic and geometric measurements.* J Biomech, 2004. **37**(11): p. 1787-91.
143. Dunbar, W.L., Jr., et al., *An evaluation of three-dimensional diarthrodial joint contact using penetration data and the finite element method.* J Biomech Eng, 2001. **123**(4): p. 333-40.
144. Nickel, J.C., et al., *Laboratory stresses and tractional forces on the TMJ disc surface.* J Dent Res, 2004. **83**(8): p. 650-4.
145. Nickel, J.C., et al., *Static and dynamic loading effects on temporomandibular joint disc tractional forces.* J Dent Res, 2006. **85**(9): p. 809-13.
146. Tanaka, E., et al., *Biomechanical behaviour of bovine temporomandibular articular discs with age.* Arch Oral Biol, 2001. **46**(11): p. 997-1003.

147. del Pozo, R., et al., *The regional difference of viscoelastic property of bovine temporomandibular joint disc in compressive stress-relaxation.* Med Eng Phys, 2002. **24**(3): p. 165-71.
148. Allen, K.D. and K.A. Athanasiou, *A surface-regional and freeze-thaw characterization of the porcine temporomandibular joint disc.* Ann Biomed Eng, 2005. **33**(7): p. 951-62.
149. Stairmand, J.W., S. Holm, and J.P. Urban, *Factors influencing oxygen concentration gradients in the intervertebral disc. A theoretical analysis.* Spine, 1991. **16**(4): p. 444-9.
150. Holm, S., et al., *Nutrition of the intervertebral disc: solute transport and metabolism.* Connect Tissue Res, 1981. **8**(2): p. 101-19.
151. Bartels, E.M., et al., *Oxygen and lactate concentrations measured in vivo in the intervertebral discs of patients with scoliosis and back pain.* Spine, 1998. **23**(1): p. 1-7; discussion 8.
152. Kuo, J., et al., *Effect of mechanical loading on electrical conductivity in porcine TMJ discs.* J Dent Res, 2011. **90**(10): p. 1216-20.
153. Gu, W.Y., M.A. Justiz, and H. Yao, *Electrical conductivity of lumbar anulus fibrosis: Effects of porosity and fixed charge density.* Spine, 2002. **27**(21): p. 2390-2395.
154. Shen, G. and M.A. Darendeliler, *The adaptive remodeling of condylar cartilage---a transition from chondrogenesis to osteogenesis.* J Dent Res, 2005. **84**(8): p. 691-9.
155. Moses, J.J. and D.C. Topper, *A functional approach to the treatment of temporomandibular joint internal derangement.* J Craniomandib Disord, 1991. **5**(1): p. 19-27.
156. Mow, V.C., et al., *Biphasic creep and stress relaxation of articular cartilage in compression? Theory and experiments.* J Biomech Eng, 1980. **102**(1): p. 73-84.
157. Lai, W.M., J.S. Hou, and V.C. Mow, *A triphasic theory for the swelling and deformation behaviors of articular cartilage.* J Biomech Eng, 1991. **113**(3): p. 245-58.
158. Maroudas, A.I., *Balance between swelling pressure and collagen tension in normal and degenerate cartilage.* Nature, 1976. **260**(5554): p. 808-9.
159. del Palomar, A.P., et al., *Clenching TMJs-loads increases in partial edentates: a 3D finite element study.* Ann Biomed Eng, 2008. **36**(6): p. 1014-23.
160. Soboleva, U., L. Laurina, and A. Slaidina, *Jaw tracking devices--historical review of methods development. Part I.* Stomatologija, 2005. **7**(3): p. 67-71.
161. Lemoine, J.J., et al., *Radiographic analysis for jaw motion normalization.* J Oral Maxillofac Surg, 2005. **63**(7): p. 961-7.
162. Enciso, R., et al., *The virtual craniofacial patient: 3D jaw modeling and animation.* Stud Health Technol Inform, 2003. **94**: p. 65-71.
163. Krebs, M., et al., *A new method for three-dimensional reconstruction and animation of the temporomandibular joint.* Ann Acad Med Singapore, 1995. **24**(1): p. 11-6.
164. Woltring, H.J. and E.B. Marsolais, *Optoelectric (Selspot) gait measurement in two- and three-dimensional space--a preliminary report.* Bull Prosthet Res, 1980. **10-34**: p. 46-52.
165. Seemann, R., et al., *Pseudodynamic MRI differs from natural opening of the temporomandibular joint.* Oral Surg Oral Med Oral Pathol Oral Radiol Endod, 2008. **105**(3): p. 371-8.
166. Fushima, K., et al., *Analysis of the TMJ intraarticular space variation: a non-invasive insight during mastication.* Med Eng Phys, 2003. **25**(3): p. 181-90.

167. Stowell, A.W., R.J. Gatchel, and L. Wildenstein, *Cost-effectiveness of treatments for temporomandibular disorders: biopsychosocial intervention versus treatment as usual.* J Am Dent Assoc, 2007. **138**(2): p. 202-8.
168. Slade, G.D., et al., *Study methods, recruitment, sociodemographic findings, and demographic representativeness in the OPPERA study.* The journal of pain : official journal of the American Pain Society, 2011. **12**(11 Suppl): p. T12-26.
169. Werner, J.A., B. Tillmann, and A. Schleicher, *Functional anatomy of the temporomandibular joint. A morphologic study on human autopsy material.* Anat.Embryol.(Berl), 1991. **183**(1): p. 89-95.
170. Nickel, J.C. and K.R. McLachlan, *In vitro measurement of the frictional properties of the temporomandibular joint disc.* Arch.Oral Biol., 1994. **39**(4): p. 323-331.
171. Ahmad, M., et al., *Research diagnostic criteria for temporomandibular disorders (RDC/TMD): development of image analysis criteria and examiner reliability for image analysis.* Oral surgery, oral medicine, oral pathology, oral radiology, and endodontics, 2009. **107**(6): p. 844-60.
172. Schiffman, E.L., et al., *The Research Diagnostic Criteria for Temporomandibular Disorders. I: overview and methodology for assessment of validity.* Journal of orofacial pain, 2010. **24**(1): p. 7-24.
173. Solberg, W.K., T.L. Hansson, and B. Nordstrom, *The temporomandibular joint in young adults at autopsy: a morphologic classification and evaluation.* J.Oral Rehabil., 1985. **12**(4): p. 303-321.
174. Pullinger, A.G., D.A. Seligman, and W.K. Solberg, *Temporomandibular disorders. Part I: Functional status, dentomorphologic features, and sex differences in a nonpatient population.* The Journal of prosthetic dentistry, 1988. **59**(2): p. 228-35.
175. Milam, S.B., *Pathogenesis of degenerative temporomandibular joint arthritides.* Odontology., 2005. **93**(1): p. 7-15.
176. Rees, L.A., *The structure and function of the mandibular joint.* Br.Dent.J., 1954. **96**: p. 125-133.
177. Leonardi, R., et al., *Expression of vascular endothelial growth factor in human dysfunctional temporomandibular joint discs.* Arch.Oral Biol., 2003. **48**(3): p. 185-192.
178. Yamaguchi, A., et al., *Role of hypoxia and interleukin-1beta in gene expressions of matrix metalloproteinases in temporomandibular joint disc cells.* Arch.Oral Biol., 2005. **50**(1): p. 81-87.
179. Tojyo, I., et al., *Effect of hypoxia and interleukin-1beta on expression of tenascin-C in temporomandibular joint.* Oral Dis., 2008. **14**(1): p. 45-50.
180. Kuo, J., et al., *Regional Cell Density Distribution and Oxygen Consumption Rates in Porcine TMJ Discs: An Explant Study.* Osteoarthritis Cartilage, 2011.
181. Mills, D.K., et al., *An animal model for studying mechanisms in human temporomandibular joint disc derangement.* J.Oral Maxillofac.Surg., 1994. **52**(12): p. 1279-1292.
182. Herring, S.W., et al., *Temporomandibular joint in miniature pigs: anatomy, cell replication, and relation to loading.* Anat.Rec., 2002. **266**(3): p. 152-166.
183. Gu, W.Y., et al., *Diffusivity of ions in agarose gels and intervertebral disc: Effect of porosity* Annals of Biomedical Engineering, 2004. **32**: p. 1710-1717.

184. Jackson, A.R., F. Travascio, and W.Y. Gu, *Effect of mechanical loading on electrical conductivity in human intervertebral disk.* J Biomech Eng, 2009. **131**(5): p. 054505.
185. Koolstra, J.H. and T.M. van Eijden, *Combined finite-element and rigid-body analysis of human jaw joint dynamics.* J.Biomech., 2005. **38**(12): p. 2431-2439.
186. Yao, H., et al., *Effects of Swelling Pressure and Hydraulic Permeability on Dynamic Compressive Behavior of Lumbar Annulus Fibrosus.* Annals of Biomed Engng, 2002. **30**: p. 1234-1241.
187. Gu, W.Y. and M.A. Justiz, *Apparatus for measuring the swelling dependent electrical conductivity of charged hydrated soft tissues.* J Biomech Engng, 2002. **124**: p. 790-793.
188. Frank, E.H., et al., *Physiochemical and bioelectrical determinants of cartilage material properties*, in *Biomechanics of Diarthrodial Joints*, V.C. Mow, D.O. Wood, and S.L. Woo, Editors. 1990, Spring-Verlag: New York. p. 261-282.
189. Maroudas, A., *Physicochemical properties of cartilage in the light of ion exchange theory.* Biophys.J, 1968. **8**(5): p. 575-595.
190. Almarza, A.J., et al., *Biochemical analysis of the porcine temporomandibular joint disc.* Br.J.Oral Maxillofac.Surg., 2006. **44**(2): p. 124-128.
191. Kuo, J., et al., *The region-dependent biphasic viscoelastic properties of human temporomandibular joint discs under confined compression.* J Biomech, 2010. **43**(7): p. 1316-21.
192. Quinn, T.M., P. Kocian, and J.J. Meister, *Static compression is associated with decreased diffusivity of dextrans in cartilage explants.* Arch Biochem Biophys, 2000. **384**: p. 327-334.
193. Quinn, T.M., V. Morel, and J.J. Meister, *Static compression of articular cartilage can reduce solute diffusivity and partitioning: implications for the chondrocyte biological response.* J Biomech, 2001. **34**(11): p. 1463-1469.
194. Jackson, A.R., et al., *Effect of compression and anisotropy on the diffusion of glucose in annulus fibrosus.* Spine (Phila Pa 1976.), 2008. **33**(1): p. 1-7.
195. Yuan, T.Y., et al., *Strain-dependent oxygen diffusivity in bovine annulus fibrosus.* J Biomech Eng, 2009. **131**(7): p. 074503.
196. Gross, A.E., et al., *Fresh osteochondral allografts for posttraumatic knee defects: long-term followup.* Clinical orthopaedics and related research, 2008. **466**(8): p. 1863-70.
197. *Worldwide markets and emerging technologies for tissue engineering and regenerative medicine*, in *Marketing and Technology Reports*2009, InteLab Corporation.
198. Taylor, M.J. and K.G.M. Brockbank, *Frontiers in biopreservation technology: Challenges for the storage of living tissues and engineered constructs*, in *Anti-aging Medical Therapeutics*, R.M. Klatz and R. Goldman, Editors. 2003, Health Quest Publications: Marina Del Rey. p. 515-26.
199. Brockbank, K.G., J.F. Carpenter, and P.E. Dawson, *Effects of storage temperature on viable bioprosthetic heart valves.* Cryobiology, 1992. **29**(5): p. 537-42.
200. Williams, S.K., et al., *Prolonged storage effects on the articular cartilage of fresh human osteochondral allografts.* The Journal of bone and joint surgery. American volume, 2003. **85-A**(11): p. 2111-20.
201. Ball, S.T., et al., *The effects of storage on fresh human osteochondral allografts.* Clinical orthopaedics and related research, 2004(418): p. 246-52.

202. Allen, R.T., et al., *Analysis of stored osteochondral allografts at the time of surgical implantation.* The American journal of sports medicine, 2005. **33**(10): p. 1479-84.
203. Malinin, T., H.T. Temple, and B.E. Buck, *Transplantation of osteochondral allografts after cold storage.* The Journal of bone and joint surgery. American volume, 2006. **88**(4): p. 762-70.
204. Black, J., et al., *Articular cartilage preservation and storage. II. Mechanical indentation testing of viable, stored articular cartilage.* Arthritis and rheumatism, 1979. **22**(10): p. 1102-8.
205. Onuma, K., et al., *Cold preservation of rat osteochondral tissues in two types of solid organ preservation solution, culture medium and saline.* Cell and tissue banking, 2009. **10**(1): p. 1-9.
206. Rodrigo, J., E. Thompson, and C. Travis, *4 degree C preservation of avascular osteocartilaginous shell allografts in rats.* Trans Orthop Res Soc, 1980. **5**: p. 72.
207. Wayne, J.S., et al., *Long-term storage effects on canine osteochondral allografts.* Acta orthopaedica Scandinavica, 1990. **61**(6): p. 539-45.
208. Oates, K.M., et al., *Effect of tissue culture storage on the in vivo survival of canine osteochondral allografts.* Journal of orthopaedic research : official publication of the Orthopaedic Research Society, 1995. **13**(4): p. 562-9.
209. Rohde, R.S., R.K. Studer, and C.R. Chu, *Mini-pig fresh osteochondral allografts deteriorate after 1 week of cold storage.* Clinical orthopaedics and related research, 2004(427): p. 226-33.
210. Williams, R.J., 3rd, J.C. Dreese, and C.T. Chen, *Chondrocyte survival and material properties of hypothermically stored cartilage: an evaluation of tissue used for osteochondral allograft transplantation.* The American journal of sports medicine, 2004. **32**(1): p. 132-9.
211. Kim, W., et al., *Functional Viability of Chondrocytes Stored at 4 degrees C.* Tissue engineering, 1996. **2**(1): p. 75-81.
212. Teng, M.S., A.S. Yuen, and H.T. Kim, *Enhancing osteochondral allograft viability: effects of storage media composition.* Clinical orthopaedics and related research, 2008. **466**(8): p. 1804-9.
213. Brockbank, K.G., et al., *Impact of Hypothermia upon Chondrocyte Viability and Cartilage Matrix Permeability after 1 Month of Refrigerated Storage.* Transfusion medicine and hemotherapy : offizielles Organ der Deutschen Gesellschaft fur Transfusionsmedizin und Immunhamatologie, 2011. **38**(6): p. 387-392.
214. Brockbank, K.G., A.E. Heacox, and K. Schenke-Layland, *Guidance for removal of fetal bovine serum from cryopreserved heart valve processing.* Cells, tissues, organs, 2011. **193**(4): p. 264-73.
215. O'Brien, J., et al., *Investigation of the Alamar Blue (resazurin) fluorescent dye for the assessment of mammalian cell cytotoxicity.* European journal of biochemistry / FEBS, 2000. **267**(17): p. 5421-6.
216. Maroudas, A., *Physicochemical properties of cartilage in the light of ion exchange theory.* Biophysical journal, 1968. **8**(5): p. 575-95.
217. Frank, E.H., et al., *Physiochemical and bioelectrical determinants of cartilage material properties*, in *Biomechanics of Diarthrodial Joints*, V.C. Mow, D.O. Wood, and S.L. Woo, Editors. 1990, Springer-Verlag: New York. p. 261-82.

218. Gu, W.Y., et al., *Diffusivity of ions in agarose gels and intervertebral disc: Effect of porosity.* Annals of Biomedical Engineering, 2004. **32**(12): p. 1710-1717.
219. Jackson, A. and W. Gu, *Transport Properties of Cartilaginous Tissues.* Current rheumatology reviews, 2009. **5**(1): p. 40-50.
220. Stockwell, R.A., *Chondrocytes.* J Clin Pathol Suppl (R Coll Pathol), 1978. **12**: p. 7-13.
221. Yao, H. and W.Y. Gu, *Convection and diffusion in charged hydrated soft tissues: a mixture theory approach.* Biomechanics and modeling in mechanobiology, 2007. **6**(1-2): p. 63-72.
222. Beaver, R.J., et al., *Fresh osteochondral allografts for post-traumatic defects in the knee. A survivorship analysis.* The Journal of bone and joint surgery. British volume, 1992. **74**(1): p. 105-10.
223. Bakay, A., et al., *Osteochondral resurfacing of the knee joint with allograft. Clinical analysis of 33 cases.* International orthopaedics, 1998. **22**(5): p. 277-81.
224. LaPrade, R.F., et al., *Refrigerated osteoarticular allografts to treat articular cartilage defects of the femoral condyles. A prospective outcomes study.* The Journal of bone and joint surgery. American volume, 2009. **91**(4): p. 805-11.
225. Lightfoot, A., J. Martin, and A. Amendola, *Fluorescent viability stains overestimate chondrocyte viability in osteoarticular allografts.* Am J Sports Med, 2007. **35**(11): p. 1817-23.
226. Brockbank, K.G.M., A.E. Heacox, and K. Schenke-Layland, *Tissue Preservation*, in *Advances in Biopreservation*, J.G. Baust and J.M. Baust, Editors. 2007, CRC Press/Taylor & Francis: Boca Raton. p. 157-96.
227. Soltz, M.A. and G.A. Ateshian, *Interstitial fluid pressurization during confined compression cyclical loading of articular cartilage.* Annals of biomedical engineering, 2000. **28**(2): p. 150-9.
228. Brockbank, K.G., et al., *Quantitative second harmonic generation imaging of cartilage damage.* Cell and tissue banking, 2008. **9**(4): p. 299-307.
229. Gu, W.Y. and H. Yao, *Effects of hydration and fixed charge density on fluid transport in charged hydrated soft tissues.* Annals of Biomedical Engineering, 2003. **31**(10): p. 1162-1170.
230. Votteler, M., et al., *Raman spectroscopy for the non-contact and non-destructive monitoring of collagen damage within tissues.* Journal of biophotonics, 2012. **5**(1): p. 47-56.
231. Jackson, A.R., et al., *A Conductivity Approach to Measuring Fixed Charge Density in Intervertebral Disc Tissue.* Annals of Biomedical Engineering, 2009. **37**(12): p. 2566-2573.
232. Lai, W.M., J.S. Hou, and V.C. Mow, *A TRIPHASIC THEORY FOR THE SWELLING AND DEFORMATION BEHAVIORS OF ARTICULAR-CARTILAGE.* Journal of Biomechanical Engineering-Transactions of the Asme, 1991. **113**(3): p. 245-258.
233. Yao, H., et al., *Effects of swelling pressure and hydraulic permeability on dynamic compressive behavior of lumbar annulus fibrosus.* Annals of Biomedical Engineering, 2002. **30**(10): p. 1234-1241.
234. Detamore, M.S. and K.A. Athanasiou, *Structure and function of the temporomandibular joint disc: Implications for tissue engineering.* Journal of Oral and Maxillofacial Surgery, 2003. **61**(4): p. 494-506.

235. Urban, J.P.G. and J.F. McMullin, *SWELLING PRESSURE OF THE INTERVERTEBRAL DISK - INFLUENCE OF PROTEOGLYCAN AND COLLAGEN CONTENTS.* Biorheology, 1985. **22**(2): p. 145-157.
236. Best, B.A., et al., *COMPRESSIVE MECHANICAL-PROPERTIES OF THE HUMAN ANULUS FIBROSUS AND THEIR RELATIONSHIP TO BIOCHEMICAL-COMPOSITION.* Spine, 1994. **19**(2): p. 212-221.
237. Urban, J.P.G., S. Holm, and A. Maroudas, *DIFFUSION OF SMALL SOLUTES INTO THE INTERVERTEBRAL-DISK - AS INVIVO STUDY.* Biorheology, 1978. **15**(3-4): p. 203-223.
238. Urban, J.P.G., et al., *NUTRITION OF INTERVERTEBRAL-DISK - INVIVO STUDY OF SOLUTE TRANSPORT.* Clinical Orthopaedics and Related Research, 1977(129): p. 101-114.
239. Gu, W.Y. and M.A. Justiz, *Apparatus for measuring the swelling dependent electrical conductivity of charged hydrated soft tissues.* Journal of Biomechanical Engineering-Transactions of the Asme, 2002. **124**(6): p. 790-793.
240. Gu, W.Y., W.M. Lai, and V.C. Mow, *A mixture theory for charged-hydrated soft tissues containing multi-electrolytes: Passive transport and swelling behaviors.* Journal of Biomechanical Engineering-Transactions of the Asme, 1998. **120**(2): p. 169-180.
241. Allen, K.D. and K.A. Athanasiou, *Tissue engineering of the TMJ disc: A review.* Tissue Engineering, 2006. **12**(5): p. 1183-1196.
242. Almarza, A.J. and K.A. Athanasiou, *Design characteristics for the tissue engineering of cartilaginous tissues.* Annals of Biomedical Engineering, 2004. **32**(1): p. 2-17.
243. Johns, D.E. and K.A. Athanasiou, *Design characteristics for temporomandibular joint disc tissue engineering: learning from tendon and articular cartilage.* Proceedings of the Institution of Mechanical Engineers Part H-Journal of Engineering in Medicine, 2007. **221**(H5): p. 509-526.
244. Tanaka, E., et al., *Viscoelastic properties of the human temporomandibular joint disc in patients with internal derangement.* Journal of Oral and Maxillofacial Surgery, 2000. **58**(9): p. 997-1002.
245. Gallo, L.M., et al., *Stress-field translation in the healthy human temporomandibular joint.* Journal of Dental Research, 2000. **79**(10): p. 1740-1746.
246. Nickel, J.C. and K.R. McLachlan, *IN-VITRO MEASUREMENT OF THE FRICTIONAL-PROPERTIES OF THE TEMPOROMANDIBULAR-JOINT DISC.* Archives of Oral Biology, 1994. **39**(4): p. 323-331.
247. Fields, A.J., et al., *Influence of Biochemical Composition on Endplate Cartilage Tensile Properties in the Human Lumbar Spine.* Journal of Orthopaedic Research, 2014. **32**(2): p. 245-252.
248. Kwan, M.K., T.H.C. Lin, and S.L.Y. Woo, *ON THE VISCOELASTIC PROPERTIES OF THE ANTEROMEDIAL BUNDLE OF THE ANTERIOR CRUCIATE LIGAMENT.* J Biomech, 1993. **26**(4-5): p. 447-452.
249. Detamore, M.S. and K.A. Athanasiou, *Tensile properties of the porcine temporomandibular joint disc.* Journal of Biomechanical Engineering-Transactions of the Asme, 2003. **125**(4): p. 558-565.
250. Beatty, M.W., et al., *Strain rate dependent orthotropic properties of pristine and impulsively loaded porcine temporomandibular joint disk.* Journal of Biomedical Materials Research, 2001. **57**(1): p. 25-34.

251. Johnson, G.A., et al., *TENSILE AND VISCOELASTIC PROPERTIES OF HUMAN PATELLAR TENDON.* Journal of Orthopaedic Research, 1994. **12**(6): p. 796-803.
252. Kalpakci, K.N., et al., *An Interspecies Comparison of the Temporomandibular Joint Disc.* Journal of Dental Research, 2011. **90**(2): p. 193-198.
253. PR, H., *Treatment of scoliosis. Correction and internal fixation by spine instrumentation.* J Bone Joint Surg Am, 1962. **44**: p. 591-610.
254. Moe, J.H., et al., *Harrington instrumentation without fusion plus external orthotic support for the treatment of difficult curvature problems in young children.* Clin Orthop Relat Res, 1984(185): p. 35-45.
255. Campbell, R.M., Jr., *Spine deformities in rare congenital syndromes: clinical issues.* Spine (Phila Pa 1976), 2009. **34**(17): p. 1815-27.
256. Oetgen, M.E. and L.C. Blakemore, *Growing Rods in Early-Onset Scoliosis.* Seminars in Spine Surgery, 2012. **24**(3): p. 155-163.
257. Akbarnia, B.A., et al., *Dual growing rod technique for the treatment of progressive early-onset scoliosis: a multicenter study.* Spine (Phila Pa 1976), 2005. **30**(17 Suppl): p. S46-57.
258. Thompson, G.H., B.A. Akbarnia, and R.M. Campbell, Jr., *Growing rod techniques in early-onset scoliosis.* J Pediatr Orthop, 2007. **27**(3): p. 354-61.
259. Thompson, G.H., et al., *Comparison of single and dual growing rod techniques followed through definitive surgery: a preliminary study.* Spine (Phila Pa 1976), 2005. **30**(18): p. 2039-44.
260. Wang, S., et al., *Dual growing rods technique for congenital scoliosis: more than 2 years outcomes: preliminary results of a single center.* Spine (Phila Pa 1976), 2012. **37**(26): p. E1639-44.
261. Akbarnia, B.A., et al., *Dual growing rod technique followed for three to eleven years until final fusion: the effect of frequency of lengthening.* Spine (Phila Pa 1976), 2008. **33**(9): p. 984-90.
262. Bess, S., et al., *Complications of growing-rod treatment for early-onset scoliosis: analysis of one hundred and forty patients.* J Bone Joint Surg Am, 2010. **92**(15): p. 2533-43.
263. Yang, J.S., et al., *Growing rod fractures: risk factors and opportunities for prevention.* Spine (Phila Pa 1976), 2011. **36**(20): p. 1639-44.
264. Hicks, J.M., et al., *Complications of pedicle screw fixation in scoliosis surgery: a systematic review.* Spine (Phila Pa 1976), 2010. **35**(11): p. E465-70.
265. Sankar, W.N., D.C. Acevedo, and D.L. Skaggs, *Comparison of complications among growing spinal implants.* Spine (Phila Pa 1976), 2010. **35**(23): p. 2091-6.
266. Watanabe, K., et al., *Risk factors for complications associated with growing-rod surgery for early-onset scoliosis.* Spine (Phila Pa 1976), 2013. **38**(8): p. E464-8.
267. Schroerlucke, S.R., et al., *How does thoracic kyphosis affect patient outcomes in growing rod surgery?* Spine (Phila Pa 1976), 2012. **37**(15): p. 1303-9.
268. Coe, J.D., et al., *Influence of bone mineral density on the fixation of thoracolumbar implants. A comparative study of transpedicular screws, laminar hooks, and spinous process wires.* Spine (Phila Pa 1976), 1990. **15**(9): p. 902-7.
269. Halvorson, T.L., et al., *Effects of Bone Mineral Density on Pedicle Screw Fixation.* Spine (Phila Pa 1976), 1994. **19**(21): p. 2415-2420.
270. Butler, T.E., Jr., et al., *The strength and stiffness of thoracic implant anchors in osteoporotic spines.* Spine (Phila Pa 1976), 1994. **19**(17): p. 1956-62.

271. Gross, R.H., *An alternate method of fixation for management of early-onset deformity with thoracic kyphosis.* J Pediatr Orthop, 2012. **32**(6): p. e30-4.
272. Mahar, A.T., et al., *Biomechanical comparison of different anchors (foundations) for the pediatric dual growing rod technique.* Spine J, 2008. **8**(6): p. 933-9.
273. Liljenqvist, U., et al., *Pullout strength of pedicle screws versus pedicle and laminar hooks in the thoracic spine.* Acta Orthop Belg, 2001. **67**(2): p. 157-63.
274. DiAngelo, D.J. and K.T. Foley, *An improved biomechanical testing protocol for evaluating spinal arthroplasty and motion preservation devices in a multilevel human cadaveric cervical model.* Neurosurg Focus, 2004. **17**(3): p. E4.